The Structure and Dynamics of Tropical Forests In Relation to Climate Variability

The structure and dynamics of tropical forests

in relation to climate variability

A dissertation presented

by

Shirley Xiaobi Dong

to

The Department of Organismic and Evolutionary Biology

in partial fulfillment of the requirements
for the degree of
Doctor of Philosophy
in the subject of
Biology

Harvard University
Cambridge, Massachusetts

April 2011

Dissertation Advisor | Author

Professor Paul R. Moorcroft | **Shirley Xiaobi Dong**

The structure and dynamics of tropical forests

in relation to climate variability

Abstract

Although trends and changes in environmental forcing over tropical regions have been recognized, the question remains: how do tropical forests respond to current and future global climate change? Results from long-term studies of permanent forest plots have reported different, and in some cases opposing, trends in tropical forest dynamics in response to climate variability. Researchers remain divided as to whether tropical forests are likely to become net carbon sources or net carbon sinks under ongoing climate change. In this thesis, I use both empirical field measurement data analyses and mathematical modeling approaches to study the structure and dynamics of tropical forests in relation to climate variability. I examine tree growth rates calculated from long-term plot censuses with 5-year intervals and dendrometer band measurements with 3- or 6-month intervals to analyze changes in trees' growth responses to differences in the mean climate forcing at different sites and to temporal variation in precipitation, temperature and solar radiation at different locations. The results reveal new information about relationships between tree growth and climate variability and offer plausible explanations for conflicting trends in tree growth rates observed across

different tropical forests over time. In the modeling studies, I use an integral projection model combined with allometric scaling theories to relate tree demographic rates to differences in forest structure. The ability of this model to predict steady-state stem size-frequency distributions of the forests provides the opportunity to gain insights into the demographic history of the forest. I then develop a new dynamic scaling theory that incorporates the two-way interaction between tree demography and forest structure. It can predict the transient, time-dependent dynamics of forest demography and structure as forests reach their steady-state equilibrium, and can capture the characteristic timescales for these processes. This dynamic scaling theory can also be applied in non-equilibrium situations, such as the dynamics of forest re-growth following natural or human disturbances, or transient changes in forest demography and size distributions following climate change.

Table of Contents

List of Figures

List of Tables

Acknowledgments

I have been extremely fortunate to get to know many wonderful people and receive a lot of help, guidance and support from them in the past six years. Among them all, I owe my greatest gratitude to my advisor, Paul Moorcroft, for everything he has taught me and everything he has helped me with. If I were to make a list of them, it would probably be longer than this thesis itself. Besides, any verbal description I could possibly come up with would just seem too weak. So I guess all I can and will say here, is that I can never thank him enough for everything he has done for me.

I also thank the rest of my graduate committee: Peter Ashton, Stuart Davies, David Foster, and Noel Michele Holbrook, for their advice throughout the years of my doctoral research. I have benefited greatly from their valuable knowledge, thoughts and comments through discussing my projects and preliminary results with them. A special thank goes to Stuart, who not only helped to pave the way to start my field project, but also was always there to help me and answer my questions. I really could not have done it without his help and support.

It has been a great privilege to get to know and work with many brilliant people in

the lab and I thank my past and current lab-mates for their support: Alex Antonarakis, Gil Bohrer, Mike Dietze, James Forester, Jaclyn Hatala, Takeshi Ise, Jonna Katajisto, Adrienne Keller, Yeonjoo Kim, Naomi Levine, Dan Lipsitt, Jeff Lo, Marcos Longo, Heather Lynch, David Medvigy, Tom Powell, Abby Swann, and Ke Zhang. I also need to thank Carla Barger, Ivelise Bermudez, Melissa van Ee, Heather Ehlers, Pam Greene, Katie Parodi, Chris Preheim, and William Tootle, for their tremendous help in administrative and logistics support for my study and/or my fieldwork.

I received permission from the following institutions to enter and conduct field research in the forest reserves and to use relevant data for analysis: Center for Tropical Forest Science, Smithsonian Tropical Research Institute, Forest Research Institute of Malaysia, Royal Forest Department of Thailand, Xishuangbanna Tropical Botanical Garden, Chinese Academy of Sciences. I thank the researchers there for their collaboration and support for my project; and among them, the most important are: Sarayudh Bunyavejchewin, Min Cao, Christine Dawn Fletcher, Abdul Rahman bin Kassim, Somboon Kiratiprayoon, Helene Muller-Landau, Nur Supardi Md. Noor, and Hua Zhu. The climate data used in Chapter 3 for Pasoh were from the meteorological station run by Forestry and Forest Products Research Institute, Japan and Forest Institute of Malaysia. And the climate data for Xishuangbanna were from the Xishuangbanna Station for Tropical Rain Forest Ecosystem Studies (XSTRE). I thank Yoshiko Kosugi and Xiaobao Deng, respectively, for providing the data.

During my field trips for the dendrometer band project, I received a lot of help at each of the sites I visited. And I am the most indebted to: Muhammad Firdaus bin

Abdullah Sani at Pasoh Forest Reserve, Malaysia; Pitoon Kongnoo at Khao Chong Peninsular Botanical Garden (KC), Thailand; Manop Kaewfoo at Huai Kha Khaeng Wildlife Sanctuary (HKK), Thailand; Wenfu Zhang at Xishuangbanna Tropical Botanical Garden (XSBN), China; and Pablo Ramos at Barro Colorado Island (BCI), Panama. During part or entire length of my each visit, they made all the initial logistical arrangements, accompanied me to and showed me around the forest plots, translated and/or communicated to the field assistants, took good care of me and helped me greatly in every possible way. I would never have been able to manage the field trips and finish the fieldwork without them. For the same reason, I would also like to list and thank all the field assistants, although I don't even know some of their last names. Banding nearly ten thousand trees and re-measuring all the dendrometers every three or six months would not be possible without all their help; and therefore I owe my gratitude to: Aboi, Bob, Din, Helmi, Rauf at Pasoh; Et, Kai, Koon, Ong, Vee at KC; Biek, Bui, Kong, Mu, Nei, Yong at HKK; Defu Chen, Yunchao Deng, Lancai He, Laosan Li, Shao'an Li, Mengnan Liu, Jiu Ma, Jinhua Xiong, Jiang Yu at XSBN. In addition, Razman scanned and sent the datasheets from Pasoh and Dongfen Dai entered the data; Kae entered and sent all the data from KC and HKK. I am very grateful for all their help.

There are also a lot of people at Harvard who have offered me their support and/or provided me with great opportunities at various stages of my life in graduate school. So I would like to thank: Ginny Drislane of the ELP program for her coach in English and introduction to American culture and history; Christine Herot, Frank McNamara

and Sheila Reindl of the Bureau of Study Council for their various workshops that helped me adjusting to the work, study, and life style here; Tom Judson and John Hall for giving me the opportunities to teach Math 19a; Cam Webb for the opportunities to teach the Harvard summer course in Borneo; Virginia Maurer of the Derek Bok Center for coaching me and making all the efforts to help me become a better teacher; Rebekah Maggor for the voice and speech coaching; Rob Campbell for helping me rehearse my sections and providing his insights as an undergraduate student; Barbara Powell for reading and editing this thesis in addition to all her support throughout these years; Laura Malisheski, Robin Mount and Amy Sanford of the Office of Career Services for the workshops and individual meetings to help my job search; Darryl Ziegler of Harvard International Office for all his help with visa-related questions; Tom Dodson of the Office for Scholarly Communications for the opportunity to work as an Open Access Fellow; Scott Smider of Cambridge Queen's Head Pub for the opportunities to work at various events; and Kevin Ebert of Harvard Museum of Natural History for selling my paper flowers at the museum gift shop.

Finally, I would like to thank my families and friends for their lasting support. By families, I refer to not only my family back in China, but also my host family here in Cambridge. I thank Barbara, Art, Ben, Julia, Allie, Nancy, Carl, and all the Powells for their love and care in all these years. I have never spent a holiday alone and always know I have a home to turn to when in need. I also thank the following friends for being the most important part of my life during part or all of the past six years: Shuang Chen, Xiao Fang, Naiqing Gu, Bin Guo, Rui Guo, Chong Han, Ling Han, Lin He,

Hannie Heny, Wei Huang, Zhan Li, Lihan Liu, Lihong Liu, Jiayuan Luo, Minmin Luo, Teng Ma, Xiaofei Ma, Lin Qian, Wenjie Tang, Xiaolu Wan, Weiye Wang, Yaheng Wang, Yihua Wang, Fan Xiang, Liwei Yan, Gang Yu, Min Zhang, Tingting Zhang, Yanling Zhang, and Hong Zi. I cannot imagine how my life would have been without their company. I treasure their friendship and am forever grateful for their love and support.

To my parents.

Chapter 1

Introduction

With approximately 59% of global vegetation carbon, 27% of global soil carbon (Dixon et al. 1994), and more than half of the world's biodiversity (Wilson 1988), tropical forests are receiving increasing attention by scientists and researchers from various disciplines. They not only face threats from deforestation and fragmentation, but also challenges of ongoing changes in global climate (Bawa and Markham 1995). Although trends in environmental forcing, including temperature, atmospheric CO_2, solar radiation, and precipitation, over the tropical regions have been recognized (Malhi and Wright 2004; IPCC 2007), the responses of tropical forests to current and future global climate variability and change remain poorly understood. In this thesis, I use empirical field measurement data and mathematical modeling to study the structure and dynamics of tropical forests in relation to climate variability.

1.1 Background: observed changes in different tropical forests

In order to gain insights into the composition, structure and dynamics of tropical forests, long-term sample plots have been set up in all three major tropical regions: Neotropics, South and Southeast Asia, and Africa. Two of the most prominent plot networks are the Forest Dynamics Plot Network of the Center for Tropical Forest Science (CTFS, Losos and Leigh 2004), and the Amazon Forest Inventory Network (RAINFOR, Malhi et al. 2002). Standardized protocols for site selection and sampling methods within each network[1] aim for consistent measurement and data collection. The protocols not only ensure correct detection of the temporal trend in the variation of forest structure and dynamics, but also make possible comparative studies of the spatial patterns among the sites in the network. Despite the differences in size and coverage of their plots[2], as well as the minimum size of trees measured[3], both networks are long-term, permanent plots in which individual trees are identified, mapped, and measured in multiple censuses.

The multiple censuses of the sites allow the researchers in each network to

[1] RAINFOR started as a collection of sample plots established and monitored by independent researchers. The network has since been advocating standardized sampling techniques and methodology to ensure coherence across all sites (Malhi et al. 2002).

[2] The CTFS network is pan-tropical, with large plots of sizes between 2 and 50 hectares (Losos and Leigh 2004). All the RAINFOR sites are located across Amazonia, with plot sizes ranging from 0.4 to 9.0 hectares, about 1 hectare on average (Baker et al. 2004a).

[3] The minimum size of tree stems being measured at CTFS plots is 1 cm DBH (diameter at breast height, ~1.3m, Losos and Leigh 2004). The minimum size of trees recorded in the RAINFOR network is 10 cm DBH (Baker et al. 2004a).

examine the trend in the total biomass changes of the forests, as well as the variation in rates of turnover (recruitment, mortality and growth). Analyses of the RAINFOR plot network measurements have indicated a significant regional-scale carbon sink in old-growth Amazonian forests, with an increase of above-ground dry biomass of 1.21 ± 0.43 Mg ha^{-1} yr^{-1} (unweighted), or 0.98 ± 0.38 Mg ha^{-1} yr^{-1} (weighted by monitoring effort), for trees that are more than 10 cm in diameter (Baker et al. 2004b). Stand-level changes within 50 RAINFOR plots across South America also showed a significant increase in basal area over time, along with increasing stem density, recruitment and mortality rates (Lewis et al. 2004). Such trends in the changes of forest structure and dynamics have been confirmed in subsequent analyses from RAINFOR data. For example, Phillips et al. (2004) concluded that the growth and productivity of Amazon forests are being stimulated by widespread environmental changes, with significantly increasing turnover rates in almost every region and environmental zone that they have examined over 25 years (1976-2001).

In contrast, analyses of data from the CTFS network have found either no such trends, or changes in opposite direction. When estimating the above-ground biomass (AGB) change in the 50-hectare Forest Dynamics Plot on Barro Colorado Island (BCI), Chave et al. (2003) found no statistically significant increase in AGB over the 15-year average (1985-2000). A more recent study using data from all of the five censuses completed for the same site revealed that relative basal area growth actually decreased over time, as did sapling growth rates and mortality rates; such trends were also found in Pasoh, a Southeast Asian plot in Malaysia (Feeley et al. 2007). In another old-

growth tropical rain forest at La Selva, Costa Rica, a site that is independent from the RAINFOR and CTFS networks, decreased canopy growth rates were also found in six canopy species during 1984-2000 (Clark et al. 2003).

In all these studies, researchers have suggested climate change as an explanation for the observed changes in tropical forest structure and dynamics; however, their conclusions are different, or sometimes at odds, with each other. For example, the La Selva study found a negative correlation between the annual diameter growth rate of trees and the annual mean of daily minimum temperature (Clark et al. 2003). A similar trend was confirmed in the CTFS study by Feeley et al. (2007). In contrast, the RAINFOR researchers suggested that increasing temperature may be the underlying cause of accelerating forest dynamics (Lewis et al. 2004). Other environmental forcing, such as rising atmospheric CO_2 and/or changes in sunlight and cloud cover, have also been proposed as the major drivers of the directional change in forest dynamics (Lewis et al. 2004). Scientists have yet to reach consensus on how tropical forests are responding to on-going climate change and whether they are likely to become net carbon sources or sinks (Clark 2004a, b; Clark 2007; Malhi and Phillips 2004).

1.2 Research objectives and approaches

The conflicting findings and unresolved debate about the impacts of climate variability and change on tropical forests described above motivated my doctoral

research.

Specifically, I sought to address two inter-related sets of questions:

(1) Are tropical forests changing in their dynamics and structure as a result of on-going climate change? If so, in which direction? And why?

(2) To what extent can we account for the different structure and dynamics of different tropical forests? And to what extent do these differences affect their responses to changes in environmental forcing?

During my doctoral research, I used both empirical field measurement data analyses and mathematical modeling approaches to address these questions.

The field measurement data I used in my studies all came from forest plots within the CTFS plot network. I had access to long-term census data from five CTFS plots (Pasoh and Lambir in Malaysia, Huai Kha Khaeng and Khao Chong in Thailand, and Barro Colorado Island in Panama). I used the *c.* 5-year census measurements in various analyses throughout the thesis, including an analysis of climate variability on patterns of tree growth. I also initiated an extensive dendrometer-based study of tropical tree growth, in which I installed nearly ten thousand dendrometer bands across trees in four Southeast Asian forests within the CTFS plot network (Pasoh in Malaysia, Huai Kha Khaeng and Khao Chong in Thailand, and Xishuangbanna in China). These dendrometer bands are re-measured and tree growth data are recorded every three or six months since 2007, except for Xishuangbanna, where measurements began in 2009. The much shorter measurement intervals made possible by the dendrometer bands

enabled me to examine the inter- and intra-annual variations in tree growth responses to climate variability that are not captured in the original 5-year plot-wide census data.

The second component of my thesis research was the application of mathematical models to understand the relationship between the differences in the observed tree demographic rates and the resulting differences in tropical forest structure at different sites. I tested and compared the ability of size-structured models using phenomenological functions to relate observed forest demographic rates and current forest structure to gain insights into the demographic history of the forest. I then developed a new dynamic scaling theory that yields more accurate predictions and capable of studying and predicting the transient dynamics of forest demography and structure.

1.3 Chapter synopses

In Chapter 2, I compare changes in tree growth rates measured across *c.* 5-year census intervals at four long-term permanent tropical forest research plots (Pasoh, Lambir, Huai Kha Khaeng, and Barro Colorado Island) in relation to variation in solar radiation, temperature and precipitation. The results indicate that a combination of incoming solar radiation and minimum night-time temperature variability explain most of the observed variability in five-year tree growth rates, and can explain conflicting trends in tree growth rates seen in different tropical forests.

In Chapter 3, I present results from the dendrometer band study at four tropical forest plots along a latitudinal gradient (Pasoh, Khao Chong, Huai Kha Khaeng, and Xishuangbanna). These inter- and intra-annual growth measurements revealed new information about relationships between tree growth and climate variability, including effects of precipitation, that were not apparent in the analyses using the 5-year census data. I then compared the responses of five representative species groups with different life history traits. I also examined the impact of light availability, wood density, and topography on tree growth rates in different forests.

In Chapter 4, I present a size-structured model that relates current forest demographic rates to the forest structure that would result from these demographic rates if they are maintained. The ability of this model to predict steady-state stem size-frequency distributions of the forests provides the opportunity to gain insights into the demographic history of the forest, as is shown in case studies of three different forest plots in Southeast Asia (Lambir, Pasoh, and Huai Kha Khaeng). I then discuss and compare some of the predictions from metabolic scaling theory, using the same study sites.

In Chapter 5, I introduce a new size-structured model formulation that incorporates these models to yield more accurate predictions of the observed size distributions and growth and mortality rates. The dynamic scaling theory presented in this chapter builds upon the basic assumptions of conventional metabolic scaling theory, retaining the allometric relationship for canopy leaf area as a function of tree size. However, it also incorporates the density-dependent impact of forest structure upon forest light

profiles and resulting tree demographic rates. In addition, his model is capable of predicting both the transient, time-dependent dynamics of forest demography and structure as the forests reach their steady-state equilibrium, and the characteristic timescales for these processes.

In Chapter 6, I conclude the thesis and bring together the findings from the empirical and modeling studies presented in all of the four main chapters. I then point out the implications of the results, and highlight several directions for future studies.

Chapter 2

Observed patterns and trends in tree growth rates across tropical forests in relation to climate variability

As discussed in chapter 1, although trends in environmental forcing over tropical regions have been recognized, the responses of tropical forests to current and future global climate change remain poorly understood. Researchers remain divided as to whether tropical forests are likely to become net carbon sources or net carbon sinks under ongoing climate change. They are also debating whether the changes of the forests are caused by increased temperature, rising atmospheric CO_2, or as a result of other changes in environmental forcing. In this chapter, I review changes in tree growth rates at four long-term permanent tropical forest research plots in relation to variation in solar radiation, temperature and precipitation that were examined in earlier studies. I have found a positive correlation between temporal variation in stand-level

tree growth rates and variation in incoming solar radiation, and a negative correlation between tree growth rates and night-time temperatures. Taken alone, neither solar radiation variability nor the negative effects of night-time temperature explain the changes in growth rates at all sites. However, when considered together these two climate variables explain most of the observed changes in tree growth rates over time. Moreover, these effects of solar radiation and temperature variability explain conflicting trends in tree growth rates across different tropical forests.

2.1 Introduction

Although trends in environmental forcing, including temperature, atmospheric CO_2, solar radiation, and precipitation, over tropical regions have been recognized (Malhi and Wright 2004; IPCC 2007), the responses of tropical forests to current and future global climate change remain poorly understood. For example, researchers have found apparently conflicting trends in changes in above-ground biomass (e.g., Baker et al. 2004; Chave et al. 2008), and remain divided as to whether tropical forests are likely to become net carbon sources or net carbon sinks under increased temperature, rising atmospheric CO_2, or as a result of other changes in environmental forcing (Clark 2004a, b; Lewis et al. 2004; Malhi.and Phillips 2004; Phillips et al. 2004; Feeley et al. 2007; Gloor et al. 2009).

This uncertainty is linked to ongoing debate on whether and how tropical forests are changing in their structure and dynamics as a result of climate change (e.g., Clark et al. 2003; Clark 2004b; Lewis et al. 2004; Phillips et al. 2004). Results from long-term studies of permanent forest plots reported different, and in some cases opposing, trends in tropical forest dynamics. For example, researchers with the Amazon Forest Inventory Network (RAINFOR, Malhi et al. 2002) concluded that the growth and productivity of Amazon forests are being stimulated by widespread environmental changes, with significantly increasing turnover rates (i.e. the average rate of biomass growth plus biomass mortality) in almost every region and environmental zone that they have examined over 25 years (1976-2001, Phillips et al. 2004). However, in an independent study at La Selva, Costa Rica, the researchers found out that growth rates decreased in six canopy species during 1984-2000 (Clark et al. 2003); and the same trend of decelerating growth was also reported from large forest dynamics plots in Panama and Malaysia (Feeley et al. 2007). Both these studies found a negative correlation between the annual diameter growth rate of trees and the annual mean of daily minimum temperature. This finding is at odds with the conclusions of the RAINFOR study, which suggested that increasing temperature may be the underlying cause of accelerating forest dynamics (Lewis et al. 2004).

While many studies have focused on the impacts of increasing temperature and CO_2, the differential responses seen in the above-mentioned studies of tropical forests may be linked to changes in other aspects of climate forcing. In particular, plant growth and productivity in the tropics is thought to be strongly limited by light (solar

radiation) as compared to temperature and water availability (Graham et al. 2003; Nemani et al. 2003; Wright & Calderon 2006). Since variation in cloud cover occurs at much smaller spatial scales, differences in solar radiation forcing could potentially provide an explanation for the observed differences in the trends of tropical forest dynamics in different areas. In this chapter, I examine changes in tree growth rates at four long-term permanent tropical forest research plots in relation to changes in their solar radiation forcing, in addition to the effects of temperature and precipitation that were examined in afore-mentioned earlier studies. The objectives are to determine the extent to which tropical forests respond to variation in climate forcing and to ascertain whether the results that I find could potentially explain the differing trends in forest dynamics observed in different regions and studies.

2.2 Methods

2.2.1 Study sites

The study sites were chosen from the Center for Tropical Forest Science (CTFS) network of large-scale forest dynamics plots. Four plots which had been censused three or more times at *c.* 5-year intervals were chosen because two or more census intervals were needed to examine changes in growth rates over time (Table 2.1). Barro

Colorado Island (BCI) in Panama is covered by lowland moist forest dominated by Bombacaceae and Leguminosae; Huai Kha Khaeng (HKK) in Thailand is a seasonal dry forest dominated by Dipterocarpaceae. Lambir in Malaysian Borneo and Pasoh in Peninsular Malaysia are lowland mixed dipterocarp forests. Both BCI and HKK are semi-evergreen forests with significant and sometimes severe dry season, while Lambir and Pasoh are evergreen forests with no or less than one month dry season (Losos and Leigh 2004). All plots were censused at *c.* 5-year intervals using standardized methods. That is, all trees whose stem diameter at breast height (~1.3 m) was more than 1 cm were mapped, tagged, identified to species, and measured in diameter (Condit 1998). The census years used in this study for each site are listed in Table 2.1.

2.2.2 Tree growth rates

For each census interval, the yearly diameter growth rate (in cm per year) and relative diameter growth rates (in percentage diameter change per year) of each individual tree were calculated for all trees that were alive and greater than 1 cm diameter at breast height (DBH) in each census interval. Specifically, the absolute and relative change in diameter of each tree between each census was divided by the length of each corresponding census interval to obtain yearly absolute and relative growth rates.

Table 2.1 The forest dynamics plots (FDPs) used in this study and their site characteristics

Site	Latitude	Longitude	Plot area (ha)	Census Years	Elevation (m a.s.l.)	Dry season (months)	Canopy height (m)	Stand density (thousand)
Barro Colorado Island, Panama	9°09' N	79°51' W	50	1985, 1990, 1995, 2000, 2005	120-160	3	20-40	208
Huai Kha Khaeng Wildlife Sanctuary, Thailand	15°37' N	99°12' E	50	1994, 1999, 2004	549-638	6	40-55	113
Lambir Hills National Park, Sarawak, Malaysia	4°10' N	114°01' E	52	1992, 1997, 2002	104-244	0	40-60	362
Pasoh Forest Reserve, Malaysia	2°58' N	102°18' E	50	1986, 1990, 1995, 2000, 2005	80-104	1	35	296

Rainfall is the average annual total; dry season length is the number of calendar months with average rainfall < 100 mm. T_{max} and T_{min} are the average daily maximum and minimum temperatures respectively. All data are from Losos and Leigh 2004.

Consistent with earlier analyses (e.g. Condit et al. 2006), excluded from the calculation were: (i) trees that grew at a rate greater than 7.5 cm diameter per year; (ii) trees that shrunk more than 25% of their initial DBH; (iii) trees that were measured at different heights in two consecutive censuses (usually due to growing buttresses or damaged stems); and (iv) trees whose main stem had broken and re-sprouted. In other words, this study included only trees that were measured at exactly the same place on the stem in both of the consecutive censuses, and that did not grow or shrink at biologically unrealistic rates (as such cases are usually due to measurement errors). In addition, trees with negative growth rates of smaller magnitude than 25% were included, but their growth rates were set to zero.

Figure 2.1 shows the stand-level mean absolute growth rates (in diameter, cm/year) calculated for each census interval at the four sites, and as expected, the long-term average growth rates vary among these forests due to differences in their physical environment. Soil nutrient storage, particularly phosphorus, is higher in tropical dry forests (Murphy and Lugo 1986). Topography may also contribute to the significantly higher growth rates observed at HKK. For the purpose of this study I controlled for the site-level differences in the baseline (long-term mean) tree growth rates by computing the deviations of growth rates for each census interval from their long-term mean (over the entire census history). For example, the five-year mean growth rate at HKK was 0.23 cm/year during the first census interval (1994-1999), it then decreased to 0.21 cm/year during the second census intervals (1999-2004). But at Lambir, the five-year stand-level mean growth rate increased from 0.065 cm/year to 0.067 cm/year

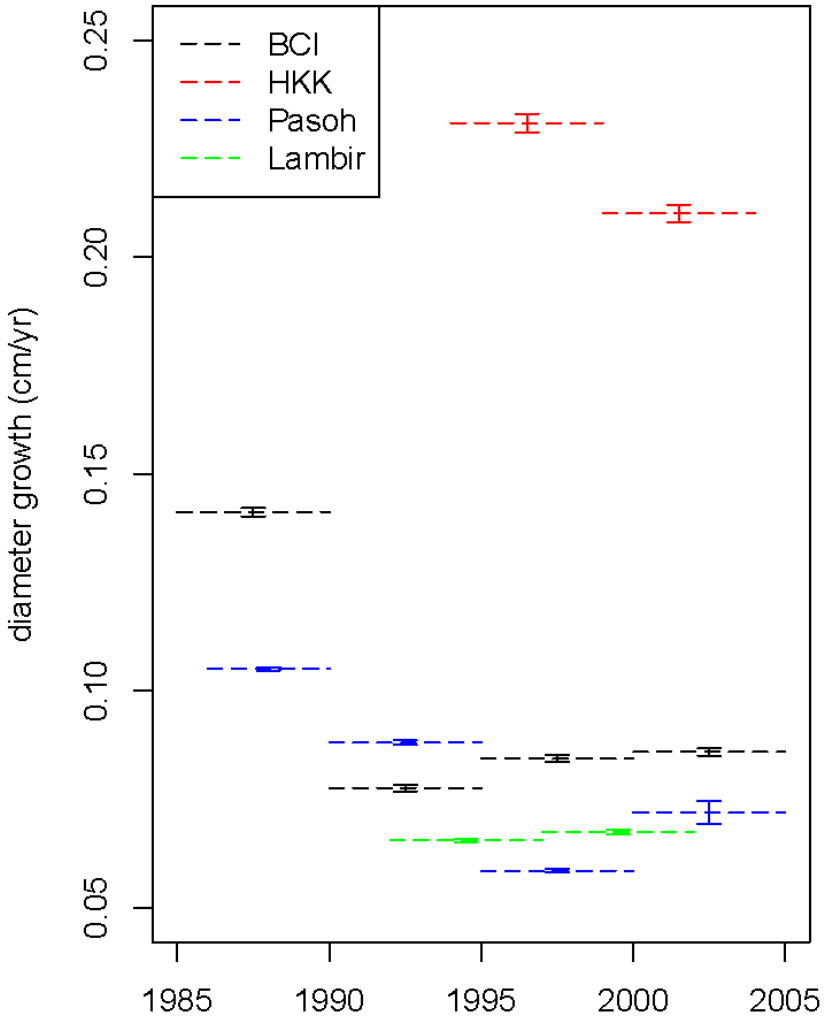

Figure 2.1 Stand-level mean diameter absolute growth (cm/yr) at BCI (black), HKK (red), Pasoh (blue), and Lambir (green). Each dashed horizontal line represents the mean growth rate over that census interval. The solid vertical lines with horizontal bars show the 95% confidence interval of the mean growth rates.

between the two census intervals (1992-1997 and 1997-2002). In terms of directions, these correspond to a decrease of 0.02 cm/year for HKK and an increase of 0.002 cm/year for Lambir).

2.2.3 Climatological Data

Since none of the CTFS plots has an on-site meteorological station[1], and it is difficult to evaluate the quality and consistency of data obtained from local meteorological stations, I used monthly climate data from the NOAA/NCEP Climate Prediction Center (http://iridl.ldeo.columbia.edu/docfind/databrief/cat-atmos.html). Specifically, for precipitation, average annual precipitation (mm/year) for each census period was calculated from the product PREC/L (Precipitation REConstruction over Land; Chen et al. 2002) by adding the raw monthly data and dividing by the census interval. In a similar manner, monthly mean daily minimum, maximum and mean temperatures (ºC) were obtained from the product EVE (Ropelewski et al. 1985) and then averaged to yearly mean values for each of these temperature measures.

Estimates of the solar radiation forcing at each site during each census interval were obtained from the satellite-based radiation measurements of the International Satellite Cloud Climatology Project (ISCCP, http://isccp.giss.nasa.gov/). The gridded

[1] There have been plans to set up on-site meteorological stations at several plots within the CTFS network as part of its new measurement program to quantify inter- and intra-annual variation in forest carbon dynamics in relation to climate (http://www.ctfs.si.edu/group/Carbon). In the summer of 2009, two meteorological stations were installed in two plots in Thailand (Huai Kha Khaeng and Khao Chong) and one more will be deployed at Barro Colorado Island in Panama soon.

ISCCP-FD RadFlux dataset (Zhang et al. 2004) were downloaded to obtain shortwave downwelling flux at surface (W/m^2). Then the latitude and longitude coordinates of each site were used to locate the nearest land grid cell. The original data were recorded at 3-hour intervals, which were averaged to daily mean values in this study.

Mean values of all the above climate variables were calculated for each census interval (from July of the year of one census to June of the year of the next census) for each site, and compared with the local mean over the entire period when the forests were monitored (from July of the year of the first census to June of the year of the last census; Figures 2.2-2.4). The long-term local means of the climate variables at each site differ significantly from one another. As I did with the tree diameter growth rates, I examined the impact of changes in climate by computing deviations of the climate variables from their long-term mean at each site. This approach has advantages when the available climate data had not been collected locally at each site, since the regional data is likely to be different from the local climate conditions (particularly for sites such as HKK, which is mountainous). While the absolute temperature should be expected to be lower than the regional estimates by about 4 degrees, the pattern of variability in temperature is likely to be similar.

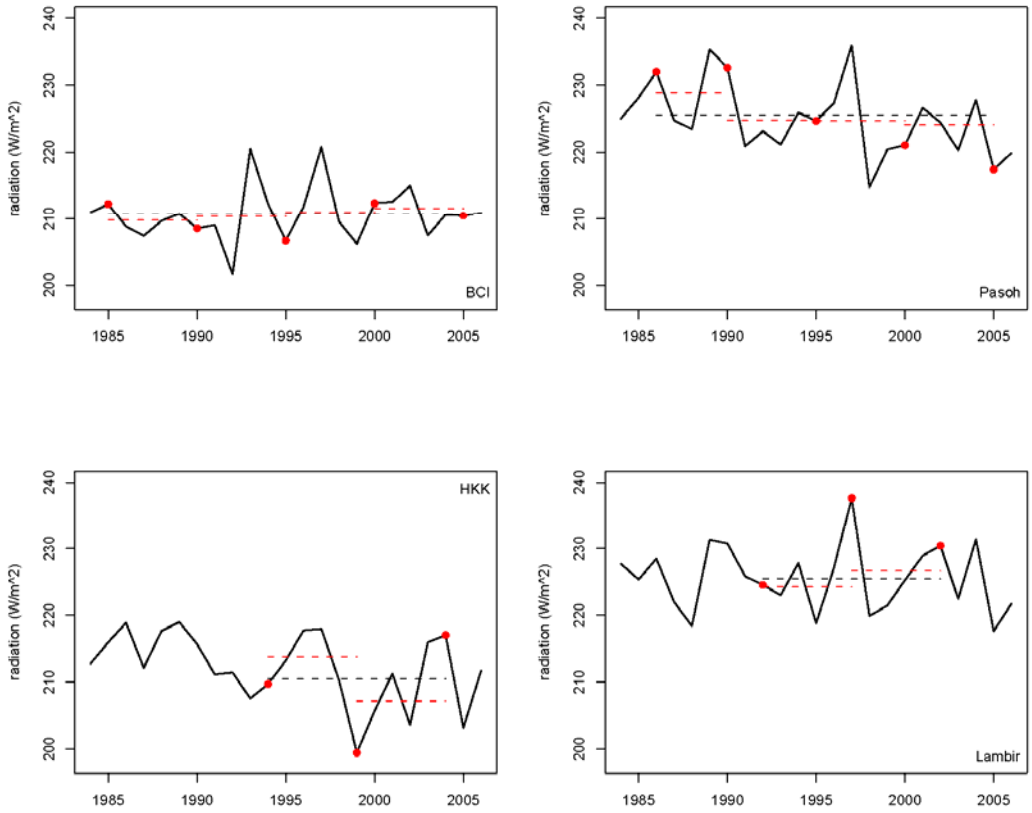

Figure 2.2 Changes in annual mean incoming solar radiation (W/m^2) at each site from 1984 to 2006. The annual values are calculated from July of one year to June of the next year. See Section 2.2.3 for details and data sources. The red dots indicate the time of each census taken place at each site. The red dashed lines are the mean over each census interval, while the black dashed lines are the mean over the entire study period. The differences between each red dashed line to the corresponding black line are the deviations used in the analysis (see Section 2.2.3).

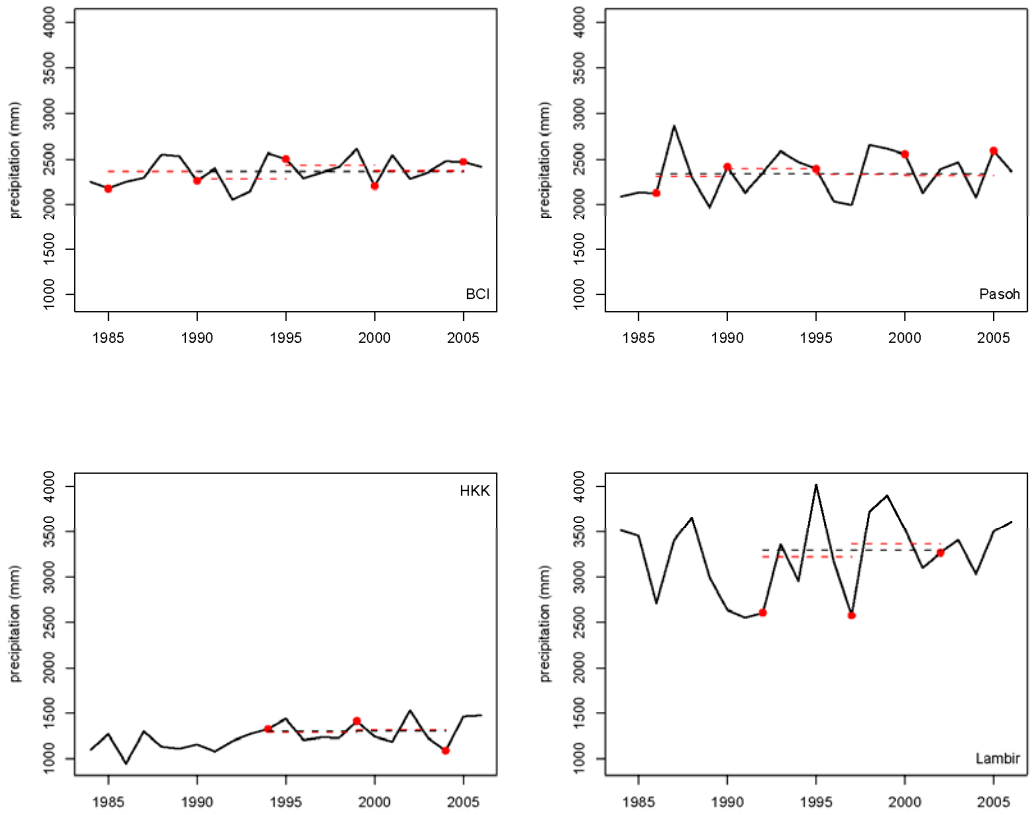

Figure 2.3 Changes in annual total precipitation (mm) at each site from 1984 to 2006. The annual values are calculated from July of one year to June of the next year. See Section 2.2.3 for details and data sources. The red dots indicate the time of each census taken place at each site. The red dashed lines are the mean over each census interval, while the black dashed lines are the mean over the entire study period. The differences between each red dashed line to the corresponding black line are the deviations used in the analysis (see Section 2.2.3).

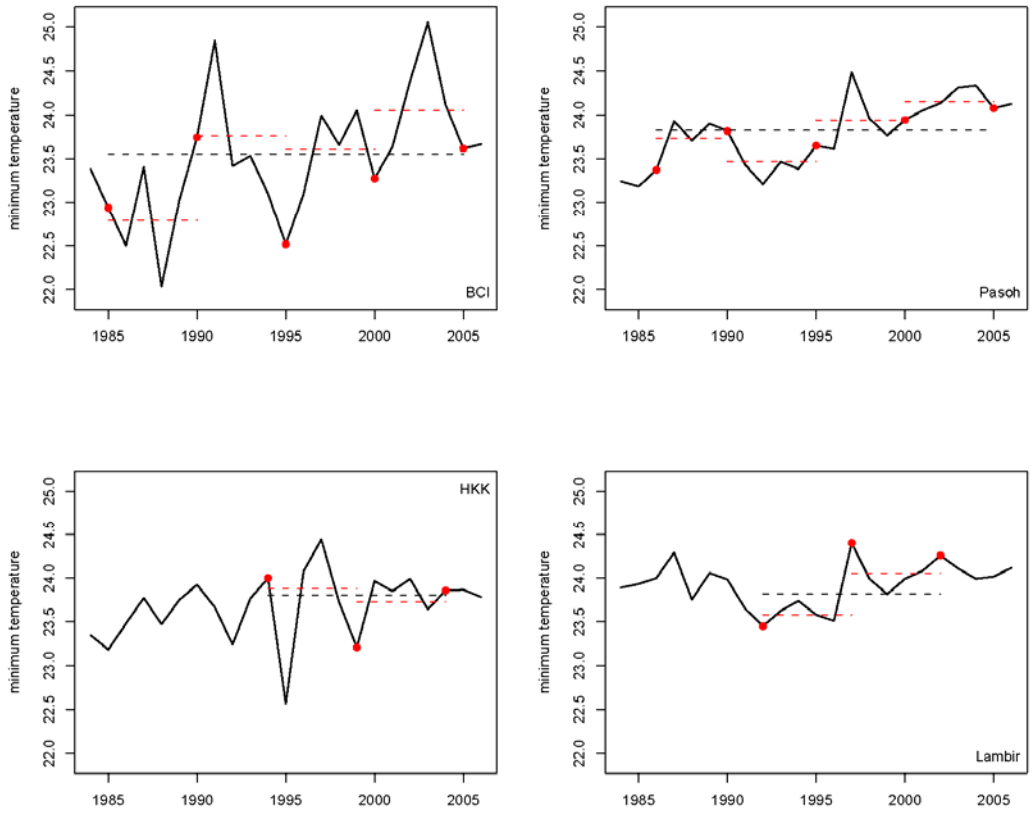

Figure 2.4 Changes in annual daily minimum temperature at each site from 1984 to 2006. The annual values are calculated from July of one year to June of the next year. See Section 2.2.3 for details and data sources. The red dots indicate the time of each census taken place at each site. The red dashed lines are the mean over each census interval, while the black dashed lines are the mean over the entire study period. The differences between each red dashed line to the corresponding black line are the deviations used in the analysis (see Section 2.2.3).

2.3 Results

Both absolute growth rates (in cm diameter) and relative growth rates were examined, and they displayed nearly identical trends of changes throughout the analyses, so only data and graphs using absolute growth rates are presented here. The deviations of inter-census growth rates from the mean for the entire study period were plotted against the climate deviations of the same time period. When the regression model was fitted, differences in variances and sample sizes of different sites and census intervals were taken into account.

The analysis showed that variations in stand-level growth rates (cm diameter per year) were positively correlated with incoming solar radiation (R^2=0.34, p=0.045, Figure 2.5). When only the three Asian sites (HKK, Pasoh, Lambir), where there had been greater directional changes in solar radiation, were examined the relationship was even more significant statistically (R^2=0.61, p=0.02). The magnitude of the effect was the greatest at Pasoh, where the absolute growth rate dropped by 0.007 cm/year per watt/m^2 decrease in incoming solar radiation over the census intervals. At HKK and Lambir, the $\Delta G/\Delta R$ ratio (unit change of growth rate per unit change of radiation) was 0.003 and 0.0008 (cm/year per watt/m^2), respectively.

Total annual precipitation was negatively correlated with solar radiation at all the three Asian sites, but not at BCI (Table 2.2). There was no negative relationship between stand-level tree growth rates and total precipitation either in all sites (R^2<0.01,

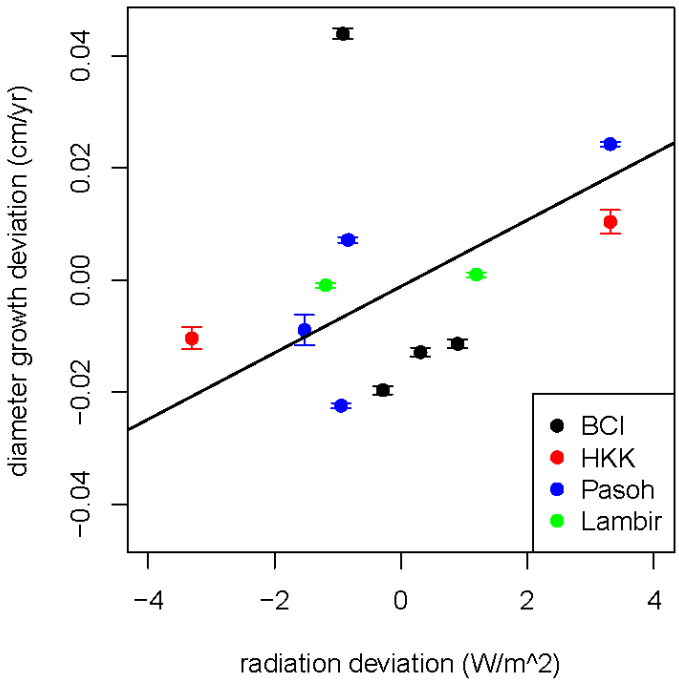

Figure 2.5 Stand-level mean diameter absolute growth (cm/yr) deviation and solar radiation (W/m^2) deviations at BCI (black), HKK (red), Pasoh (blue), and Lambir (green). The solid line with horizontal bars show the 95% confidence interval of the mean growth rates.

Table 2.2 Correlation coefficients (and 95% confidence intervals) between solar radiation and other climate variables at each site. The confidence intervals for bold values do not overlap zero.

Site	BCI	HKK	Lambir	Pasoh
Precip.	-0.35 (-0.66 to 0.06)	**-0.68 (-0.85 to -0.39)**	**-0.60 (-0.81 to -0.26)**	**-0.69 (-0.85 to -0.39)**
T_{min}	0.04 (-0.37 to 0.43)	0.16 (-0.26 to 0.53)	0.31 (-0.11 to 0.63)	0.01 (-0.39 to 0.41)
T_{max}	**0.48 (0.10 to 0.74)**	**0.51 (0.13 to 0.75)**	0.20 (-0.22 to 0.56)	0.02 (-0.39 to 0.42)
T_{mean}	0.34 (-0.07 to 0.66)	0.37 (-0.04 to 0.67)	0.29 (-0.12 to 0.62)	0.02 (-0.39 to 0.42)

p=0.96, Figure 2.6) or within the Asian sites (R^2<0.01, p=0.87). Therefore, the observed changes in tree growth rates are much more likely to be influenced by solar radiation (light) than by precipitation (water).

A negative relationship is found between stand-level tree growth rates and daily minimum temperature when all the sites are considered (R^2=0.34, p=0.05, Figure 2.7). However, the statistical significance is strongly affected by the single point of high growth rate at BCI during the period 1985-1990 (R^2=0.21, p=0.16 when this census

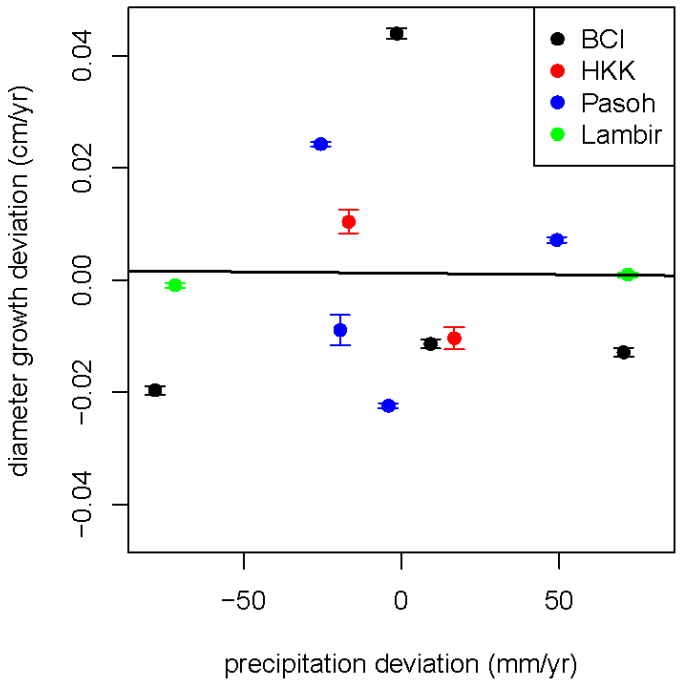

Figure 2.6 Stand-level mean diameter absolute growth (cm/yr) deviation and total precipitation (mm) deviations at BCI (black), HKK (red), Pasoh (blue), and Lambir (green). The solid line with horizontal bars show the 95% confidence interval of the mean growth rates.

interval is taken out). Growth rates are negatively correlated with daily minimum temperature at the two sites Pasoh and BCI; however, this relationship cannot be found at the other two sites (Lambir and HKK).

When the meteorological variables are inserted into a multiple regression model, the effects of incoming solar radiation and minimum temperature identified in the above univariate analyses increase in significance. The model shows that stand-level tree growth rates are positively correlated with solar radiation and negatively correlated with daily minimum temperature (R^2=0.88, p<0.001, Figure 2.8).

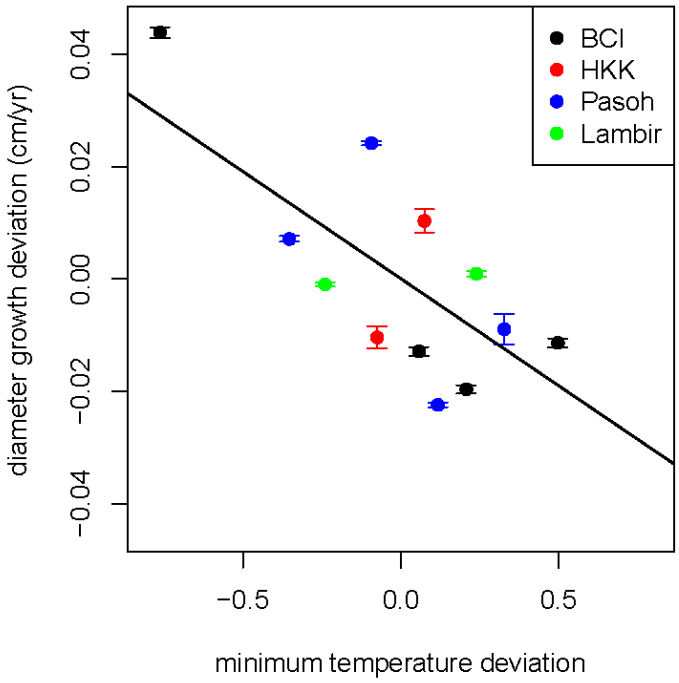

Figure 2.7 Stand-level mean diameter absolute growth (cm/yr) deviation and daily minimum temperature deviations at BCI (black), HKK (red), Pasoh (blue), and Lambir (green). The solid line with horizontal bars show the 95% confidence interval of the mean growth rates.

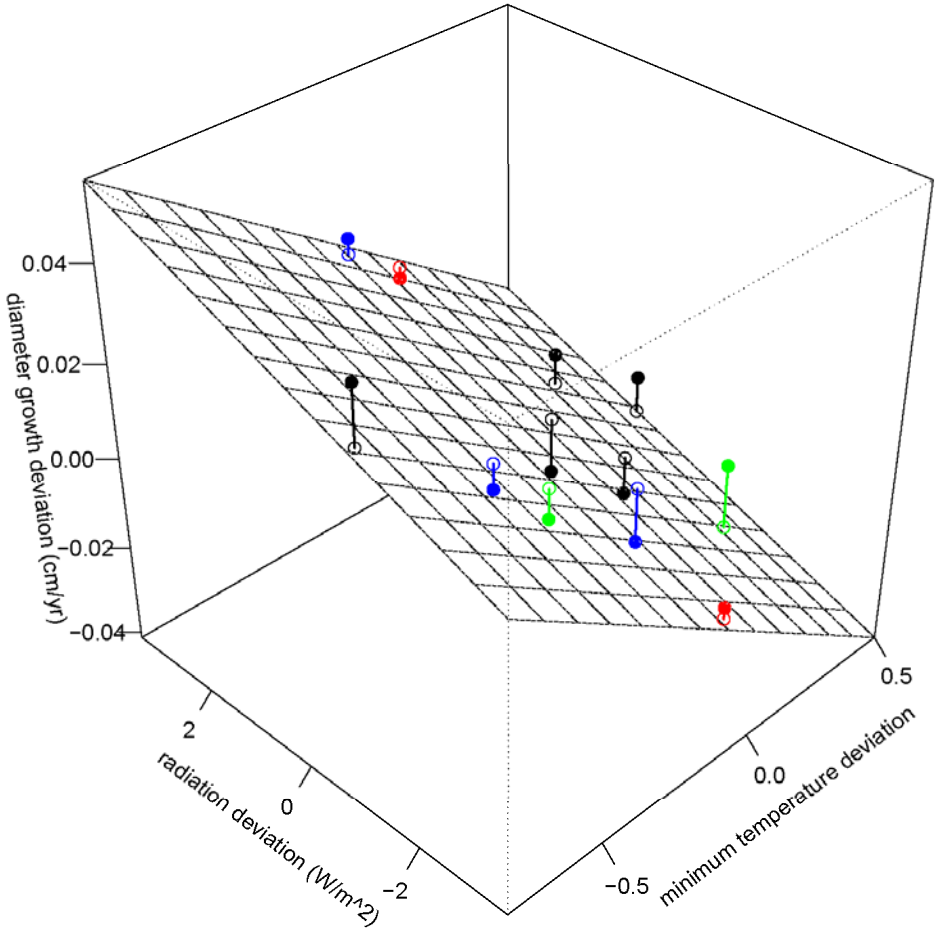

Figure 2.8 Stand-level mean diameter absolute growth deviation (cm/yr) in relation to solar radiation (W/m^2) and daily minimum temperature deviations at BCI (black), HKK (red), Pasoh (blue), and Lambir (green). The solid points are the observed data points, and the open points are their projections on the plane fitted in multiple linear regression.

Therefore, increases in tree growth rates are associated with increases in solar radiation and decreases in daily minimum temperature. In the cases where deviations in solar radiation cannot account for the observed changes in tree growth rates (e.g. BCI, especially between censuses 1985 and 1990), deviations in daily minimum temperature largely explain the residuals due to a negative relationship between growth and temperature. Similarly, the unexplained increase in tree growth rates at HKK as temperature increased (Figure 2.7) is explained by a concurrent increase in solar radiation between the two census intervals.

2.4 Discussion

This study showed positive relationships between ecosystem-level tropical tree growth rates and solar radiation (Figure 2.5) and a negative relationship between growth rates and daily minimum temperature (Figure 2.7). There was no correlation between growth rates and precipitation (Figure 2.6).

When examined as single factors, the positive impact of incoming solar radiation more strongly explains changes in observed tree growth rates than the negative impact of increasing temperature, especially when looking at the trends of changes at each individual site (Figures 2.5 and 2.7). While there is a significant negative relationship between growth rate and temperature, the relationship is weak when the extreme high value of growth between censuses 1985 and 1990 at BCI is taken out of the sample

(Figure 2.7). And trends in growth rate variations did not respond negatively to temperature variations at HKK and Lambir. Nevertheless, although temperature alone was insufficient to explain the observed different trends in growth rate variations at site level, a multiple linear regression parameterizing both incoming solar radiation and daily minimum temperature showed strong correlation with tree growth rates (Figure 2.8). It indicates that temperature also plays an important role in affecting tree growth rates and explains growth rate changes in areas that have not experienced much difference in average radiation. In particular, at BCI, where decreasing stand-level tree growth rates were observed when mean solar radiation did not vary much between the census intervals but mean daily minimum temperature had increased over time, the negative impact of rising temperature explains the growth decrease at this site.

The results of this study thus suggest a plausible explanation for the differing results obtained in earlier studies of the response of tropical forests to climate change. As noted in Section 2.1, Amazon forests have been observed to be experiencing accelerated dynamics over the past several decades, including significantly increased rates of tree growth and mortality, recruitment rates and above-ground biomass (Baker et al. 2004b; Lewis et al. 2004; Phillips et al. 2004). However, a separate study conducted at BCI, Panama did not show the same trends (Chave et al. 2003). Decreasing growth rates were also reported both at BCI and Pasoh (Malaysia) during a time period overlapping the above mentioned studies conducted in Amazon (Feeley et

al. 2007), and a similar deceleration was also observed in Costa Rican tropical forests (Clark et al. 2003).

Whereas the above studies focused on changing temperature and atmospheric CO_2 concentrations as explanatory factors for observed trends in tropical forest dynamics, the results of this analysis indicate that solar radiation variability is also an important aspect of environmental forcing affecting the dynamics of tropical tree growth. Tree growth rates at HKK, Pasoh, and Lambir all responded positively to increased solar radiation (Figure 2.5). However, in contrast to the more spatially uniform trends in atmospheric CO_2 and temperature, each site experienced different trends and magnitudes of changes in solar radiation forcing over the past few decades, giving rise to spatially-variable trends in patterns of tree growth rates. The previously noted study by Nemani et al. 2003 has shown large scale patterns in observed changes in solar radiation forcing were different between regions (Nemani et al. 2003, Figure 1D). Note that specifically, the tropical regions where plant growth is more limited by light availability (Nemani et al. 2003, Figure 1A) have experienced differing trends in solar radiation variation. This pattern, together with the results of this study, suggests that solar radiation variability provides consistent explanation for the conflicting results of earlier studies.

To better understand the observed trends in stand-level mean growth rates, I examined the histograms of the growth deviations of individual trees at each site for all census intervals. The changes in distribution of individual growth deviation illustrate how the trends in mean stand-level growth rates arise from the responses of

individual trees (Figures 2.9-2.12). For example, at HKK (Figure 2.11), the distribution was right-skewed (i.e. more individuals with increased growth rates, skewness = 2.91) over the period 1994-1999, while the later census interval 1999-2004 had a left-skewed (skewness = -2.91) distribution of relative growth deviation (i.e. more individuals with decreased growth rates). The two distributions are significantly different from each other as shown by Kolmogorov-Smirnov test ($D = 0.4251$, $p < 0.001$). Thus the increased stand-level mean growth rate did not result from the exceptional performance of just a few individuals or species, but rather from a systematic shift.

Two of the four plots in this study (HKK and BCI) are seasonal forests with significant dry seasons (Table 2.1) and are partially deciduous in the canopy. The dynamics of tree growth will be different in the dry season, when diameter growth will slow or stop. Assuming that most of the annual net growth observed is gained during the wet season, I also looked at the correlation between growth variation and changes in mean wet season monthly precipitation (calculated for months with >100 mm rainfall). However, I still didn't find any significant positive relationship (R^2=0.29, p=0.27 for HKK and BCI; R^2=0.15, p=0.22 for all sites).

Although extreme high values of growth rate are most likely due to measurement error (see Section 2.2), stand-level mean growth rates can still sometimes be greatly influenced by a few fast-growing individuals and species. The topographical location of trees may also affect their growth rates, for example, in seasonal forests; trees in swales grow faster than those on the ridges because soil water availability is sustained

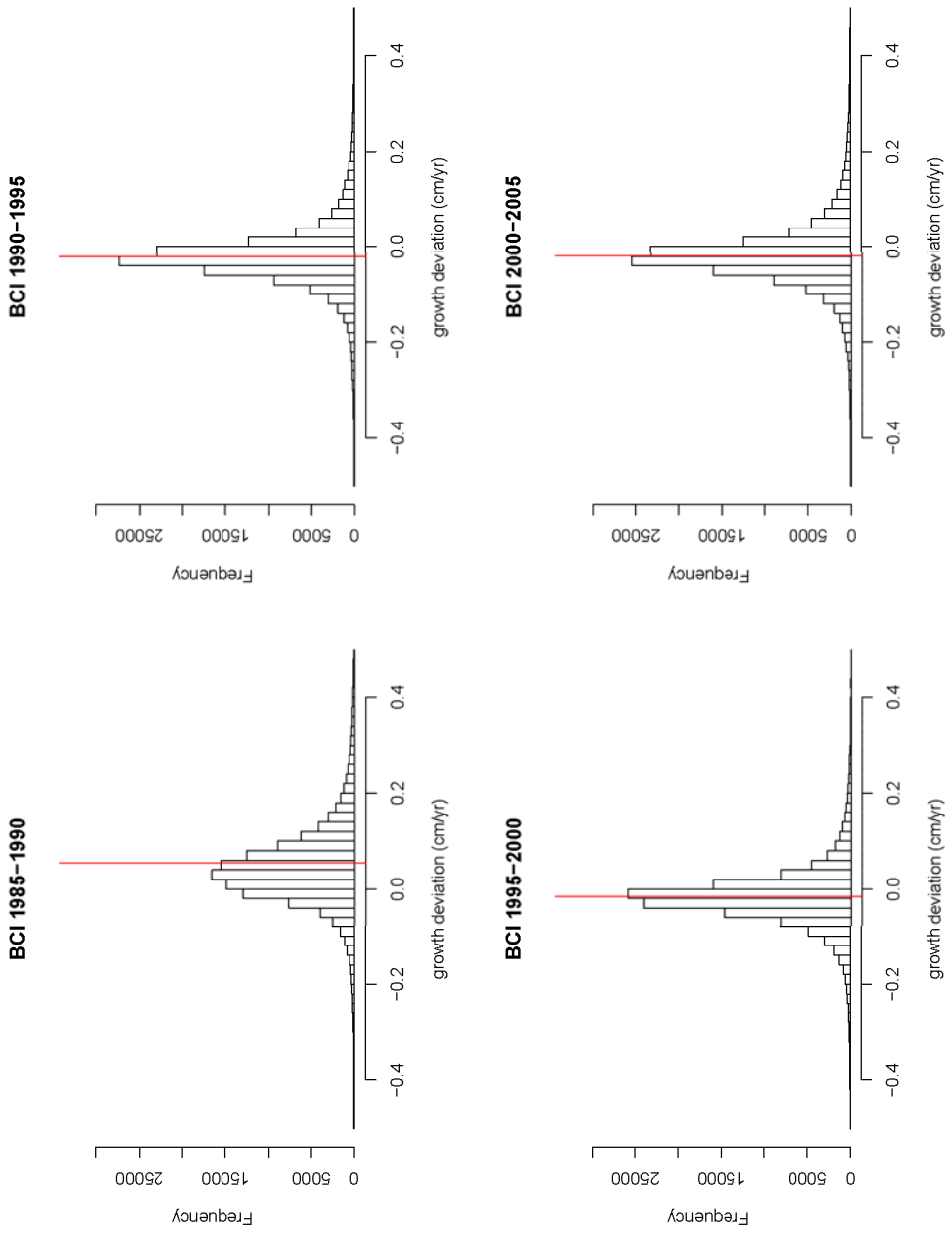

Figure 2.9 Histogram of individual absolute growth (cm/yr) deviation for each census interval at BCI. The vertical red line indicates the stand-level mean growth deviation.

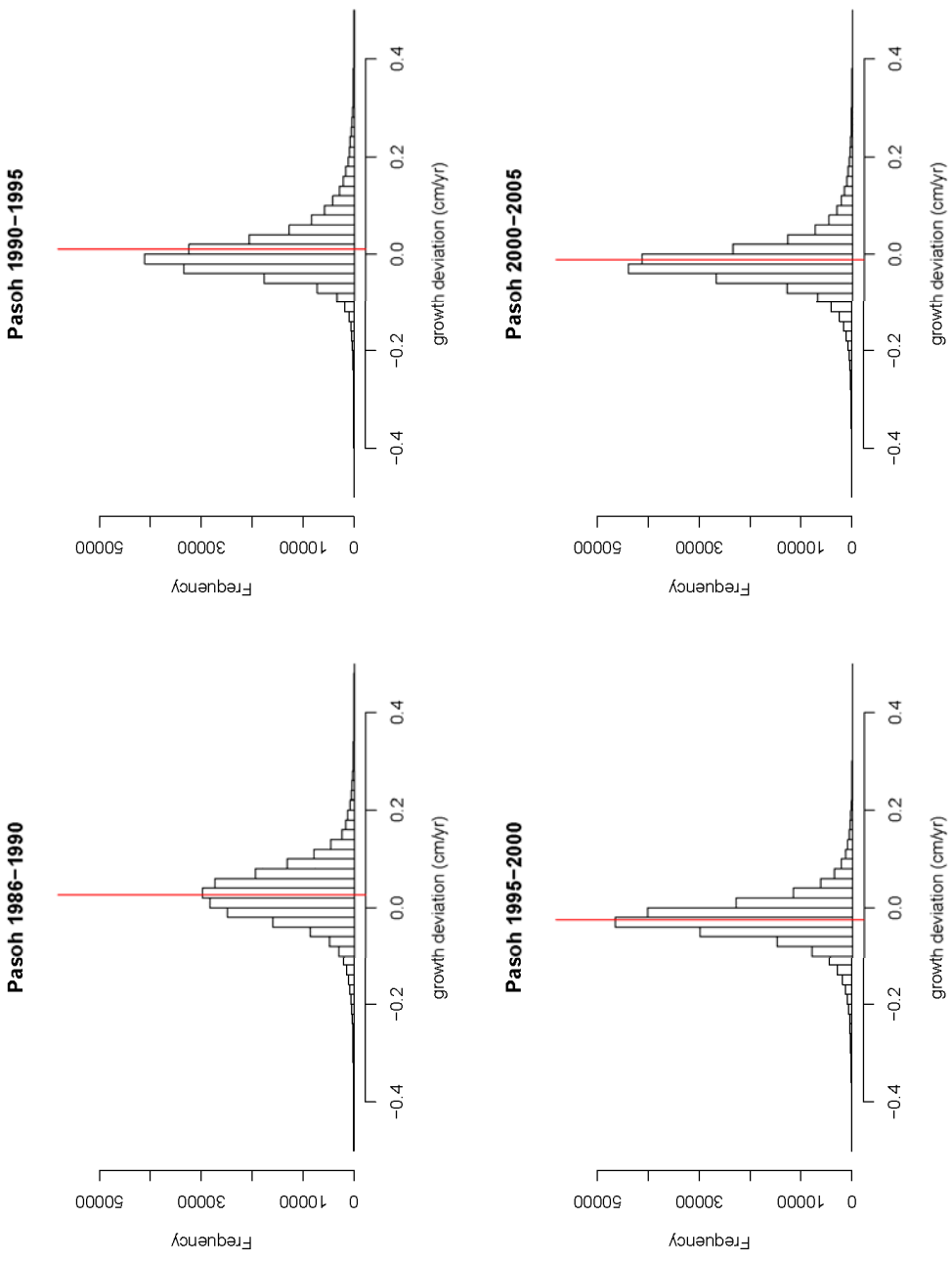

Figure 2.10 Histogram of individual absolute growth (cm/yr) deviation for each census interval at Pasoh. The vertical red line indicates the stand-level mean growth deviation.

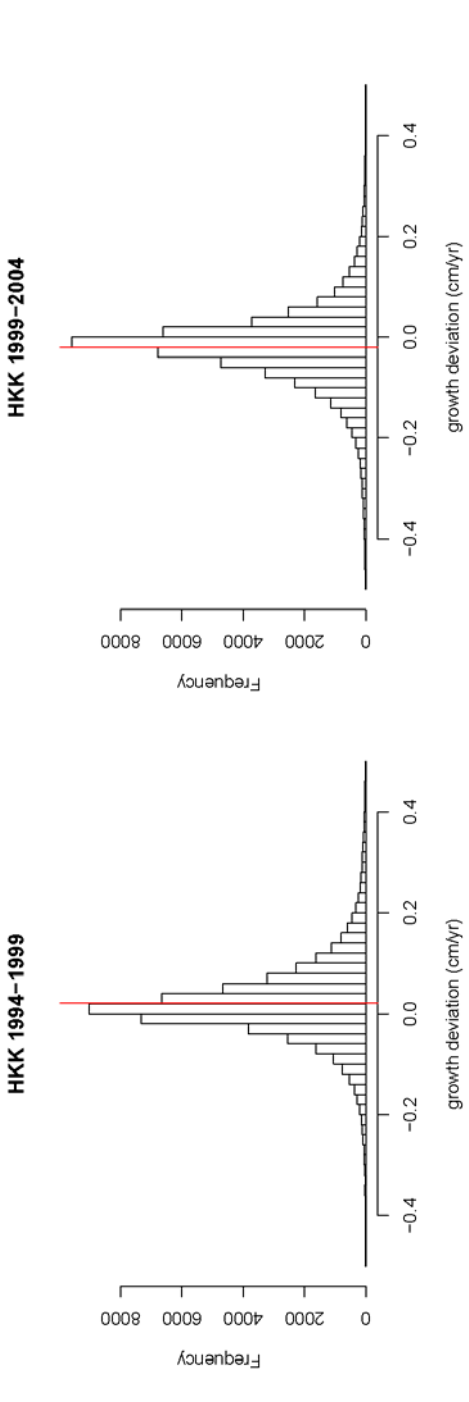

Figure 2.11 Histogram of individual absolute growth (cm/yr) deviation for each census interval at HKK. The vertical red line indicates the stand-level mean growth deviation.

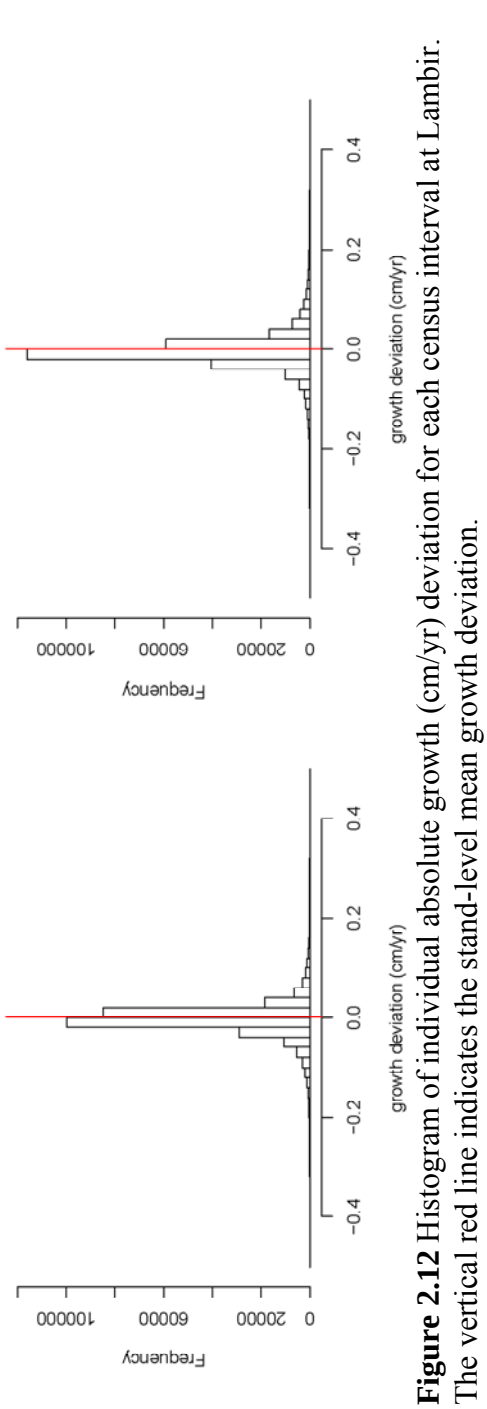

Figure 2.12 Histogram of individual absolute growth (cm/yr) deviation for each census interval at Lambir. The vertical red line indicates the stand-level mean growth deviation.

for a longer time during the dry season.

The magnitudes of the variation in growth rates documented in this study here appear to be relatively modest: the largest detected variation in mean diameter growth rate, found at the BCI plot, was only 0.06 cm/yr (Figure 2.1). However, it is important to realize that this variation in growth rate was associated with only 1.81 watt/m^2 variation in level of solar radiation forcing between census periods, - equivalent to only 0.86% of the average annual solar radiation. However, as Figures 2.2-2.4 illustrates, the 5-year census intervals average over substantial amounts of inter-annual variability in climate forcing. The yearly average radiation deviations at BCI range from -9.04 watt/m^2 in 1992 to +10.06 watt/m^2 in 1997, while the five-year-census-interval average radiation deviations only range between -0.92 watt/m^2 and +0.90 watt/m^2; and mean absolute deviation of yearly average radiation is 3.06 watt/m^2, versus 0.60 watt/m^2 for census intervals. The same pattern is also observed at all the other sites, where both the range of radiation variations and their mean absolute deviation from the average are substantially larger from year to year than between census intervals (Pasoh: -10.40 ~ +10.80 watt/m^2 versus -1.53 ~ +3.31 watt/m^2 and 4.39 watt/m^2 versus 1.65 watt/m^2; HKK: -11.06 ~ +7.49 watt/m^2 versus -3.30 ~ +3.30 watt/m^2 and 4.91 watt/m^2 versus 3.30 watt/m^2; Lambir: -6.63 ~ +12.21 watt/m^2 versus -1.19 ~ +1.19 watt/m^2 and 4.03 watt/m^2 versus 1.19 watt/m^2). Comparing to a timescale of 5 years solar radiation variability between census periods, all sites have shown more than 3-fold increases in the variability of solar radiation forcing from year to year.

It is therefore likely that the 5-year average growth rates measured by the current censuses mask substantial shorter-term variation in tree growth rates in response to inter-annual climate variability within census interval periods. Given the responses to small changes in 5-year average climate conditions detected in this study, I anticipate that inter- and intra- annual growth rates will vary substantially in response to the higher order of magnitude variability in environmental factors that occurs at annual to sub-annual timescales.

The dendrometer study provides a great opportunity to quantify inter- and intra-annual variation in forest dynamics. These measurements will enable examination of the relationship between tree growth rates and environmental variability at these shorter time scales. Having more frequent measurements of tree growth will also pave the way for conducting rigorous independent tests about how changes in temperature, precipitation, and/or solar radiation affect tree demographic rates in different tropical forest formations. The recent addition of short-term observation of tree growth to the long-term census records at the participating CTFS plots thus promises to greatly improve our current understanding of responses of tropical forest dynamics in relation to climate change. These short-term measurements will be particularly powerful when combined with the less-frequent, longer term census information used in this study, because it will facilitate understanding of how effects of short-term climate variability on tree growth and mortality rates translate into effects on longer timescales. In the following chapter, I will present results from the dendrometer measurement data collected in four Southeast Asian forests over the past three years.

Chapter 3

Dendrometer band measurements of tropical tree growth rates along a latitudinal gradient

The growth rates used in the analyses in Chapter 2 were measured in *c.* 5-year intervals, and thus would inevitably mask shorter-term variation in tropical trees' growth response to inter-and intra-annual climate variability within those census interval periods. Here, I present results from a newly initiated and on-going study in which dendrometer bands are used to measure inter- and intra-annual variations in tree growth rates at four tropical forest plots along a latitudinal gradient in Southeast Asia. These results reveal new information about relationships between tree growth and climate variability that were not evident in the analyses using the 5-year census data.

3.1 Introduction

When tree growth rates at four long-term permanent tropical forest research plots were examined in Chapter 2 in relation to variation in climate variability, most of the observed changes in tree growth rates over time could be explained by the combined effects of two of the climate variables: incoming solar radiation and night-time temperature (Figure 2.8). However, when taken alone, neither solar radiation nor the night-time temperature explained the changes in growth rates at all sites (Figures 2.5 and 2.7; Section 2.3). Precipitation showed no direct influence on tree growth (Figure 2.6). The weakness of the relationships is likely due to the infrequency of measurements. All of the four forest plots studied in Chapter 2 are measurement approximately only every 5 years. A 5-year interval is too long to capture the impact of climate variability, which changes much more in magnitude on finer time scale than its long-term mean. It is therefore likely that the 5-year average growth rates measured by the current censuses mask substantial shorter-term variation in tree growth rates in response to inter-annual climate variability within census interval periods. Annual growth rates may have varied substantially in response to greater variability in environmental factors that occurs at annual to sub-annual timescales (Figures 2.2-2.4). Those variations were not captured in the measurements due to the coarse time resolution.

In order to capture the inter- and intra-annual variations in forest dynamics, and further examine the relationship between tree growth rates and environmental

variability at these shorter time scales, in 2007, I initiated an extensive study to measure short-term rates of tree growth using dendrometer bands at four sites in the CTFS plot network. Metal dendrometers have been used successfully to monitor diameter growth in temperate forests for several decades (Keeland and Sharitz, 1993) and have been recently applied to measure tree growth rates in tropical and subtropical forests (Pelissier and Pascal 2000; Da Silva et al. 2002; Rice et al. 2004; O'Brien et al. 2008; Yan et al. 2006). This study is the first of its kind within the CTFS plot network. All of the four sites (Pasoh in Malaysia, Khao Chong and Huai Kha Khaeng in Thailand, and Xishuangbanna in China) are in the Southeast Asia region and the forests are all dominated by the same family, Dipterocarpaceae. Situated along a latitudinal gradient 5 to 8 degrees apart from one another, these study sites differ in temperature, seasonality, topography as well as other environmental factors. The intrinsic similarity and extrinsic difference make these forests perfect subjects to study and compare the impact of changes in environmental forcing. Here, I present results from the dendrometer measurements over the first three years of the study.

3.2 Methods

3.2.1 Site selection and sampling design

The four study sites are chosen from the Center for Tropical Forest Science (CTFS)

network of large-scale forest dynamics plots: Pasoh Forest Reserve in Malaysia, Khao Chong Peninsular Botanical Garden and Huai Kha Khaeng Wildlife Sanctuary in Thailand, and Xishuangbanna Tropical Botanical Garden in China (hereafter Pasoh, Khao Chong or KC, Huai Kha Khaeng or HKK, and Xishuangbanna or XSBN). The four sites are all situated in Mainland Southeast Asia, 5 to 8 degrees in latitude apart from one another on the Indochina and Malay peninsular (Figure 3.1). Along the latitudinal gradient, the length of the dry season increase from 1 month at Pasoh, the southernmost plot, to 6-8 months at Xishangbanna, the northernmost plot (Table 3.1).

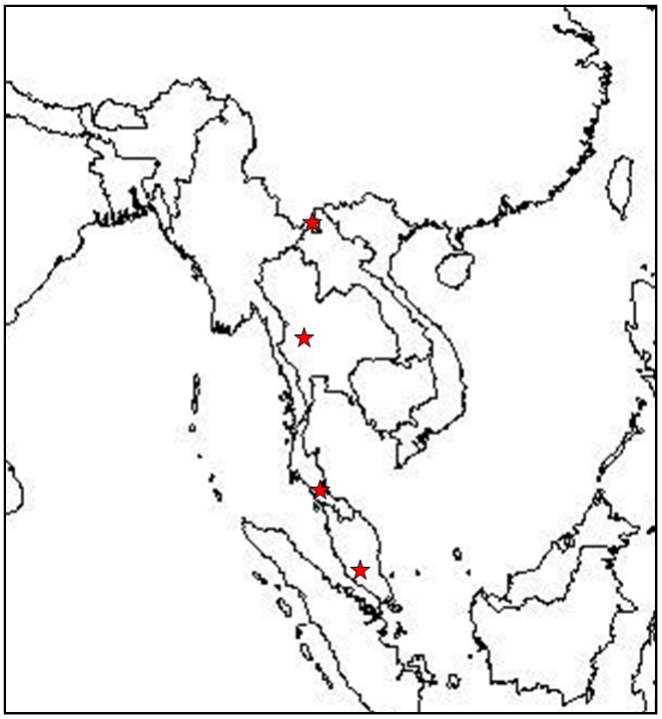

Figure 3.1 Location of the study sites (red stars). From south to north: Pasoh, Malaysia; Khao Chong, Thailand; Huai Kha Khaeng, Thailand; and Xishuangbanna, China. Latitudinal and longitudinal coordinates of each site are listed in Table 3.1.

Table 3.1 Summary of the study sites.

Site	Pasoh	Khao Chong	Huai Kha Khaeng	Xishuangbanna
Latitude	2.982	7.54347	15.6324	21.6117
Longitude	102.313	99.798	99.217	101.574
Elevation (m)	66-90	116-348	549-638	709-869
Plot size (ha)	50	24	50	20
Dimensions (m)	1000 x 500	600 x 400	1000 x 500	500 x 400
Dry season (month)	1	2-3	6	6-8
Total number of trees	335,400	121,500	72,500	95,834
Total number of species	814	593	251	468
Number of sampled trees	2,639	2,310	2,397	2,413
Number of sampled species	455	305	168	249

Despite their differences in climatic and topographic conditions, all of the four forest plots are dipterocarp forests and share common families and genera. Some species are present at two or more sites (e.g. *Cynometra malaccensis* is found at both Pasoh and KC; *Duabanga grandiflora* is found at KC, HKK, and XSBN).

All canopy trees larger than 80 cm in diameter at breast height (DBH) were included in the sample and banded throughout all four plots. The rest of the trees were sampled using 100 size-stratified nested plots that were randomly placed within the area of each study plot. Each set of subplots consists of:

(1) a 40m x 40m subplot in which all trees larger than 40 cm DBH are included;

(2) a 20m x 20m subplot (centered within the 40m x 40m subplot) in which all trees larger than 20 cm DBH are included;

(3) a 10m x 10m subplot (centered within the 20m x 20m subplot) in which all trees larger than 10 cm DBH are included;

(4) a 5m x 5m subplot (centered within the 10m x 10m subplot) in which all trees larger than 5 cm DBH are included.

Figure 3.2 illustrates the placement of the subplots and the locations of the subplots at HKK. An identical sample design was used at all the other sites.

The size-stratified nested subplot sample includes all qualified stems present in the plot, regardless of tree species. A separate species sample was added in order to include enough trees from five important groups of trees in each forest: fast-growing

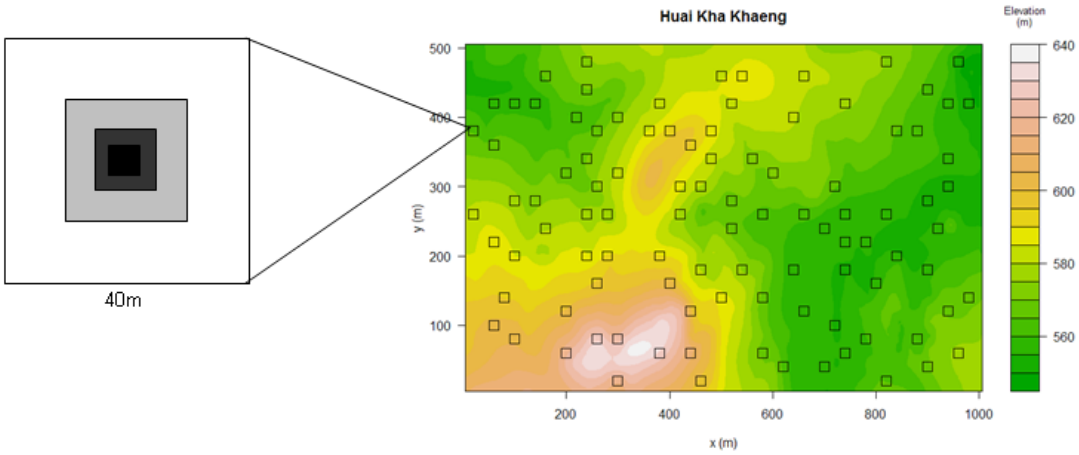

Figure 3.2 Locations of the nested subplots for size-stratified sampling at HKK. The squares on the map show the locations of the 100 sets of subplots chosen randomly over the entire plot area, overlaid on the topography of the 50-hectare plot. The magnified square on the left illustrates the nested arrangement of the subplots: trees larger than 40 cm DBH were sampled in the white area (40mx40m); trees > 20 cm and ≤ 40 cm DBH were measured in the light grey area (20mx20m); trees > 10 cm and ≤ 20 cm DBH were measured in the dark grey area (10mx10m); and trees > 5cm and ≤ 10 cm DBH were measured in the black area (5mx5m).

emergent trees, slow-growing emergent trees, Legumes (slow-medium growing canopy trees), Burseraceae (animal dispersed, slow-growing canopy trees), and pioneer species. Table 3.2 lists the species from each group chosen at the four sites. In addition to the trees chosen in the nested subplot sample, a further 60 stems (or all of the remaining stems, whichever is greater) of each species from the sampled groups were included in the study. These extra samples were similarly size-stratified, chosen randomly over the entire plot area regardless of the placement of the nested plots. The samples were chosen before the field deployment of dendrometer bands using the most recent 5-year plot census data, and the final sample size varied among the plots (Table 3.1). On average, I installed approximately 2,400 dendrometer bands at each of the four sites; and the random and species samples included over 50% of the species present in each plot.

3.2.2 Dendrometer band measurements

Stainless steel dendrometer bands were installed on every sampled tree stem at the four sites following a standardized protocol (Muller-Landau and Dong 2008), except for the trees that: (1) were already dead at the time of installation; (2) had buttresses that extended to a height too hard to reach by the available ladders (~ 8m); (3) had thorns or spines that completely covered the tree trunk; (4) were situated at an unsafe location (e.g. steep slope, or close-by bee hive). When the dendrometer bands were re-

Table 3.2 Species sample of the five important groups.

Group	Site	Species
Fast-growing emergents	Pasoh	*Shorea leprosula, Shorea parvifolia*
	Khao Chong	*Dipterocarpus grandiflorus*
	Huai Kha Khaeng	*Hopea odorata*
	Xishuangbanna	*Parashorea chinensis*
Slow-growing emergents	Pasoh	*Shorea maxwelliana, Neobalanocarpus heimii*
	Khao Chong	*Shorea gratissima*
	Huai Kha Khaeng	*Saccopetalum lineatum*
	Xishuangbanna	*Pometia tomentosa*
Legumes	Pasoh	*Cynometra malaccensis, Millettia atropurpurea*
	Khao Chong	*Cynometra malaccensis, Millettia atropurpurea*
	Huai Kha Khaeng	*Pterocarpus grandiflorum, Afzelia xylocarpa*
Burseraceae	Pasoh	*Dacryodes rostrata, Santiria laevigata*
	Khao Chong	*Dacryodes rostrata*
	Huai Kha Khaeng	*Garuga pinnata*
	Xishuangbanna	*Garuga pinnata*
Pioneers	Pasoh	*Dyera costulata, Macaranga hypoleuca, Macaranga conifera, Melicope glabra*
	Khao Chong	*Alstonia scholaris, Macaranga gigantea, Duabanga grandiflora*
	Huai Kha Khaeng	*Macaranga siamensis, Tetrameles nudiflora, Duabanga grandiflora*
	Xishuangbanna	*Castanopsis hystrix, Castanopsis indica, Duabanga grandiflora, Macaranga indica, Mallotus garrettii*

measured, the condition of the bands was examined first. Damaged or twisted bands, as well as the bands on trees that had out-grown the measurement range, were replaced with new ones. Moderately disturbed bands (e.g. bands that had been moved slightly off their original position or whose ends had flipped out) were adjusted to their normal condition. The data were discarded from the corresponding growth interval calculated in the analysis, but all measurements were still recorded for those new and adjusted dendrometer bands.

Digital calipers were used to record the window size on the dendrometer for each measurement. A detailed description and illustration of the dendrometer design and measurement guidelines can be found in the protocol by Muller-Landau and Dong (2008). The changes in window size, i.e. changes in tree circumference, between measurement intervals, are calculated and translated into changes in diameter. They were then divided by the lengths of the intervals, and used in the analysis as annualized diameter growth (mm/yr). Consistent with earlier analyses (see Chapter 2), trees that grew at a rate greater than 7.5 mm/yr in diameter were considered outliers due to measurement errors and were excluded from the analysis. Negative growth rates were expected because of the impacts of humidity and water availability on trunks resulted from differences in seasonality. However, shrinkages more than 1 mm/yr were considered unlikely, and thus considered measurement errors and excluded from the analysis. There are less than 0.5% of such outliers in each measurement intervals across all plots.

The dendrometer bands were installed at Pasoh starting from November 2007, and

at Huai Kha Khaeng and Khao Chong from December 2007. They were re-measured about every six months except for the first measurement interval, which was two months longer to allow the bands enough time to settle and tighten on the tree trunk. For logistical reasons, the installation started later at the new plot Xishuangbanna, in January 2009. The first re-measurement at Xishuangbanna was conducted in August 2009 and since then the dendrometers are re-measured every three months.

3.2.3 Auxiliary information

In addition to the dendrometer measurements, the following information was also collected in the study:

Climatological data

In this study, I examined changes in tree growth rates over different measurement intervals in relation to precipitation, minimum temperature, and solar radiation. I compiled the climatological data from several different sources:

(1) For Pasoh, daily measurements are available from a meteorological station set up on a tower above the canopy adjacent to the plot. Monthly averages are computed and used in this study.

(2) For Xishuangbanna, monthly measurements are available from Xishuangbanna Tropical Botanical Garden. The unit of solar radiation has been converted from

MJ/m^2 to W/m^2 in this study.

(3) For Khao Chong and Huai Kha Khaeng, no on-site climate data is available for the period of this study (the new meteorological stations were not set up until the summer of 2009). Monthly climate data from the NOAA/NCEP Climate Prediction Center are used in this study (see details in Chapter 2). The ISCCP dataset used in Chapter 2 for solar radiation is not up-to-date (currently available data cover through 2008), so only precipitation and temperature are studied in this analysis.

Diameter measurements

At the time of dendrometer band installation, the diameter of the tree trunk was measured at two positions: (1) the paint-marked DBH measurement position used in the 5-year plot censuses, usually at 1.3m high from the ground (Condit 1998); and (2) the position at which the dendrometer band was installed, usually 10cm above the paint mark. The second diameter measurement was taken before the installation of the band and is used as initial size in this analysis.

Crown Illumination Index (CII)

The Crown Illumination Index (CII) scores the source and relative amount of crown lighting on a five-point scale (Dawkins and Field 1978). The different values are defined as follows (see Figure 3.3 for an illustrated example):

5 = crown completely exposed (to vertical light and to lateral light within the 90

degree inverted cone encompassing the crown).

4 = full overhead light (≥90% of the vertical projection of the crown exposed to vertical light; later light blocked within some or all of the 90 degree inverted cone encompassing the crown).

3 = some overhead light (10-90% of the vertical project of the crown exposed to vertical light).

2 = lateral light (<10% of ther vertical project of the crown exposed to vertical light; crown lit laterally).

1 = no direct light (crown not lit directly either vertically or laterally).

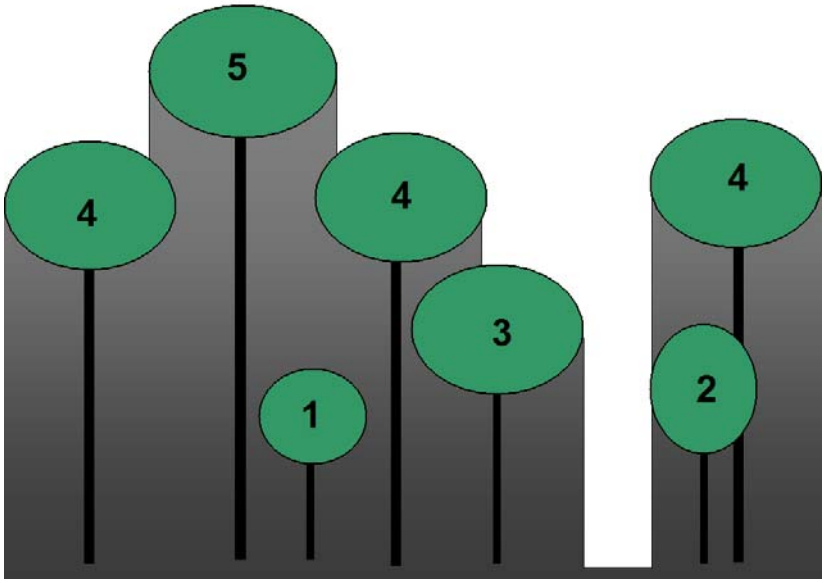

Figure 3.3 Examples of trees having different values of the crown illumination index.

Wood density

Wood density data for Pasoh, Khao Chong, and Huai Kha Khaeng were compiled from several data sources: the Wood Density Database from the World Agroforestry Centre (http://www.worldagroforestrycentre.org/sea/Products/AFDbases/WD/index.htm), Prospect: the Wood Database from the World Conservation Monitoring Centre, Version 2.1 (http://www.plants.ox.ac.uk/ofi/prospect/), and two independent studies (King et al. 2005; Suzuki 1999). The units of the raw data differ among the various sources and thus were all converted to g/cm^3 in this analysis. I have not found information for every species included in my study sample. But wood density was found to be strongly conserved within genera (Chave et al. 2006), and in the absence of even genus-level information, it is common practice to use a family-level wood density mean (e.g. Baker et al. 2004a). Therefore, wood density values are assigned to each species using the following procedure.

(1) If the wood density data is available for a species from one data source, then that value is used for that species.

(2) If multiple values are available for a species from several data sources, then the average of those values is used for that species.

(3) If no data is available for a species, but there are data for other species within the same genus, then the genus-level mean is used for that species.

(4) If no data is available for a genus, but there are data for other genera within the same family, then the family-level mean is used for that genus.

(5) If no data is available for a family, then the plot-level mean is used for that

family.

Topography

The gridded elevation data for the Xishuangbanna plot are not currently available and there is relatively little variation in topography at Pasoh. Therefore, the impact of topography on growth rates was examined for Khao Chong and Huai Kha Khaeng. Slope steepness (degree) was calculated for each quadrate (20m x 20m) from elevation measured on a 5m x 5m grid using the function "meantopo.quad" in the CTFS package for R (version 1.00, http://hosho.ees.hokudai.ac.jp/~kubo/Rdoc/library/CTFS/html/meantopo.quad.html).

3.3 Results

3.3.1 Tree growth rates and climate variability

Figure 3.4 shows the climate variability over the measurement period at each site. Monthly values are averaged over each measurement interval (red dashed lines). Consistent with previous analyses in Chapter 2, when data from all of the four sites are pooled together, deviations of the climate variables from their long-term mean at each site are computed for each measurement interval. The magnitude of climate variability

varies among the sites, and generally increases along the seasonality gradient from Pasoh (the southernmost, least seasonal site) to Xishuangbanna (the northernmost, most seasonal site, Figure 3.4).

The trends of changes in annualized mean diameter absolute growth are consistent with the trends of changes in relative growth rates; and both forms of growth rates are calculated for every measurement interval at each site (Figure 3.5). Deviations of tree growth rates are compared against deviations in climate variables by using linear regression models weighted by the variances of different measurement intervals at each site (Table 3.3). Only results for absolute growth rates are presented and discussed in this section, but all tests have been performed on both absolute and relative growth rates. The test results for relative growth rates can be found in Appendix A (Tables A.2 and A.3).

The analysis shows that variations in mean growth rates are positively correlated with both monthly precipitation (R^2=0.49, $p<0.001$, Figure 3.6a), and daily minimum temperature (R^2=0.32, p=0.009, Figure 3.6b) when all the four sites are pooled together. The northernmost site Xishuangbanna experienced the greatest variation in all aspects of the climate (Figure 3.4). Furthermore, all of the three climate variables are positively correlated with one another (see Table A.1 in Appendix A). For this reason, separate tests are conducted for the other three sites (Pasoh, KC, and HKK) to confirm the aforementioned relationships between tree growth rates and climate variability without the strong influence of the variation seen at Xishuangbanna. Both slopes of the growth-precipitation and growth-temperature correlations are steeper

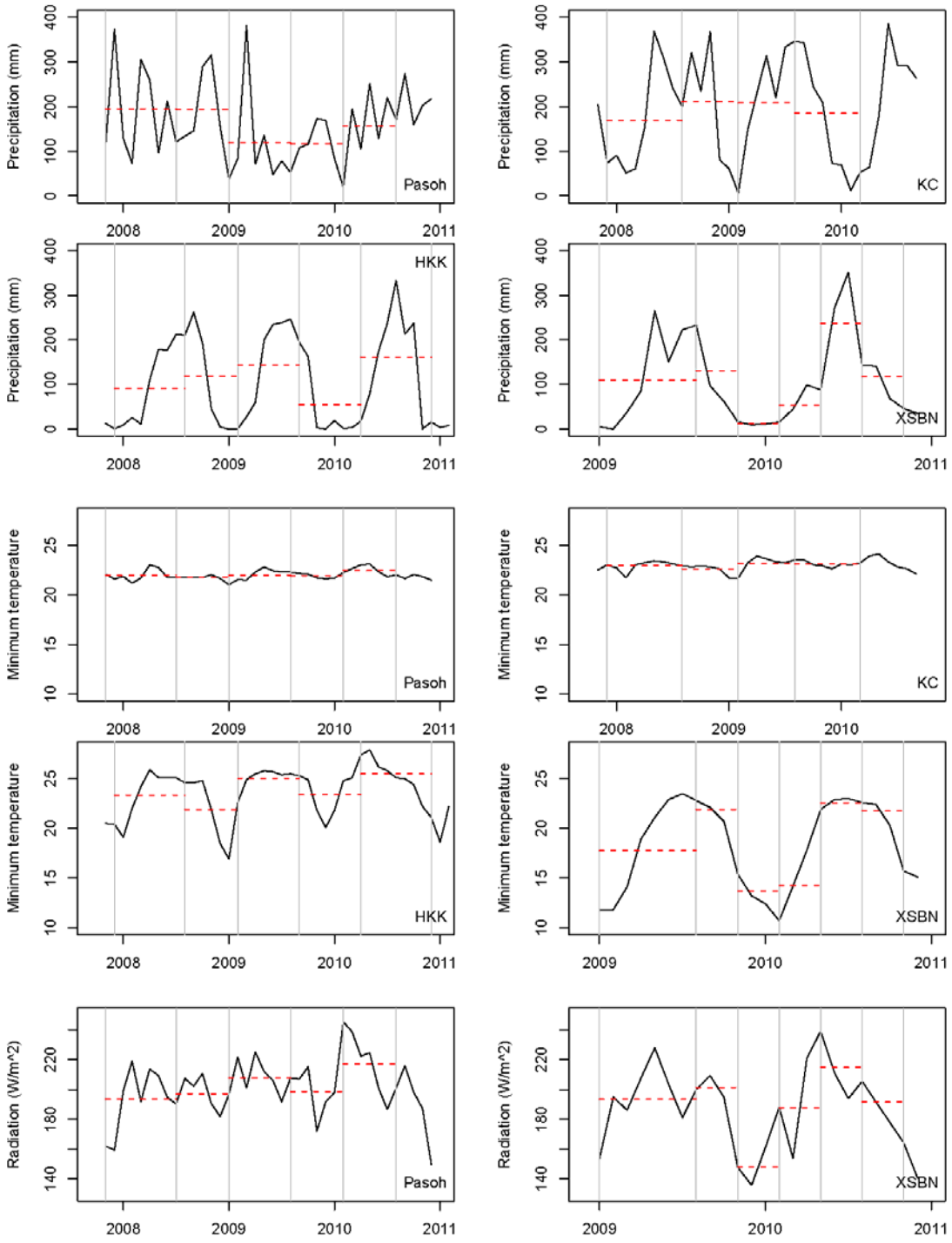

Figure 3.4 Climate variability over the measurement period at each site. The grey vertical lines separate each measurement interval. The red dashed horizontal lines show the average values over each measurement interval.

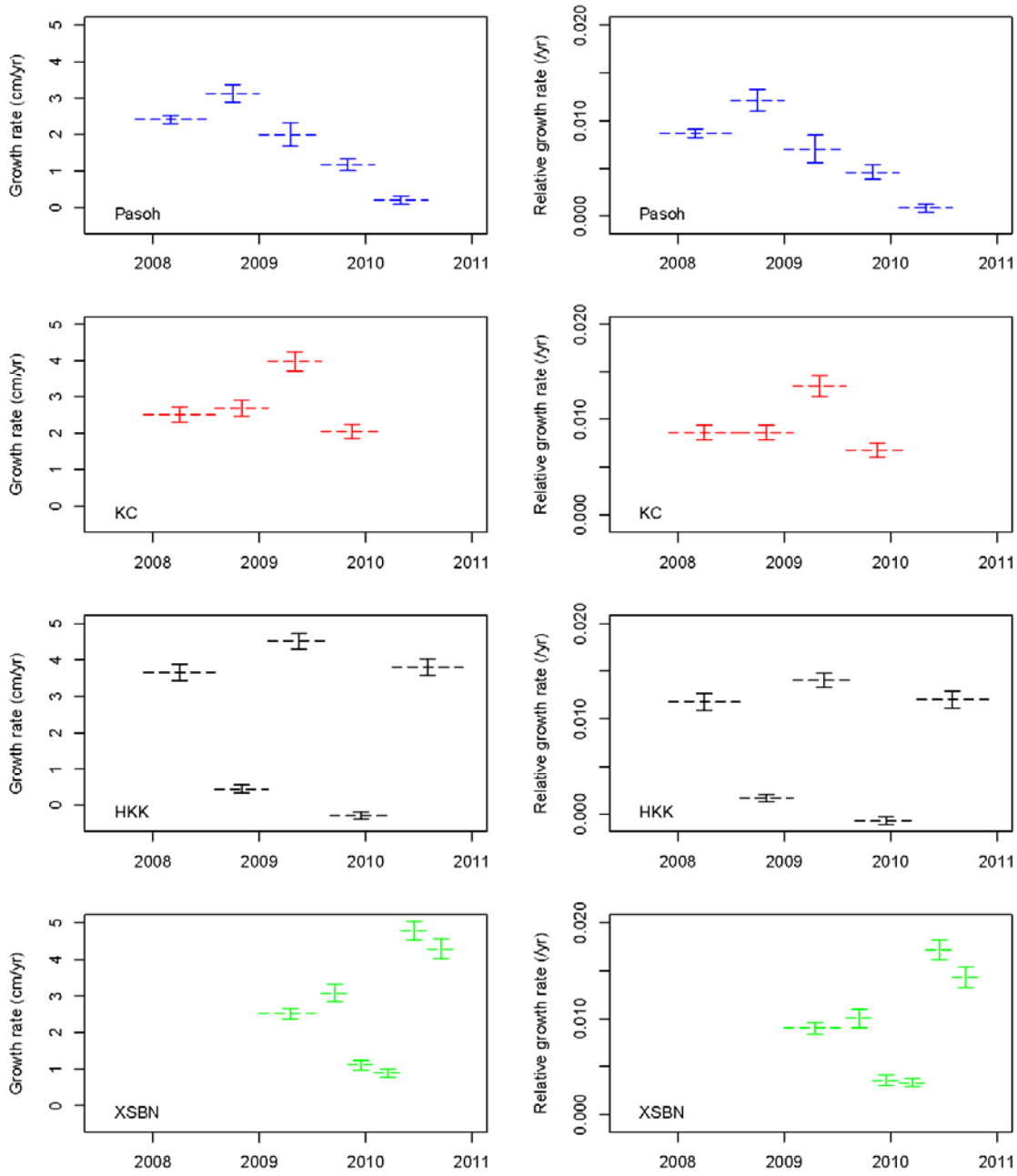

Figure 3.5 Mean diameter absolute growth (mm/yr) and relative growth (/yr) rates over time at each site. Each dashed horizontal line represents the mean growth rate over that measurement interval. The solid vertical lines with horizontal bars show the 95% confidence interval of the mean growth rates.

(a)

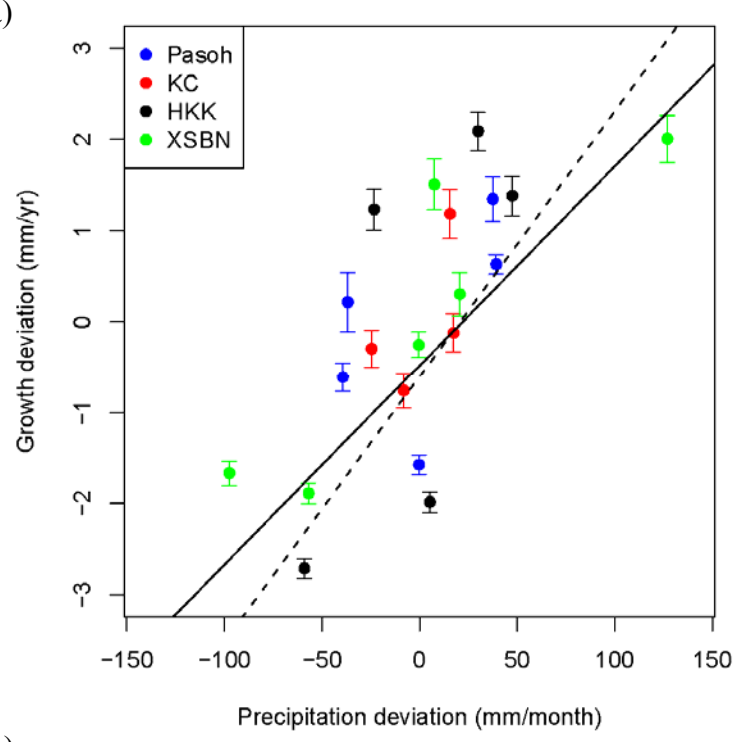

(b)

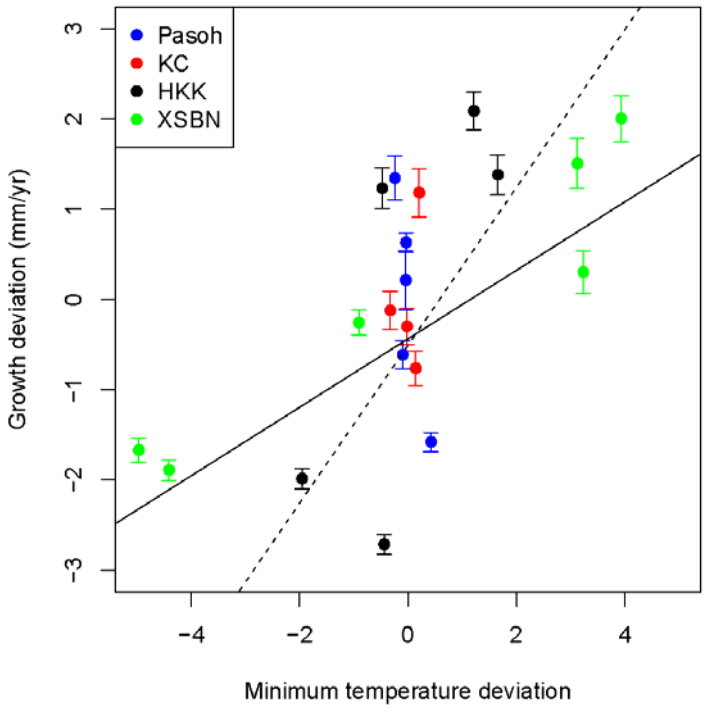

Figure 3.6 (Continues on the next page)

Figure 3.6 (Continued)

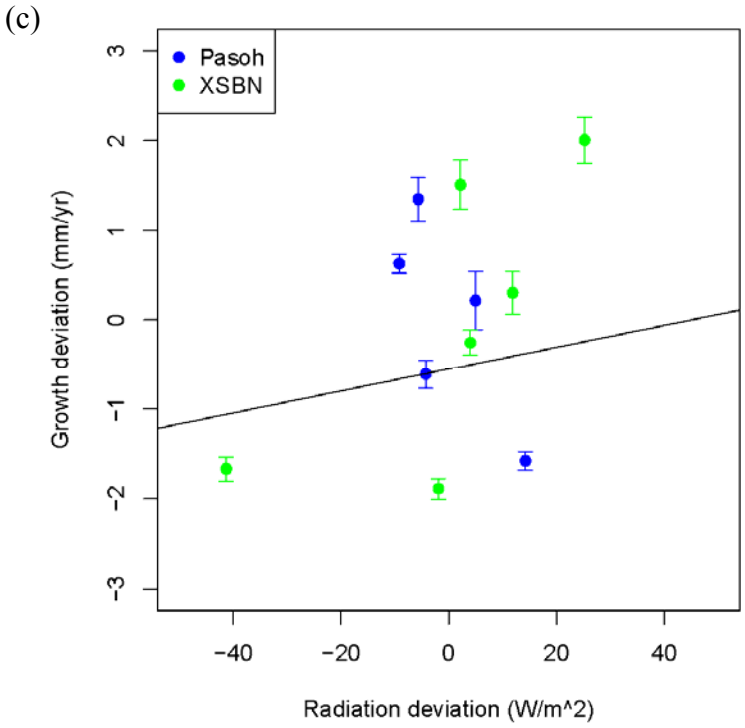

Figure 3.6 Mean diameter absolute growth (mm/yr) deviation in relation to climate variability. (a) Absolute growth deviation and monthly total precipitation deviation (mm) at Pasoh, KC, HKK, and XSBN. (b) Absolute growth deviation and monthly mean daily minimum temperature deviation at Pasoh, KC, HKK, and XSBN. (c) Absolute growth deviation and monthly mean solar radiation (W/m^2) deviation at Pasoh and XSBN. The vertical lines with horizontal bars show the 95% confidence interval of the mean growth rates. The solid black lines show the linear regression across all sites; and the dashed black lines in (a) and (b) show the linear regression across the three southern sites (excluding XSBN).

Table 3.3 Results of linear regression models of absolute growth rates against climate variables (P: precipitation; T: temperature; R: radiation). *: p≤0.05; (*): 0.05<p≤0.10.

Sites	Y	Slope	d.f.	R^2	p-value
All	P	0.022	18	0.49	<0.001*
All	T	0.38	18	0.32	0.009*
HKK, KC, Pasoh	P	0.0092	12	0.46	0.008*
HKK, KC, Pasoh	T	0.42	12	0.27	0.06(*)
Pasoh, XSBN	P	0.018	9	0.62	0.004*
Pasoh, XSBN	T	0.32	9	0.47	0.02*
Pasoh, XSBN	R	0.012	9	0.03	0.61
HKK	P	0.033	3	0.48	0.20
HKK	T	1.0	3	0.44	0.22
KC	P	0.020	2	0.29	0.46
KC	T	0.34	2	0.012	0.89
Pasoh	P	0.022	3	0.37	0.27
Pasoh	T	-3.8	3	0.77	0.05*
Pasoh	R	-0.091	3	0.81	0.03*
XSBN	P	0.019	4	0.81	0.02*
XSBN	T	0.37	4	0.92	0.002*
XSBN	R	0.037	4	0.37	0.20

when the XSBN data points are taken out (dashed lines in Figures 3.6a and 3.6b), but slightly weaker in statistical significance (Table 3.3).

There was no significant relationship between tree growth rates and incoming solar radiation (R^2=0.03, p=0.61, Figure 3.6c). The analysis of radiation effects was conducted at only Pasoh and XSBN, since solar radiation data are unavailable for the other two sites.

Table 3.4 Results of multiple linear regression models of absolute growth rates against climate variables (P: precipitation; T: temperature; R: radiation). *: $p \leq 0.05$; (*): $0.05 < p \leq 0.10$.

Sites	Y_1	Slope	p-value	Y_2	Slope	p-value	d.f.	R^2	p-value
All	P	0.019	0.02*	T	0.089	0.60	17	0.50	0.003*
HKK, KC, Pasoh	P	0.025	0.01*	T	0.65	0.08(*)	11	0.60	0.007*
Pasoh, XSBN	P	0.016	0.11	T	0.047	0.80	8	0.62	0.02*
Pasoh, XSBN	R	-0.038	0.11	T	0.49	0.007*	8	0.63	0.02*
Pasoh, XSBN	R	-0.034	0.06(*)	P	0.025	0.001*	8	0.77	0.003*
HKK	P	0.028	0.24	T	0.82	0.26	2	0.76	0.24
KC	P	0.024	0.57	T	1.08	0.75	1	0.39	0.78
Pasoh	P	0.016	0.06(*)	T	-3.39	0.02*	2	0.97	0.03*
Pasoh	R	-0.06	0.50	T	-1.25	0.63	2	0.83	0.17
Pasoh	R	-0.079	0.10(*)	P	0.01	0.42	2	0.88	0.12
XSBN	P	0.0033	0.70	T	0.32	0.11	3	0.93	0.02*
XSBN	R	-0.0086	0.54	T	0.41	0.01*	3	0.91	0.02*
XSBN	R	-0.032	0.24	P	0.029	0.03*	3	0.89	0.04*

Multiple linear regressions are used to examine the combined effect of climate variables on tree growth rates. The results of these bivariate analyses did not show any significant improvements over the univariate models (Table 3.4).

When each study site was examined separately, the slopes of growth-precipitation relationships were still uniformly positive (Figure 3.7); however, the correlation was significant only at XSBN (Table 3.3). The growth-temperature relationships at the sites varied along the latitudinal gradient from south to north, from being significantly negative at Pasoh, to being flat at KC, positive at HKK, and significantly positive at XSBN (Figure 3.8, Table 3.3). Different responses are also seen in solar radiation and

reveal the same trends as temperature at the two sites where data are available (Figure 3.9, Table 3.3). But the correlations seem to be driven by the same data points as those that determine the growth-temperature correlations, due to the positive relationship between radiation and temperature at these two sites (see Table A.1 in Appendix A). This strong correlation in radiation and temperature prevented the possibility of revealing the independent effects of radiation and temperature on tree growth rates.

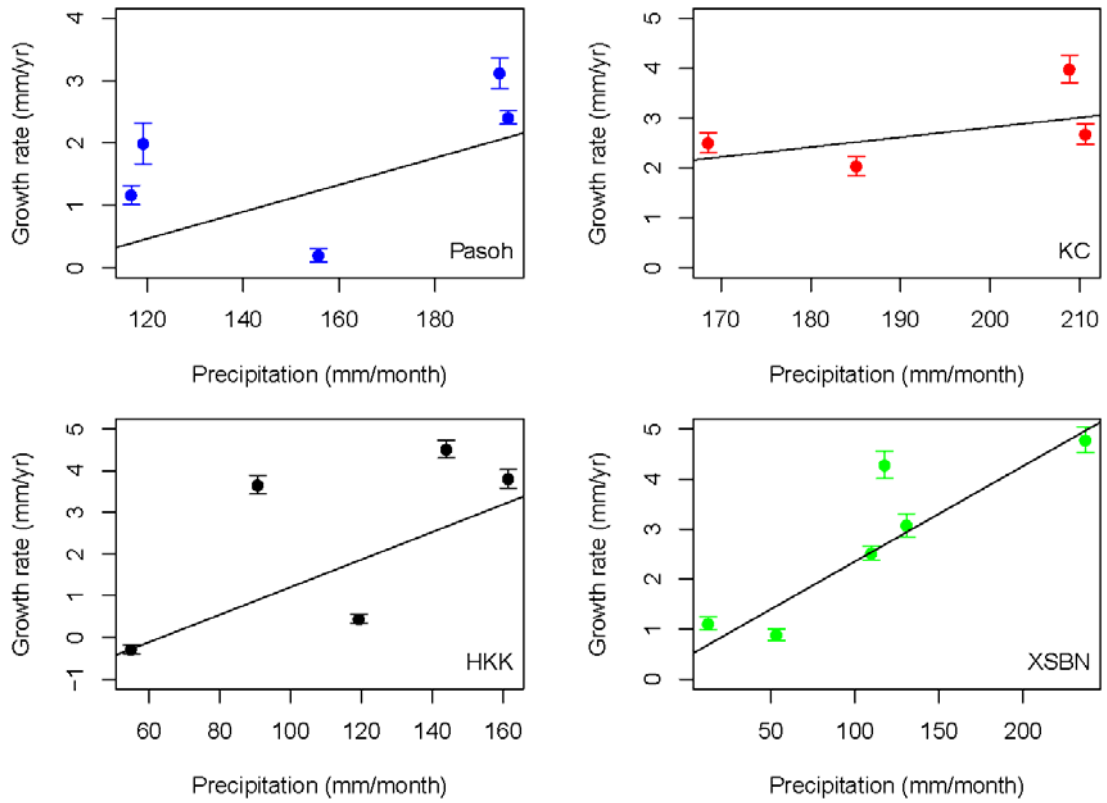

Figure 3.7 Mean diameter absolute growth (mm/yr) and precipitation (mm/month) at each site. The vertical lines with horizontal bars show the 95% confidence interval of the mean growth rates.

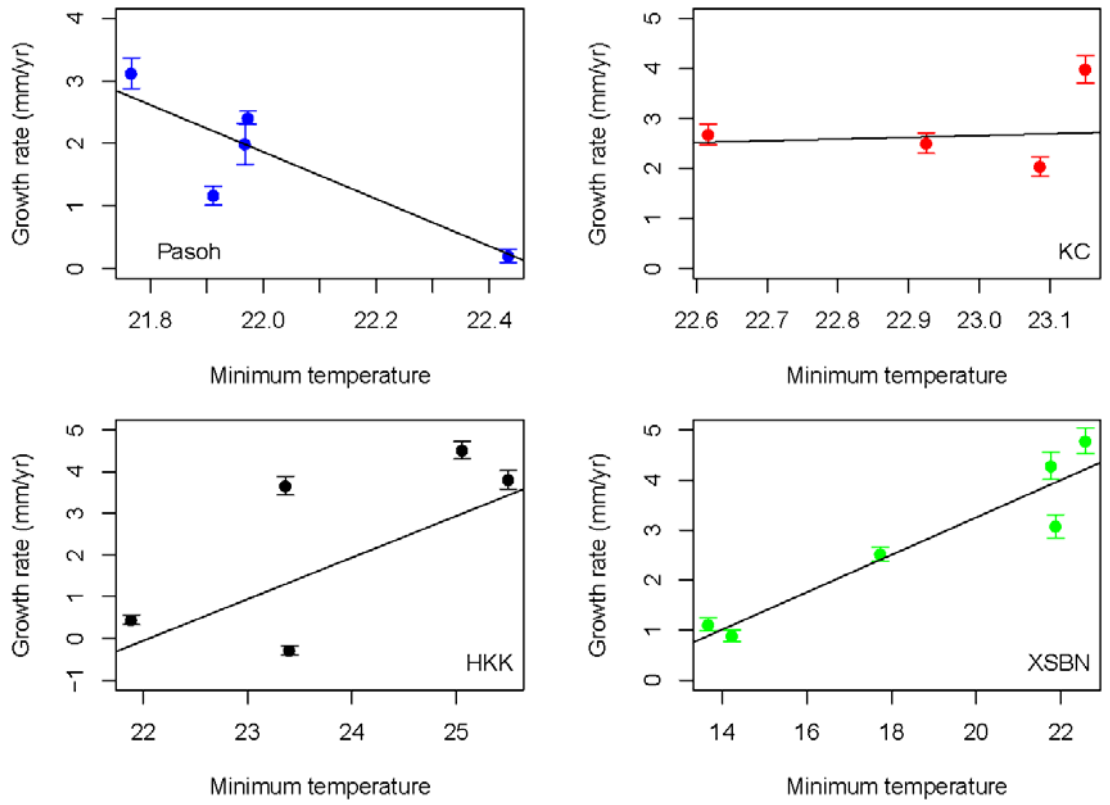

Figure 3.8 Mean diameter absolute growth (mm/yr) and minimum temperature at each site. The vertical lines with horizontal bars show the 95% confidence interval of the mean growth rates.

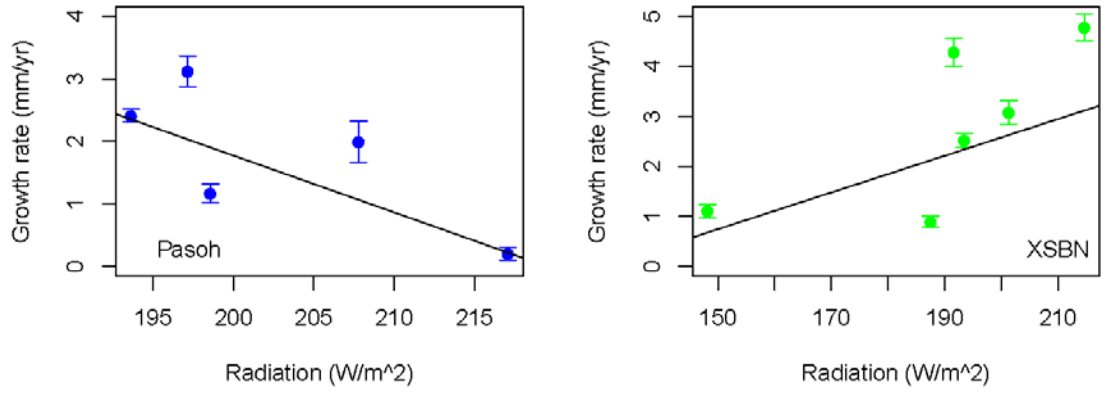

Figure 3.9 Mean diameter absolute growth (mm/yr) and solar radiation (W/m^2) at each site. The vertical lines with horizontal bars show the 95% confidence interval of the mean growth rates.

3.3.2 Tree growth rates and light availability

Both absolute and relative growth rates were examined, and they showed very different patterns in relation to light availability [as measured by the crown illumination index (CII), see Section 3.2.3]. Absolute growth rates generally increased with CII across all study sites, expect for the two dry season measurement intervals at HKK (Figure 3.10; Table 3.5). However, this trend was not found in relative growth rates, which did not change or sometimes even decreased with increases in light availability (Figure 3.11; Table 3.6).

Further analyses using multiple linear regression models which added tree size (stem diameter) and the interaction between tree size and CII as covariates revealed that the discrepancies in tree growth responses to light availability found in the simple linear regression models were due to the influence of tree size as a covariate on relative growth rates (Tables 3.7 and 3.8). While there were strong positive correlations between CII and tree diameter ($p<<0.001$ for all of the four sites) as expected, there were generally no significant impacts of tree size in the multiple linear regression models using absolute growth rates (Table 3.7). Therefore, the observed trends in changes of absolute growth rates were indeed correlated more with light availability than with size. That is, for example, when the coefficients of the model were positive, the trees grew faster because they received more light rather than because they were originally bigger. When relative growth rates were used in the multiple linear regression models, the coefficients of tree size were significantly

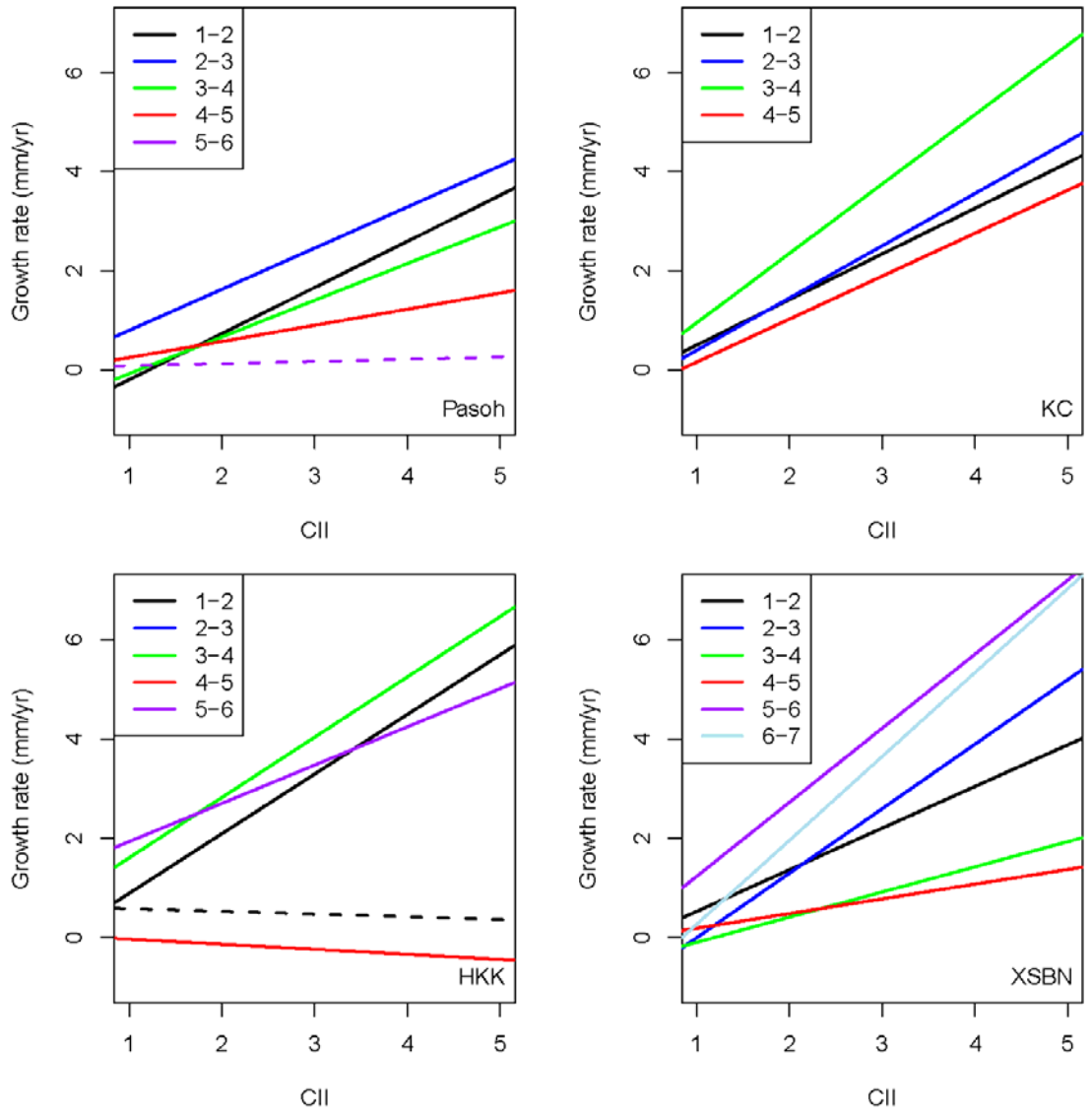

Figure 3.10 Results of linear regression models of absolute growth rates against crown illumination index (CII) for each measurement interval at each site. The solid lines show the fitted models that are statistically significant ($p<0.05$). The dashed lines show the fitted models that are not statistically significant ($p>0.05$). See the full list of test results in Table 3.5.

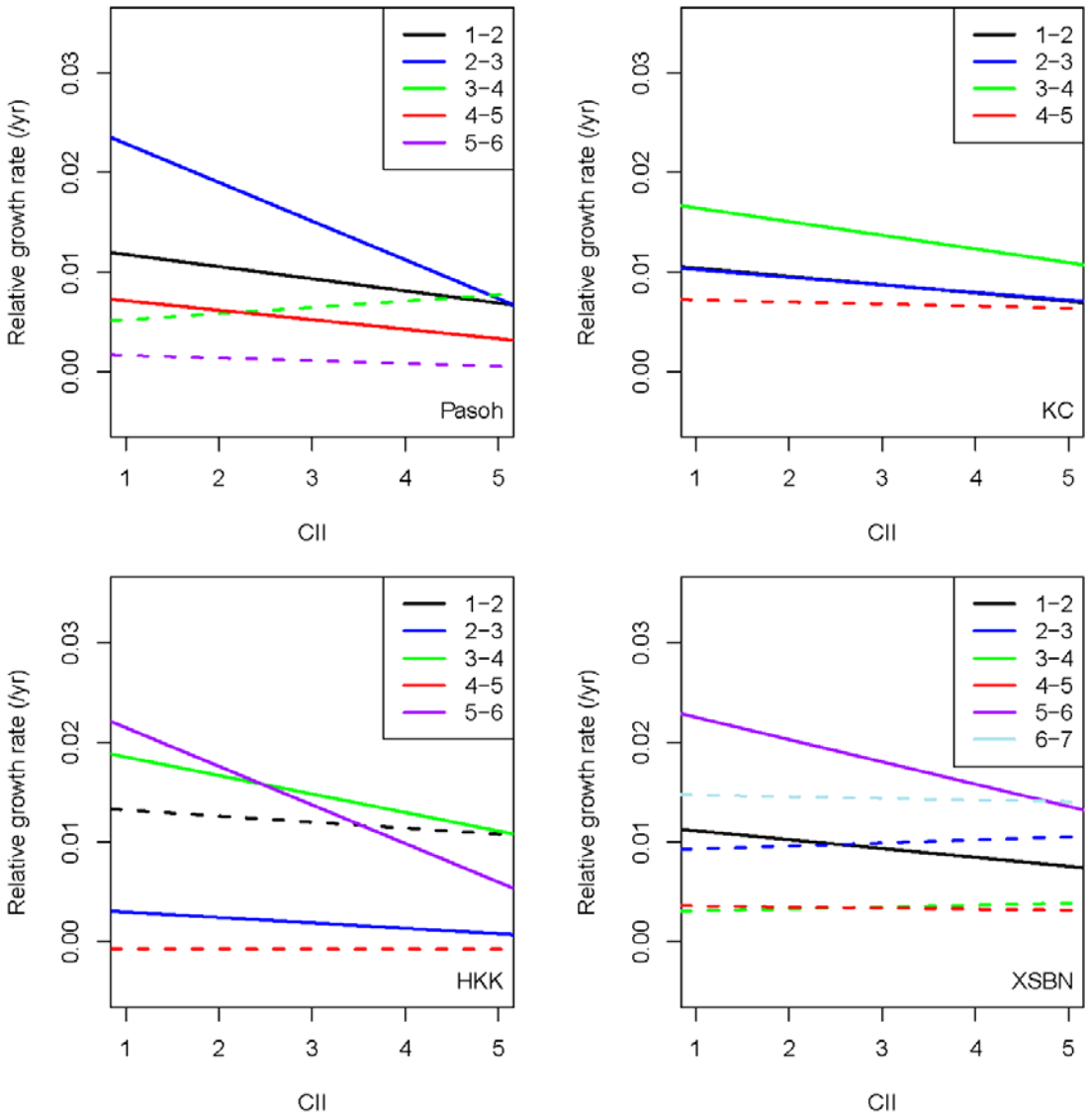

Figure 3.11 Results of linear regression models of relative growth rates against crown illumination index (CII) for each measurement interval at each site. The solid lines show the fitted models that are statistically significant ($p<0.05$). The dashed lines show the fitted models that are not statistically significant ($p>0.05$). See the full list of test results in Table 3.6.

Table 3.5 Results of linear regression models of absolute growth rates against crown illumination index (CII). *: p≤0.05; (*): 0.05<p≤0.10.

Site	Interval	Slope	d.f.	R^2	p-value
Pasoh	1-2	0.93	2365	0.14	<0.001*
Pasoh	2-3	0.83	1726	0.03	<0.001*
Pasoh	3-4	0.74	1523	0.015	<0.001*
Pasoh	4-5	0.33	1958	0.01	<0.001*
Pasoh	5-6	0.044	1894	0.0004	0.39
KC	1-2	0.92	1849	0.06	<0.001*
KC	2-3	1.05	1864	0.07	<0.001*
KC	3-4	1.4	1839	0.08	<0.001*
KC	4-5	0.87	2083	0.05	<0.001*
HKK	1-2	1.2	1433	0.10	<0.001*
HKK	2-3	-0.055	2133	0.0005	0.28
HKK	3-4	1.2	2115	0.08	<0.001*
HKK	4-5	-0.10	2228	0.002	0.04*
HKK	5-6	0.77	2269	0.03	<0.001*
XSBN	1-2	0.84	2393	0.09	<0.001*
XSBN	2-3	1.3	2357	0.08	<0.001*
XSBN	3-4	0.51	2362	0.04	<0.001*
XSBN	4-5	0.30	2337	0.02	<0.001*
XSBN	5-6	1.49	2327	0.09	<0.001*
XSBN	6-7	1.69	2303	0.10	<0.001*

Table 3.6 Results of linear regression models of relative growth rates against crown illumination index (CII). *: $p \leq 0.05$; (*): $0.05 < p \leq 0.10$.

Site	Interval	Slope	d.f.	R^2	p-value
Pasoh	1-2	-0.0012	2365	0.015	<0.001*
Pasoh	2-3	-0.0039	1726	0.03	<0.001*
Pasoh	3-4	0.00063	1523	0.0006	0.35
Pasoh	4-5	-0.00096	1958	0.004	0.004*
Pasoh	5-6	-0.00027	1894	0.0009	0.19
KC	1-2	-0.00083	1849	0.003	0.01*
KC	2-3	-0.00077	1864	0.003	0.03*
KC	3-4	-0.0014	1839	0.005	0.004*
KC	4-5	-0.00021	2083	0.0002	0.53
HKK	1-2	-0.0006	1433	0.002	0.14
HKK	2-3	-0.00055	2133	0.005	0.002*
HKK	3-4	-0.0019	2115	0.014	<0.001*
HKK	4-5	-0.000011	2228	1.7×10^{-6}	0.95
HKK	5-6	-0.0039	2269	0.04	<0.001*
XSBN	1-2	-0.00089	2393	0.006	<0.001*
XSBN	2-3	0.0003	2357	0.0003	0.44
XSBN	3-4	0.0002	2362	0.0004	0.36
XSBN	4-5	-0.00011	2337	0.0001	0.56
XSBN	5-6	-0.0022	2327	0.01	<0.001*
XSBN	6-7	-0.00017	2303	0.00007	0.69

Table 3.7 Results of multiple linear regression models of absolute growth rates against crown illumination index (C), tree size (S), and their interaction (CxS). *: $p \leq 0.05$; (*): $0.05 < p \leq 0.10$.

Interval	Slope-C	p-value	Slope-S	p-value	Slope-CxS	p-value	d.f.	R^2
Pasoh 1-2	0.70	<0.001*	0.085	<0.001*	-0.013	0.002*	2363	0.17
Pasoh 2-3	0.60	0.004*	0.16	0.001*	-0.027	0.008*	1724	0.04
Pasoh 3-4	2.07	<0.001*	0.22	0.001*	-0.052	<0.001*	1521	0.04
Pasoh 4-5	0.57	<0.001*	0.045	0.16	-0.010	0.10(*)	1956	0.01
Pasoh 5-6	0.075	0.41	0.021	0.35	-0.004	0.36	1892	0.009
KC 1-2	0.94	<0.001*	-0.069	0.002*	0.012	0.005*	1847	0.07
KC 2-3	0.93	<0.001*	-0.032	0.14	0.0072	0.11	1862	0.07
KC 3-4	1.25	<0.001*	0.0039	0.89	0.00092	0.87	1837	0.08
KC 4-5	0.81	<0.001*	-0.034	0.09(*)	0.0068	0.10(*)	2081	0.05
HKK 1-2	1.24	<0.001*	0.038	0.06(*)	-0.0071	0.11	1431	0.10
HKK 2-3	0.10	0.22	0.017	0.10(*)	-0.0044	0.04*	2131	0.003
HKK 3-4	1.34	<0.001*	0.016	0.39	-0.0040	0.32	2113	0.08
HKK 4-5	-0.11	0.18	0.0038	0.70	-0.00057	0.79	2226	0.002
HKK 5-6	0.49	0.003*	-0.0011	0.95	0.0027	0.50	2267	0.03
XSBN 1-2	1.03	<0.001*	-0.020	0.15	0.0014	0.62	2391	0.09
XSBN 2-3	1.4	<0.001*	-0.046	0.06(*)	0.0067	0.17	2355	0.08
XSBN 3-4	0.51	<0.001*	-0.026	0.055(*)	0.0047	0.10(*)	2360	0.04
XSBN 4-5	0.53	<0.001*	-0.022	0.06(*)	0.0012	0.63	2335	0.03
XSBN 5-6	1.78	<0.001*	0.015	0.56	-0.006	0.26	2325	0.09
XSBN 6-7	1.8	<0.001*	-0.054	0.055(*)	0.0083	0.15	2301	0.10

Table 3.8 Results of multiple linear regression models of relative growth rates against crown illumination index (C), tree size(S), and their interaction (CxS). *: $p \leq 0.05$; (*): $0.05 < p \leq 0.10$.

Interval	Slope-C	p-value	Slope-S	p-value	Slope-CxS	p-value	d.f.	R^2
Pasoh 1-2	-0.0002	0.96	-0.00016	0.08(*)	0.000017	0.35	2363	0.03
Pasoh 2-3	-0.0034	<0.001*	-0.00037	0.12	0.000063	0.19	1724	0.03
Pasoh 3-4	0.0059	<0.001*	0.00067	0.02*	-0.00017	0.005*	1521	0.02
Pasoh 4-5	0.00014	0.82	-0.00005	0.71	-3.7×10^{-7}	0.99	1956	0.009
Pasoh 5-6	-0.0002	0.69	-0.00006	0.54	-8.7×10^{-6}	0.63	1892	0.001
KC 1-2	0.0019	0.002*	-0.00059	<0.001*	0.00008	<0.001*	1847	0.05
KC 2-3	0.00079	0.21	-0.00039	<0.001*	0.000056	0.002*	1862	0.02
KC 3-4	0.0024	0.005*	-0.0007	<0.001*	0.00009	<0.001*	1837	0.04
KC 4-5	0.0017	0.004*	-0.00036	<0.001*	0.000046	0.007*	2081	0.02
HKK 1-2	0.0021	0.001*	-0.00037	<0.001*	0.000037	0.04*	1431	0.06
HKK 2-3	0.00004	0.89	-0.00002	0.58	-1.9×10^{-6}	0.80	2131	0.009
HKK 3-4	0.0015	0.006*	-0.00046	<0.001*	0.000049	<0.001*	2113	0.10
HKK 4-5	-0.0002	0.45	0.000004	0.90	0.000001	0.87	2226	0.0006
HKK 5-6	-0.0040	<0.001*	-0.00059	<0.001*	0.00011	<0.001*	2267	0.07
XSBN 1-2	0.00092	0.02*	-0.00034	<0.001*	0.000039	0.002*	2391	0.04
XSBN 2-3	0.0026	<0.001*	-0.0003	0.003*	0.000026	0.21	2355	0.02
XSBN 3-4	0.001	0.007*	-0.00014	0.02*	0.000015	0.20	2360	0.008
XSBN 4-5	0.0011	<0.001*	-0.00014	0.004*	0.000001	0.32	2335	0.02
XSBN 5-6	0.00083	0.25	-0.00058	<0.001*	0.000067	0.003*	2325	0.05
XSBN 6-7	0.003	<0.001*	-0.00043	<0.001*	0.00004	0.08(*)	2301	0.03

negative for most of the measurement intervals (Table 3.8). These strong negative impacts of tree size were likely due to the calculation of relative growth rates, in which tree size (stem diameter) is in the denominator of the growth metric. For both absolute and relative growth, some of the interaction terms were significantly positive, suggesting there might be some combined effects of CII and tree size (i.e. larger trees respond more to light availability than smaller ones). However, the coefficients were generally very small, and were not significant in the absolute growth models.

3.3.3 Tree growth rates and wood density

As there is no wood density dataset for the species in Xishuangbanna, only three sites were included in this analysis (Pasoh, KC, and HKK). Absolute diameter growth rates were significantly negatively correlated with wood density across most measurement intervals at all the three sites (Table 3.9; Figures 3.12-3.14), the exceptions being the last interval at Pasoh, and the second to last at HKK, the two periods that had the smallest growth rates (Figure 3.5). The results confirm that trees of lower wood density generally grow faster in diameter than those of denser wood, except when they are equally stressed and don't grow much at all. Analysis of relative growth rates showed very similar results and no obvious patterns of influence of stem size were found in the multiple linear regression analyses (see Tables A.4-A.6 in Appendix A for detailed results).

Table 3.9 Results of linear regression models of absolute growth rates against wood density. *: $p \leq 0.05$; (*): $0.05 < p \leq 0.10$.

Site	Interval	Slope	d.f.	R^2	p-value
Pasoh	1-2	-1.68	2442	0.008	<0.001*
Pasoh	2-3	-3.43	1744	0.009	<0.001*
Pasoh	3-4	-6.79	1539	0.02	<0.001*
Pasoh	4-5	-1.97	1992	0.006	<0.001*
Pasoh	5-6	0.6658	1929	0.001	0.10(*)
KC	1-2	-11.1	1850	0.11	<0.001*
KC	2-3	-9.60	1865	0.07	<0.001*
KC	3-4	-11.2	1840	0.06	<0.001*
KC	4-5	-6.49	2084	0.04	<0.001*
HKK	1-2	-5.20	1435	0.02	<0.001*
HKK	2-3	-1.55	2135	0.005	0.001*
HKK	3-4	-1.72	2117	0.002	0.05*
HKK	4-5	-0.45	2231	0.0005	0.31
HKK	5-6	-3.00	2271	0.005	0.001*

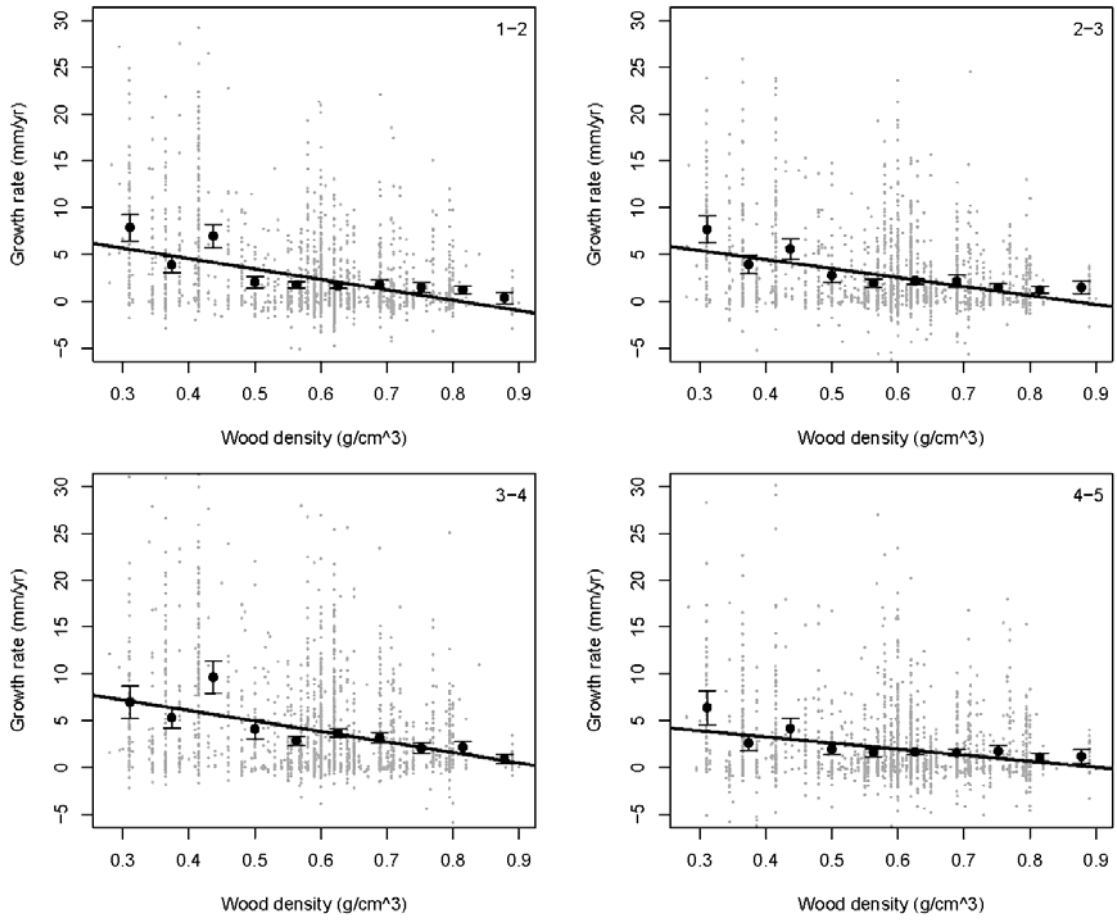

Figure 3.12 Absolute growth rates (mm/yr) and wood density (g/cm^3) during each measurement interval at Khao Chong. The grey dots are data for each individual tree; the black lines show the linear regression across all trees. The vertical lines with horizontal bars show the 95% confidence interval of the mean growth rates for ten groups of trees, grouped by increasing wood density.

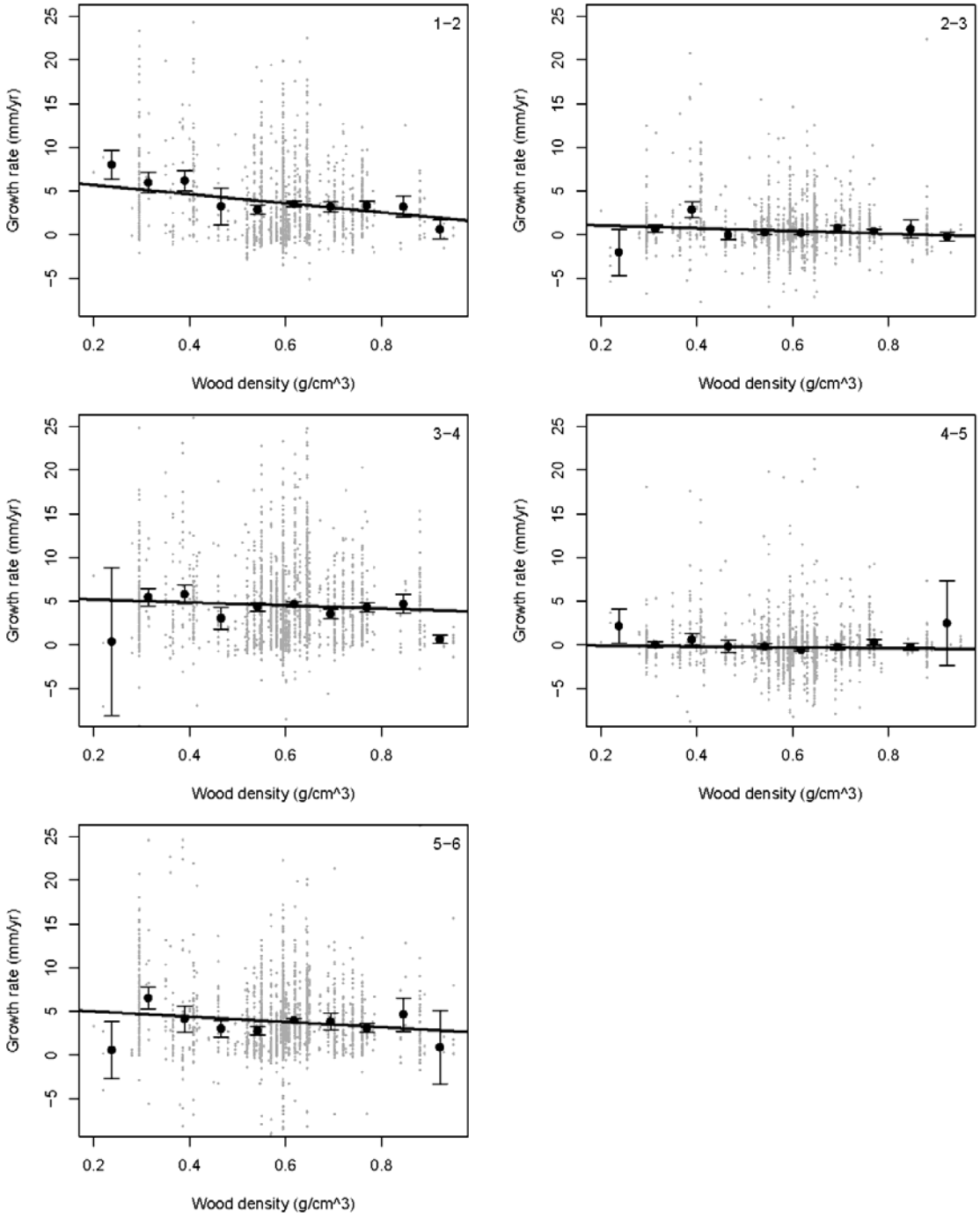

Figure 3.13 Absolute growth rates (mm/yr) and wood density (g/cm^3) during each measurement interval at Huai Kha Khaeng. The grey dots are data for each individual tree; the black lines show the linear regression across all trees. The vertical lines with horizontal bars show the 95% confidence interval of the mean growth rates for ten groups of trees, grouped by increasing wood density.

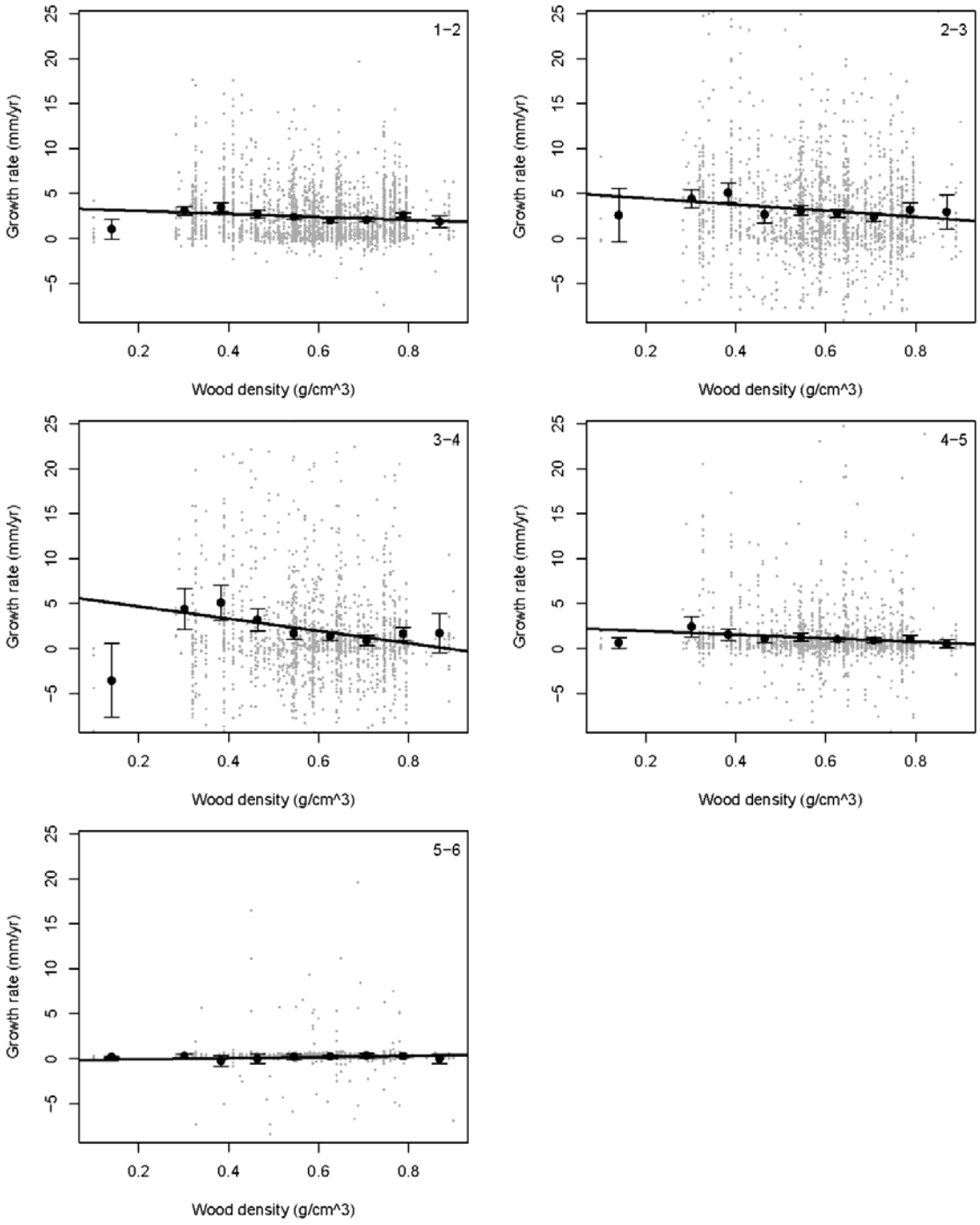

Figure 3.14 Absolute growth rates (mm/yr) and wood density (g/cm^3) during each measurement interval at Pasoh. The grey dots are data for each individual tree; the black lines show the linear regression across all trees. The vertical lines with horizontal bars show the 95% confidence interval of the mean growth rates for ten groups of trees, grouped by increasing wood density.

3.3.4 Tree growth rates and topography

Only two plots, Khao Chong and Huai Kha Khaeng, were included in the analysis. Both absolute growth rates and relative growth rates were examined and sometimes they showed different trends against changes in slope steepness.

At Khao Chong, statistically significant positive relationships with slope steepness were found in relative growth rates across all measurement intervals; but such positive relationships were found only in the first and last intervals for absolute growth rates (Table 3.10, Figure 3.15). A further analysis using multiple linear regression models which added tree size (stem diameter) and its interaction with slope steepness as co-variants revealed significantly positive impact of tree size as well as negative impact of the slope-size interaction (SSxS, Table 3.11). The coefficients became positive and statistically significant for the impact of slope steepness on absolute growth rates in

Table 3.10 Results of linear regression models of absolute growth rates (AGR) and relative growth rates (RGR) against slope steepness at Khao Chong. *: $p \leq 0.05$; (*): $0.05 < p \leq 0.10$.

Growth	Interval	Slope	d.f.	R^2	p-value
AGR	1-2	0.035	1850	0.004	0.006*
AGR	2-3	0.0086	1865	0.0002	0.51
AGR	3-4	-0.0056	1840	0.00006	0.74
AGR	4-5	0.054	2084	0.001	<0.001*
RGR	1-2	0.00017	1850	0.006	<0.001*
RGR	2-3	0.00011	1865	0.003	0.02*
RGR	3-4	0.00014	1840	0.002	0.05*
RGR	4-5	0.00032	2084	0.02	<0.001*

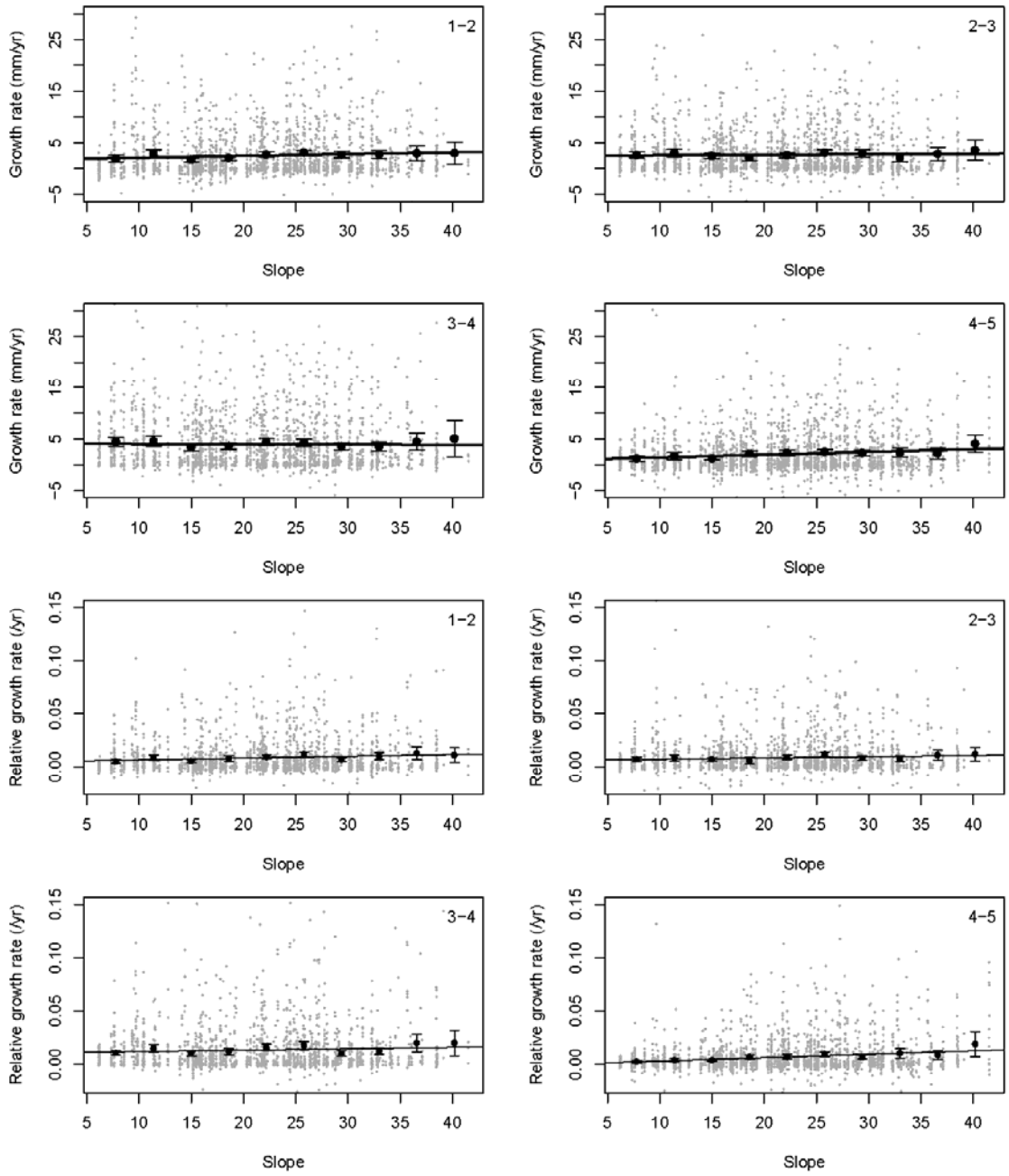

Figure 3.15 Absolute growth rates (mm/yr) and relative growth rates (/yr) against slope steepness (degree) during each measurement interval at Khao Chong. The grey dots are data for each individual tree; the black lines show the linear regression across all trees. The vertical lines with horizontal bars show the 95% confidence interval of the mean growth rates for ten groups of trees, grouped by increasing slope steepness.

Table 3.11 Results of multiple linear regression models of absolute growth rates (AGR) and relative growth rates (RGR) against slope steepness (S), tree size (s), and their interaction (Sxs) at Khao Chong. *: p≤0.05; (*): 0.05<p≤0.10.

Interval	Slope-S	p-value	Slope-s	p-value	Slope-Sxs	p-value	d.f.	R^2
AGR 1-2	0.067	0.004*	0.052	<0.001*	-0.00091	0.08(*)	1848	0.04
AGR 2-3	0.053	0.02*	0.066	<0.001*	-0.0012	0.03*	1863	0.05
AGR 3-4	0.14	<0.001*	0.15	<0.001*	-0.0041	<0.001*	1838	0.08
AGR 4-5	0.11	<0.001*	0.068	<0.001*	-0.0016	0.001*	2082	0.05
RGR 1-2	0.00029	0.001*	-0.00004	0.46	-0.000003	0.13	1848	0.03
RGR 2-3	0.00027	0.004*	0.000015	0.75	-0.000004	0.04*	1863	0.02
RGR 3-4	0.00044	<0.001*	0.00002	0.77	-0.0000075	0.007*	1838	0.03
RGR 4-5	0.00061	<0.001*	0.00013	0.005*	-0.0000084	<0.001*	2082	0.04

these multiple linear regression models. These results not only confirmed the positive relationship between slope steepness and tree growth, but also displayed the positive influence of tree size on diameter growth. Furthermore, the significantly negative coefficients for the interaction terms in three out of the four measurement intervals elucidated the nature of the impact of tree size on the tree growth responses to slope steepness in these periods. The growth of the larger-sized trees was less affected by the positive influence of steep slopes than was the growth of the smaller trees.

At Huai Kha Khaeng, no consistent patterns were found in any of the tests. The only significant positive relationship between growth rate and slope steepness was in the first measurement interval, in the simple linear regression (see Table A.7 in Appendix A). In the multiple linear regression models, only a few coefficients were statistically significant, but not for the same measurement intervals, and even the signs

were inconsistent (see Table A.8 in Appendix A), implying no consistent impact of topography on tree growth at Huai Kha Khaeng.

3.3.5 Species sample

For the species sample, I calculated the mean and variance of both absolute growth rate and relative growth rate for each species (except for the pioneer species, I grouped all the species in each plot because of the small sample sizes of each species) and examined their relationships with climate variability in the same manner as I did for the plot mean (see Section 3.3.1). Figure 3.16 shows the comparisons among fitted linear regression models of the species sample groups and the plot mean (Table 3.12). All of the five groups displayed similar trends as the plot mean. There were significant positive relationships between absolute growth rates and variations in precipitation. There were, however, no significant differences in the slopes of the growth-precipitation relationships among the species groups (Figure 3.16a). The same consistency was found in temperature responses for three of the species groups. Both of the emergent species groups and pioneer groups responded positively to variations in mean minimum temperature (Figure 3.16b). The growth-temperature relationship in Burseraceae was also positive, but very weak and marginally significant ($p=0.10$). There was no significant difference among the slopes of these growth-temperature relationships. No consistent pattern was found in growth-temperature relationship of

(a)

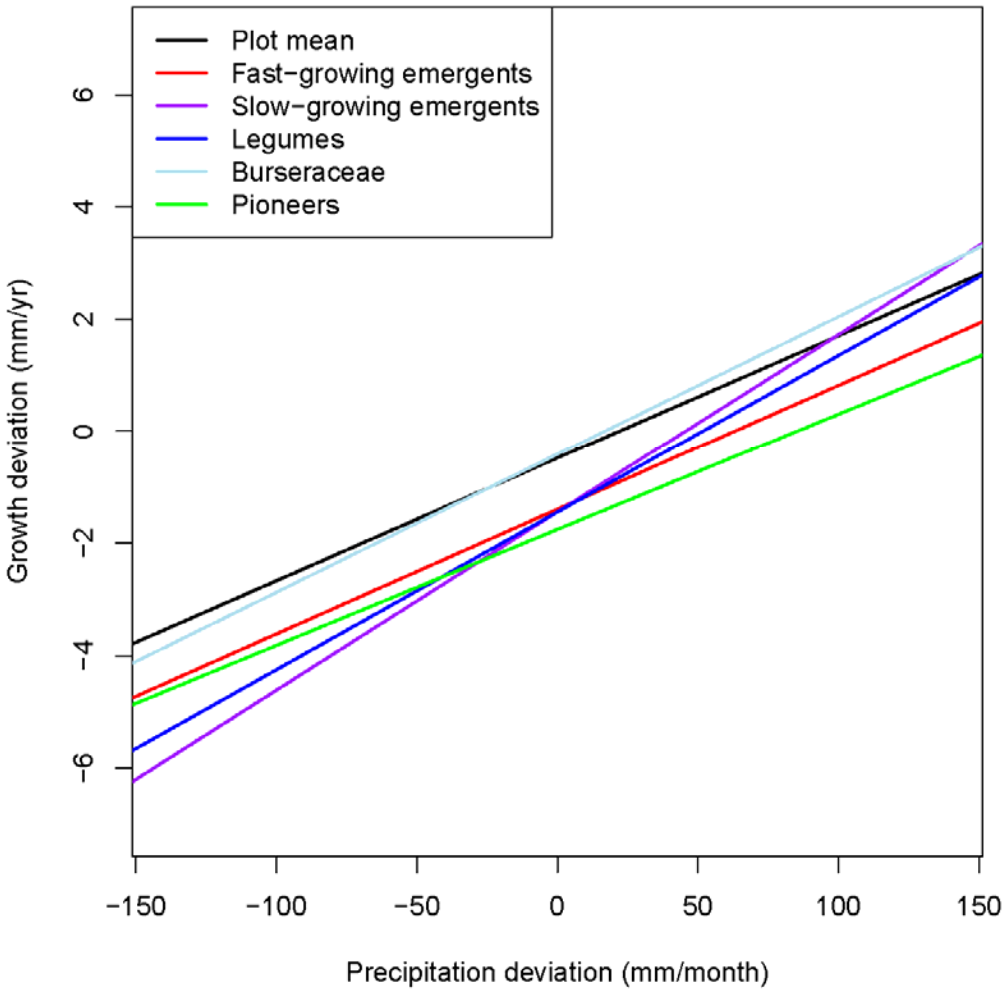

Figure 3.16 (Continues on the next page)

Figure 3.16 (Continued)

(b)

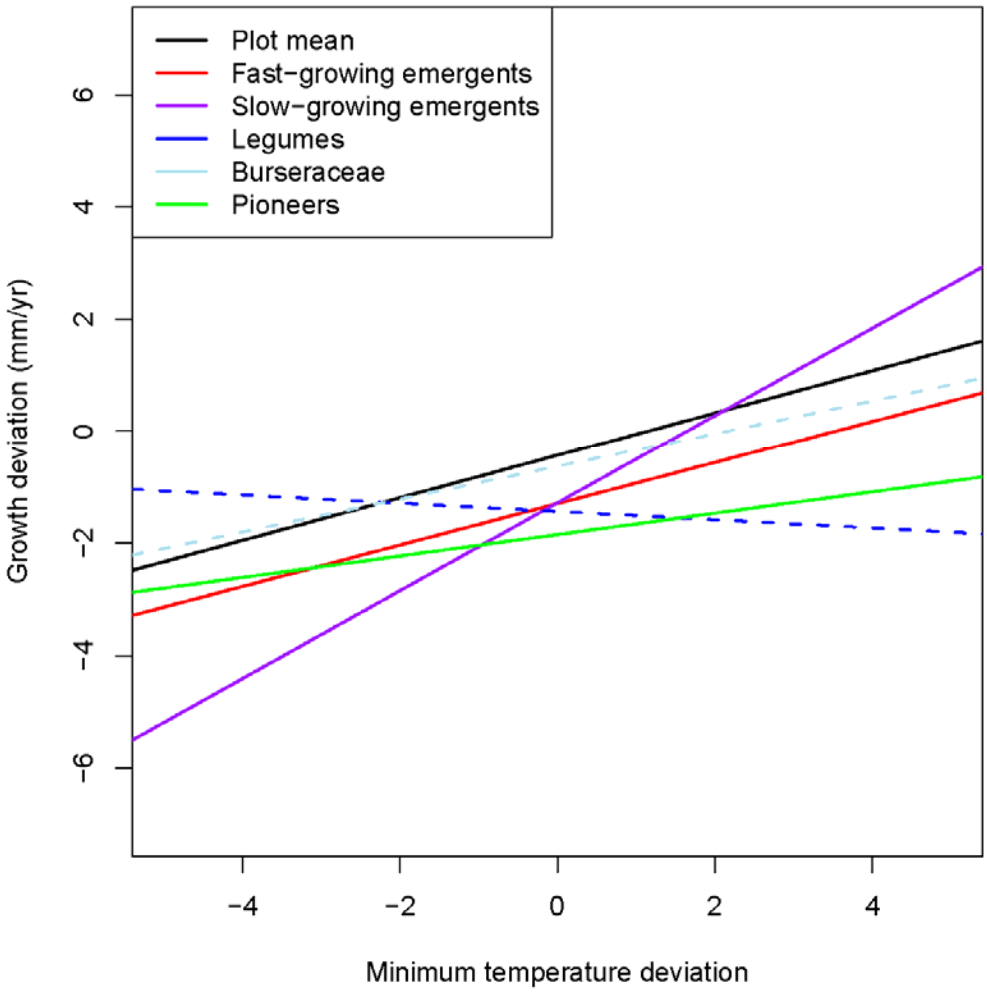

Figure 3.16 Results of linear regression models of absolute growth rates (mm/yr) against climate variability for the species sample. (a) Absolute growth deviation and monthly total precipitation deviation (mm). (b) Absolute growth deviation and monthly mean daily minimum temperature deviation. The solid lines show the fitted models that are statistically significant ($p<0.05$). The dashed lines show the fitted models that are not statistically significant ($p>0.05$).

Table 3.12 Results of linear regression models of absolute growth rates against climate variables for the species sample (P: precipitation; T: temperature; R: radiation). *: $p \leq 0.05$; (*): $0.05 < p \leq 0.10$.

Group	Y	Slope	d.f.	R^2	p-value
Fast-growing emergents	P	0.022	23	0.23	0.02*
Fast-growing emergents	T	0.37	23	0.15	0.05*
Slow-growing emergents	P	0.032	23	0.28	0.007*
Slow-growing emergents	T	0.78	23	0.37	0.001*
Legumes	P	0.028	26	0.20	0.02*
Legumes	T	-0.073	26	0.001	0.87
Burseraceae	P	0.025	23	0.45	<0.001*
Burseraceae	T	0.29	23	0.12	0.10(*)
Pioneers	P	0.025	18	0.46	0.001*
Pioneers	T	0.52	18	0.40	0.003*

the Legumes group (p=0.87).

Relative growth rates showed the same trend but weaker statistical significance than absolute growth rates (see Table A.10 in Appendix A). Both absolute and relative growth rates were plotted against precipitation and temperature deviations for each species group and the graphs were very comparable to those with the plot mean growth rates (see Figures A.1-A.10 in Appendix A).

3.4 Discussion

In this study, I examined tree diameter growth rates in relation to climate variability of all the sites, both on samples chosen randomly across the plot and on species sample groups of different life history. I also looked at the impact of light availability, wood density, and topography on tree growth at either all of the sites or where data were available.

As expected, the results of the dendrometer band study have revealed patterns that were previously not clear in the analyses using the 5-year census data. The much shorter lengths of the measurement intervals (*c.* 3 months at Xishuangbanna and *c.* 6 months at the other three sites) made it possible to examine tree growth responses to climate variability on a much shorter time scale. The dendrometer band measurements captured a much higher magnitude of change in climate variables than had conventional tape measurements (compare Figure 3.4 and Figures 2.2-2.6).

In previous analyses, precipitation was found to have no impact on tree growth because most of the variability in precipitation is masked in the five-year means (Figure 2.3). The more frequent dendrometer measurements allow us to capture not only the year-to-year differences in total precipitation, but also variations in precipitation within a year at the more seasonal sites. Therefore in this study I was able to show the positive relationship between precipitation and tree growth rate across all sites (Figure 3.6a). Such strong impact of precipitation was seen both in the plot mean growth rates and across all of the five groups in the species sample (Figure

3.16a). Growth correlations with precipitation were stronger at the more seasonal sites (Figure 3.7). Moreover, during the exceptional dry season at Huai Kha Khaeng (Nov 2009 to Apr 2010, Figure 3.4), most trees either did not grow much, or even shrunk in diameter so that the plot mean growth for that measurement interval (3-4) was negative (Figure 3.5). These results confirm the importance of dry season rainfall (Clark et al. 2010) and the negative impact of drought on tree growth (Da Costa et al. 2010; Rolim et al. 2005; Asner et al. 2004).

While the growth-precipitation relationship appears to be consistent across all of the four sites, a different and interesting pattern was found in growth-temperature relationships when each site was examined separately (Figure 3.8). At the southernmost site, Pasoh, growth rate was significantly negatively correlated with minimum temperature. This result is consistent with previous studies (e.g. Feeley et al. 2007). However, the growth-temperature correlation was reversed, i.e. significantly positive, at the northernmost site Xishuangbanna. There is a clear pattern of the growth-temperature relationship going from south to north: from strongly negative at Pasoh, flat at Khao Chong, weakly positive at Huai Kha Khaeng, and strongly positive at Xishuangbanna (Table 3.3). This suggests a possible latitudinal influence on trees' growth responses to changes in minimum temperature. The latitudinal pattern found here offers a plausible explanation for the previously mentioned inconsistent findings and the resulting debate on how tropical forests are responding to increasing temperature (e.g. Clark et al. 2003; Clark 2004b; Lewis et al. 2004; Phillips et al. 2004).

Five representative species groups of different canopy positions and life history traits were sampled in the dendrometer measurements and examined in this analysis: fast-growing emergents, slow-growing emergents, Legumes, Burseraceae, and pioneer species (Table 3.2). All species groups showed remarkably similar responses to precipitation. The positive slopes of the relationships are not significantly different from one another. With regard to temperature, three out of the five groups (fast- and slow-growing emergents and pioneers) exhibited consistent positive growth responses, while the remaining two (Burseraceae and Legumes) showed weak or no effect of temperature on growth. Again, none of the slopes were significantly different. Although species in different functional groups were thought to respond differently to climate change (for example, pioneers are less sensitive to moisture variation than other species; Condit et al. 1996), such differences are not found here. The results implied that if differences in environmental responses among the species groups exist, they are relatively small and longer observation period and/or more variation in environmental factors may be needed to detect those differences.

In this study I used Crown Illiumination Index (CII) as an indicator of light availability and recorded CII for each banded tree. The estimates are repeatable and accurate, can be performed by an observer on the ground to trees of any height (Clark and Clark 1992; Poorter et al. 2005); and have been shown to correlate well with canopy openness (Davies et al. 1998) and the amount of incident radiation (Clark et al. 1993). The results from the two sets of multiple linear regression models using absolute and relative growth rates imply that absolute growth rates are better

indicators of tree diameter growth in response to changes in light availability (compare Tables 3.5 and 3.6). More importantly, many of the coefficients for CII changed from negative to positive in the relative growth rate multiple regression models, when impact of CII was separated from that of tree size. This, together with the results from absolute growth rate, shows that light availability is in general positively correlated with tree growth. It confirms that tree growth responds positively to increases in radiation and light inception of the canopy (Chapter 2; King et al. 2005) and tree growth in the tropics is strongly limited by light availability (Graham et al. 2003; Nemani et al. 2003). The magnitude of the impact of light availability differs among measurement intervals across the sites (see the differences in slopes in Figure 3.10 and Table 3.5). In the two seasonal forests, Huai Kha Khaeng and Xishuangbanna, the slopes of the growth-light relationships were flatter during the two dry season measurement intervals (when trees didn't grow much) than those of the wet season, or sometimes even negative. At Pasoh, the slope was flat for the last measurement interval, when the mean growth rate was also very low, possibly due to high night-time temperature. This suggests that the magnitude of growth rates influences the responses of trees to light availability. Trees respond more to increase in light availability when their growth rates are less suppressed by other factors such as decreased water availability and increased night-time temperature.

A similar conclusion was drawn from the wood density analysis. Our results confirmed the negative relationships between tree growth rates and wood density found in many other studies (e.g. King et al. 2005; Enquist et al. 1999; Muller-Landau

2004). But such relationships were not seen in the measurement intervals when the tree growth rates were low (Table 3.9, Section 3.3.3).

Of the two sites examined for topographic effects (Khao Chong and Huai Kha Khaeng), only Khao Chong displayed consistent patterns of positive responses of to changes in slope steepness, influenced by the initial tree size (Figure 3.15; Table 3.11). The growth of the larger-sized trees seemed to be less affected by the positive influence of steep slopes than were the small trees, as indicated by the negative interaction term between slope steepness and tree size in the multiple linear regression models.

Although the length of this study is relatively short (two years for Xishuangbanna and a little over three years for the other three sites), and I have only conducted limited amount of measurements to date, the results presented in this chapter have shown valuable information about patterns of changes in tree growth rates in relation to variations in environmental factors. As research continues and more measurements are made, I will be able to further examine these relationships in more detail and gain more insights into the changes in forest dynamics and structure.

Chapter 4

Relating tree demographic rates to differences in tropical forest structure: a modeling approach

As introduced in Chapter 1, one of my research objectives is to relate the differences in the observed tree demography (growth and mortality rates) to differences in tropical forest structure at different sites. Mathematical models are useful tools for projecting forest dynamics forward in time in order to evaluate hypotheses that would otherwise be difficult or impossible to carry out solely by field observations. In this chapter, I present a size-structured model that uses phenomenological functions to relate current forest demographic rates to the forest structure that would result from these demographic rates if they were maintained. Using three different forest plots in Southeast Asia as case studies, I show how the ability of the model to predict steady-state stem size-frequency distributions of the forests provides the opportunity to gain insights into the demographic history of the forests. I then discuss and compare some of the predictions from metabolic scaling

theory, using the same study sites. A new dynamical theory that builds upon this analysis will be presented in the subsequent chapter.

4.1 Model formulation

An advection-reaction equation can be used to model changes in forest stem size-frequency distributions based on the given growth and mortality rates (Kohyama 1992; Kohyama 1993; Kohyama and Shigesada 1995). Let $n(z,t)$ be the number of trees of size class z at time t. The change of the number of trees over time, $\Delta n(z,t)$, is affected by the rate of mortality of trees in each particular size class as well as the shifting of the size classes due to growth, i.e., the change of the number of trees of a size class z should is governed by the number of trees that grow into this size class from smaller size classes over the time period, minus the trees that leave this size class due to either mortality or growth into larger size classes:

$$\Delta n(z,t) = \underbrace{n(z-\Delta z,t)g(z-\Delta z)\frac{\Delta t}{\Delta z}}_{\text{growth from smaller size class}} - \underbrace{n(z,t)g(z)\frac{\Delta t}{\Delta z}}_{\text{growth out of size class}} - \underbrace{n(z,t)\mu(z)\Delta t}_{\text{death}} \quad , \quad (4.1)$$

where $g(z)$ and $\mu(z)$ are functions of the growth and mortality rates, respectively, of size class z. Dividing both sides of Equation 4.1 by Δt and taking the limits $\Delta t \rightarrow 0$,

$\Delta z \rightarrow 0$ yields the following advection-reaction equation for the dynamics of forest size structure:

$$\frac{\partial n(z,\,t)}{\partial t} = \underbrace{-\frac{\partial}{\partial z}\left[g(z,\,t)n(z,\,t)\right]}_{\text{growth}} \underbrace{-\,\mu(z,\,t)n(z,\,t)}_{\text{death}} \quad . \tag{4.2}$$

Plant recruitment into the smallest size class z_0 is represented by the following boundary condition:

$$n(z_0, t) = \frac{\int_0^\infty n(z,t) f(z) dz}{g(z_0)} \quad , \tag{4.3}$$

where $f(z)$ is the fecundity of the trees of size class z. The initial condition for Equation 4.2 is just the structure of the plant community at time 0, namely, $n(z,0)$.

Equation 4.2 can be solved either analytically or numerically using appropriate functions for growth, mortality, and fecundity (functions $g(z)$, $\mu(z)$, and $f(z)$, respectively). However, it is best suited for continuous parametric growth and mortality functions; and it is also strictly deterministic: two individuals that are the same size at birth remain the same size until one of them dies (Easterling et al. 2000). Furthermore, given the discrete nature of the plot census data used in this study, a more appropriate formulation is to use an analogous discrete-time structured population model that resembles the above partial differential equation model, but accommodates stochasticity in tree growth trajectories. One such model, the integral projection model, has been introduced in Easterling et al. (2000) and predicts the

change in population density by the integral function:

$$\begin{aligned} n(y, t+1) &= \int_{\Omega} \left[p(x, y) + f(x, y) \right] n(x, t) dx \\ &= \int_{\Omega} k(y, x)\, n(x, t) dx \quad , \end{aligned} \tag{4.4}$$

where *k(y,x)* is the so-called kernel that describes all possible transitions from size *x* to size *y*. The kernel is composed of two parts, a fecundity function, *f(x,y)*, and a survival-growth function, *p(x,y)*. The integration is over the set of all possible sizes, Ω.

In this study, I developed a formulation of this kind that is able to accommodate the empirical data, tree demographic rates measured in the field. The model predicts the change of number of trees in each size classes over time as follows:

$$\Delta n(z, t) = \int_{\Omega} g(z, t \mid z')\, n(z', t)\, \Delta t\, dz' - \mu(z, t)\, n(z, t)\, \Delta t \quad , \tag{4.5}$$

where *g(z,t|z')* is the probability of trees in size class *z'* growing into size class *z* at time *t*. And fecundity of trees in each size class, *f(z,t)*, can be included in a separated equation for $\Delta n(z_1,t)$, the change of number of trees in the smallest size class, z_1:

$$\begin{aligned} \Delta n(z_1, t) &= \int_{\Omega} f(z, t) n(z, t)\, \Delta t\, dz \\ &\quad - \int_{\Omega} g(z_1, z, t) n(z_1, t)\, \Delta t\, dz - \mu(z_1, t) n(z_1, t)\, \Delta t \quad . \end{aligned} \tag{4.6}$$

In cases when fecundity data are not available, and the recruitment into the smallest size class has to be prescribed, Equation 4.6 can simply be replaced by the prescribed

fecundity function, or a constant if recruitment is assumed to stay constant over time.

The integral projection model (Equation 4.4) can be written in a matrix form and solved numerically (Childs et al. 2003). Similarly, Equation 4.5 can be approximated with the following matrix equation:

$$\begin{pmatrix} n_1(t+\Delta t) \\ n_2(t+\Delta t) \\ \vdots \\ n_i(t+\Delta t) \end{pmatrix} = \mathrm{A} \times \begin{pmatrix} n_1(t) \\ n_2(t) \\ \vdots \\ n_i(t) \end{pmatrix} \quad , \tag{4.7}$$

where n_1, n_2, …, n_i are the number of trees of different size classes, i.e. $n_z(t) = n(z,t)$. And the transition matrix A is:

$$A = \begin{bmatrix} 1-\mu_1 \Delta t - \sum_{j=2}^{i} \gamma_{1,j} \Delta t + f_1 \Delta t & f_2 \Delta t & f_3 \Delta t & \cdots & f_i \Delta t \\ \gamma_{1,2} \Delta t & 1-\mu_2 \Delta t - \sum_{j=3}^{i} \gamma_{2,j} \Delta t & 0 & \cdots & 0 \\ \gamma_{1,3} \Delta t & \gamma_{2,3} \Delta t & 1-\mu_3 \Delta t - \sum_{j=4}^{i} \gamma_{3,j} \Delta t & \cdots & 0 \\ \vdots & \vdots & \vdots & \ddots & \vdots \\ \gamma_{1,i} \Delta t & \gamma_{2,i} \Delta t & \gamma_{3,i} \Delta t & \cdots & 1-\mu_i \Delta t \end{bmatrix}, \tag{4.8}$$

where f_i is the fecundity rate of trees of size class i; μ_i is the mortality rate of trees of size class i, modeled as the probability of death of a tree in that size class following a Bernoulli distribution with parameter $\mu_i \Delta t$; and $\gamma_{i,j}$ is the probability of a tree in size class i transitioning into size class j in the next time step, following a Poisson distribution with rate parameter $g_i \Delta t$. The means used in the Bernoulli and Poisson

distributions are calculated from observed mortality and growth rates, respectively, for each tree size class at each of the study sites. The mean values are calculated after all census intervals are adjusted to five years, and then averaged across all census intervals. Therefore, the time step used in the model is always five years, i.e. $\Delta t = 5$. In this study, I used 1 cm bins for the size classes, i.e. $\Delta z = 1$. Since there are no measurements or data available at present to calculate fecundity of trees of different size classes at any of the study sites, fecundity is prescribed in the model, using the observed number of trees in the smallest size class and $n_1(t)$ is kept constant, as shown in Equation 4.9:

$$A = \begin{bmatrix} 1 & 0 & 0 & \cdots & 0 \\ \gamma_{1,2}\,\Delta t & 1-\mu_2\,\Delta t-\sum_{j=3}^{i}\gamma_{2,j}\,\Delta t & 0 & \cdots & 0 \\ \gamma_{1,3}\,\Delta t & \gamma_{2,3}\,\Delta t & 1-\mu_3\,\Delta t-\sum_{j=4}^{i}\gamma_{3,j}\,\Delta t & \cdots & 0 \\ \vdots & \vdots & \vdots & \ddots & \vdots \\ \gamma_{1,i}\,\Delta t & \gamma_{2,i}\,\Delta t & \gamma_{3,i}\,\Delta t & \cdots & 1-\mu_i\,\Delta t \end{bmatrix}. \quad (4.9)$$

4.2 Model outputs and analyses

Here I present three case studies of the model, parameterized to predict stand structure of three Southeast Asian forests: Pasoh and Lambir in Malaysia, and Huai Kha Khaeng (HKK) in Thailand (see descriptions of the study sites in Chapter 2, Section 2.2.1 and Table 2.1). Stem diameter growth rates are calculated for all trees

greater than 1 cm diameter at breast height (DBH) in each census interval. The trees are grouped into 1 cm DBH bins, i.e. the DBH of trees in size class z will be greater than or equal to z cm but smaller than (z +1) cm. Consistent with earlier analyses (e.g. Condit et al. 2006), excluded from the calculation were: (i) trees that grew at a rate greater than 7.5 cm diameter per year; (ii) trees that shrunk more than 25% of their initial DBH; (iii) trees that were measured at different heights in two consecutive censuses (usually due to growing buttresses or damaged stems); and (iv) trees whose main stem had broken and re-sprouted. Mortality rates are calculated as percentage of dead trees from those that were alive in the previous census. Only trees clearly marked as "Dead" were counted as mortalities, i.e. trees that had fallen or whose main stem had broken, but are still alive, were excluded from the calculation. Average growth and mortality rates were divided by the length of each corresponding census interval and converted back to standard 5-year rates. Because of the unreliability of tree mortality data in the 2004 census of HKK[1], only the first two censuses (1994 and 1999) are used in the calculation.

The mean growth and mortality rates calculated for each tree size class were then used as the rate parameters in the Poisson and Bernoulli distributions that respectively determine the growth and death probabilities in the transition matrix, Equation 4.8. The model is solved in MATLAB (R2006a, Natick, MA: The MathWorks, Inc.), iterating Equation 4.8 until the forest reached its projected equilibrium state.

[1] Some recorded deaths of the trees were unverified in this census, so the actual mortality rate may have been lower than that calculated from the recorded data.

4.2.1 Results

The output of the simulation is plotted against observed size distribution at each site (Figures 4.1-4.3). If the forest is at approximate equilibrium (i.e. no recent disturbance), then the size structure predicted by inserting the observed demographic rates into the model should yield the observed structure. And this is the case at Lambir (Figure 4.1), where the predicted line of stem size-frequency distribution from the simulation closely matches the observed size distribution from the field census. However, for the other two sites (Pasoh and HKK, Figures 4.2-4.3), there is a

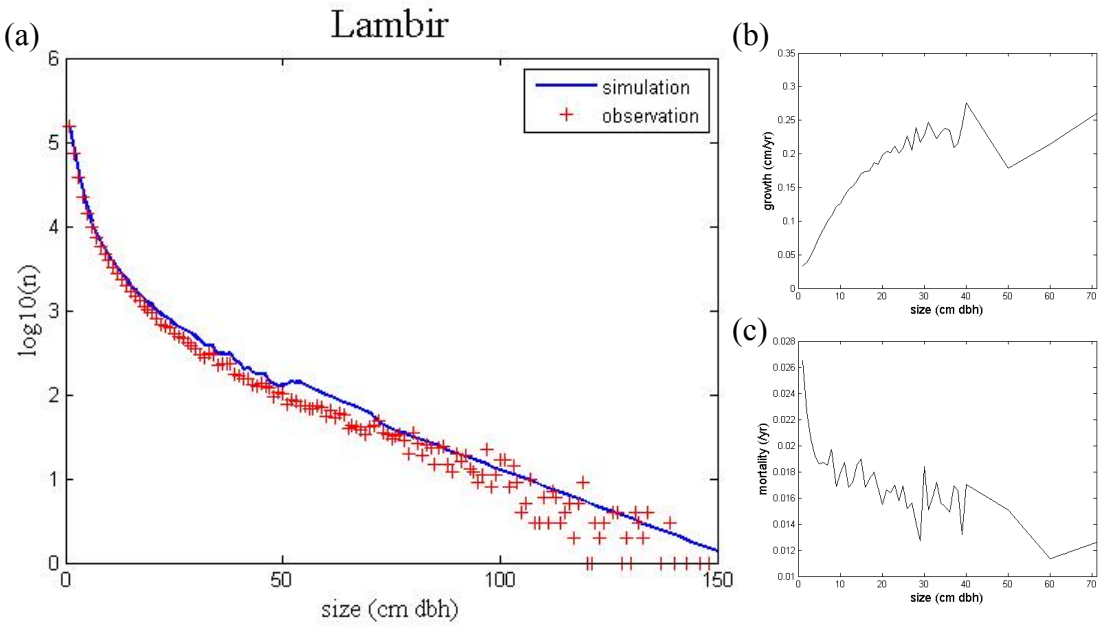

Figure 4.1 Model simulation of stem size distribution (a) at Lambir, using observed tree growth (b) and mortality (c) rates. The blue line in (a) is the model output, and the red crosses in (a) are the observed size-frequency distribution from the plot census.

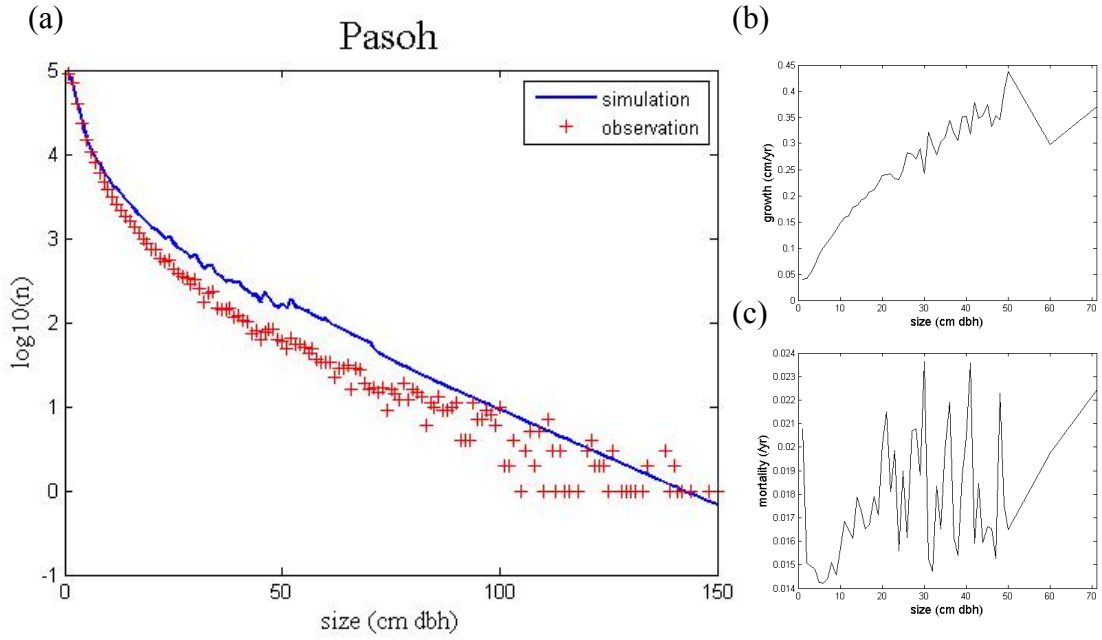

Figure 4.2 Model simulation of stem size distribution (a) at Pasoh, using observed tree growth (b) and mortality (c) rates. The blue line in (a) is the model output, and the red crosses in (a) are the observed size-frequency distribution from the plot census.

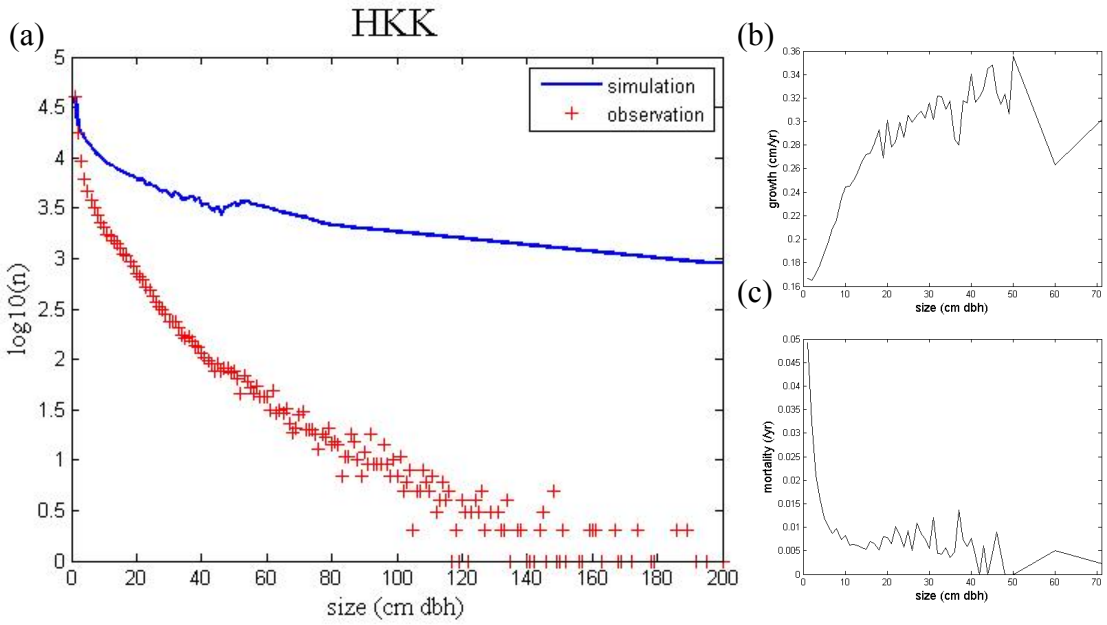

Figure 4.3 Model simulation of stem size distribution (a) at HKK, using observed tree growth (b) and mortality (c) rates. The blue line in (a) is the model output, and the red crosses in (a) are the observed size-frequency distribution from the plot census.

mismatch between the simulated versus observed size distributions. At both sites, the predicted stem abundances are higher than observed. Specifically, the predicted abundance for mid- and large-sized trees at Pasoh is, on average, twice the observed values; and at HKK, the model over-predicts trees in virtually every size class, with the discrepancies for large size classes being a ten-fold excess of individuals.

4.2.2 Further analyses

The discrepancies between simulated and observed tree size distributions at Pasoh and HKK imply that the observed tree growth and mortality rates are different from those that gave rise to their current stand structure. To better understand these differences, I adjusted the observed values of growth and mortality rates in order to detect the set of rates that are consistent with the observed size structure at the two sites. The observed demographic rates were multiplied by a monotonic function that allowed adjustment of different magnitude for different size classes:

$$G_{fit}(z) = G_{obs}(z) \cdot a\,(1 - e^{-b \cdot z}) \tag{4.10}$$

$$M_{fit}(z) = M_{obs}(z) \cdot c\,(1 - e^{-d \cdot z}) \quad , \tag{4.11}$$

where $G_{obs}(z)$ and $G_{fit}(z)$ are the observed and adjusted growth rates, respectively; and $M_{obs}(z)$ and $M_{fit}(z)$ are the observed and adjusted mortality rates, respectively. Goodness-of-fit test statistics are calculated for 10,000 iterations, each using a different set of parameters. The adjusted growth and mortality rates that yield the best

fit of the size distribution are plotted against the observed values in Figures 4.4-4.7 (see the fitted parameters in Table 4.1). The adjusted growth and mortality rates differ slightly from the observations at Pasoh, with an average 4% decrease for growth rates and an average 3% increase for mortality rates (Figures 4.4-4.5). The adjusted mortality rates are much higher than those observed at HKK (Figure 4.7), but the growth rates are roughly the same (Figure 4.6). Following the adjustments, the predicted stem size distributions using the adjusted growth and mortality rates now closely match the observed values at both sites (Figures 4.8 and 4.9).

Table 4.1 Fitted parameters for Equations 4.10 and 4.11 at each study site.

Site	a	b	c	d
Pasoh, Malaysia	0.96	1.0	1.03	1.2
HKK, Thailand	1.00	2.0	4.50	0.5

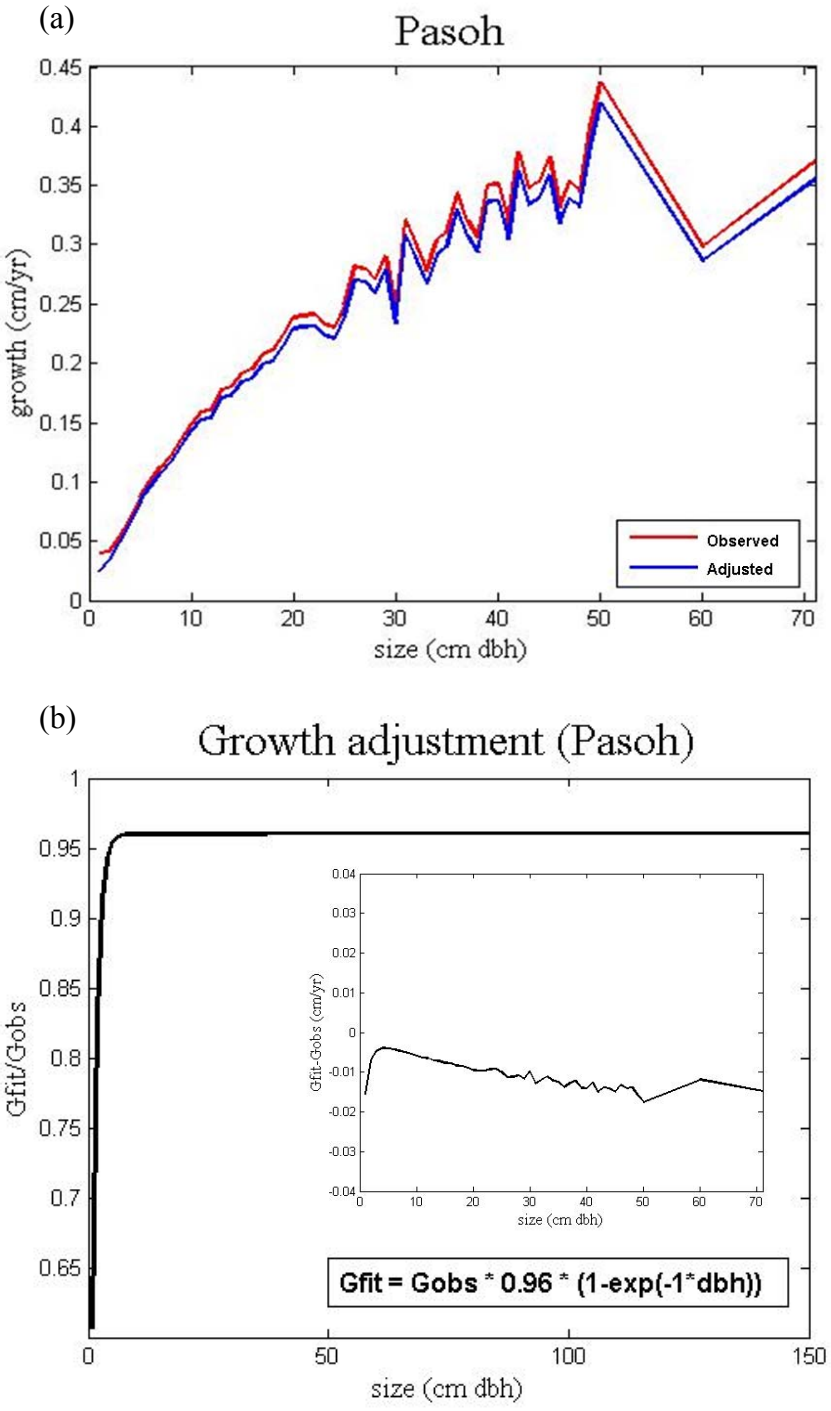

Figure 4.4 Adjusted growth rates at Pasoh. (a) Comparison of adjusted (blue line) and observed (red line) growth rates. (b) The ratio (outer panel) and difference (inner panel) of the fitted (G_{fit}) versus observed (G_{obs}) growth rates. The equation shows the functional form and parameters used in the adjustment.

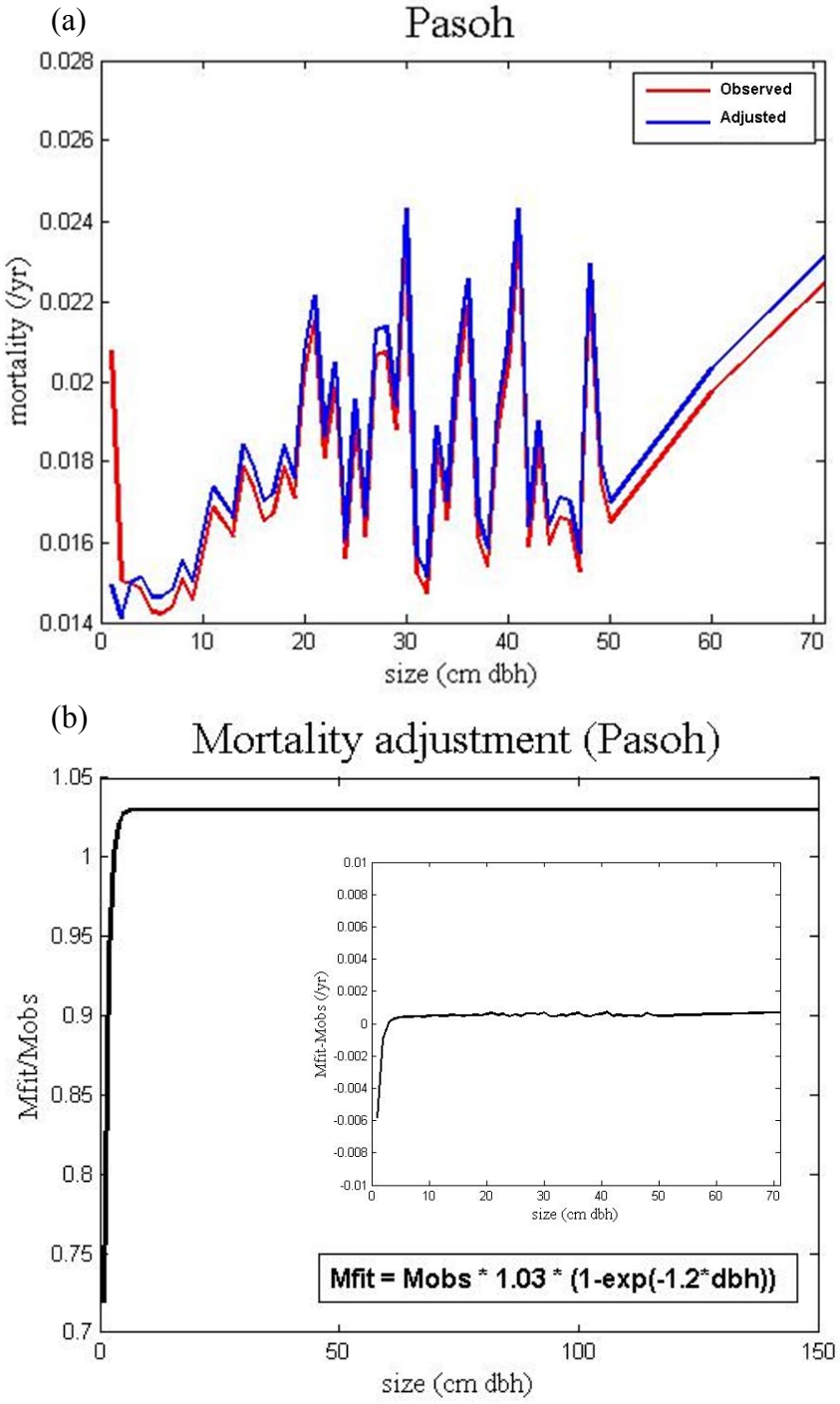

Figure 4.5 Adjusted mortality rates at Pasoh. (a) Comparison of adjusted (blue line) and observed (red line) mortality rates. (b) The ratio (outer panel) and difference (inner panel) of the fitted (M_{fit}) versus observed (M_{obs}) mortality rates. The equation shows the functional form and parameters used in the adjustment.

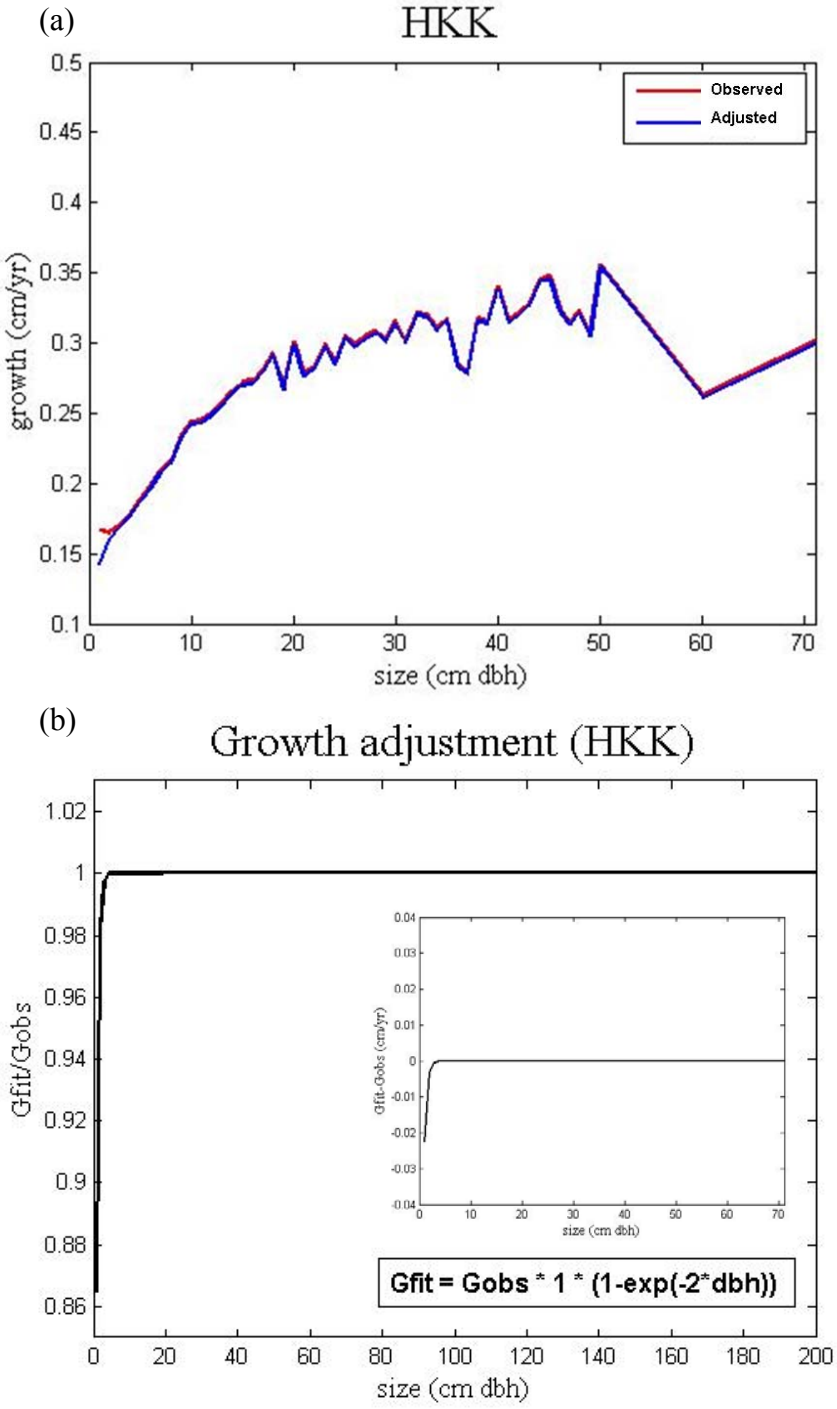

Figure 4.6 Adjusted growth rates at HKK. (a) Comparison of adjusted (blue line) and observed (red line) growth rates. (b) The ratio (outer panel) and difference (inner panel) of the fitted (G_{fit}) versus observed (G_{obs}) growth rates. The equation shows the functional form and parameters used in the adjustment.

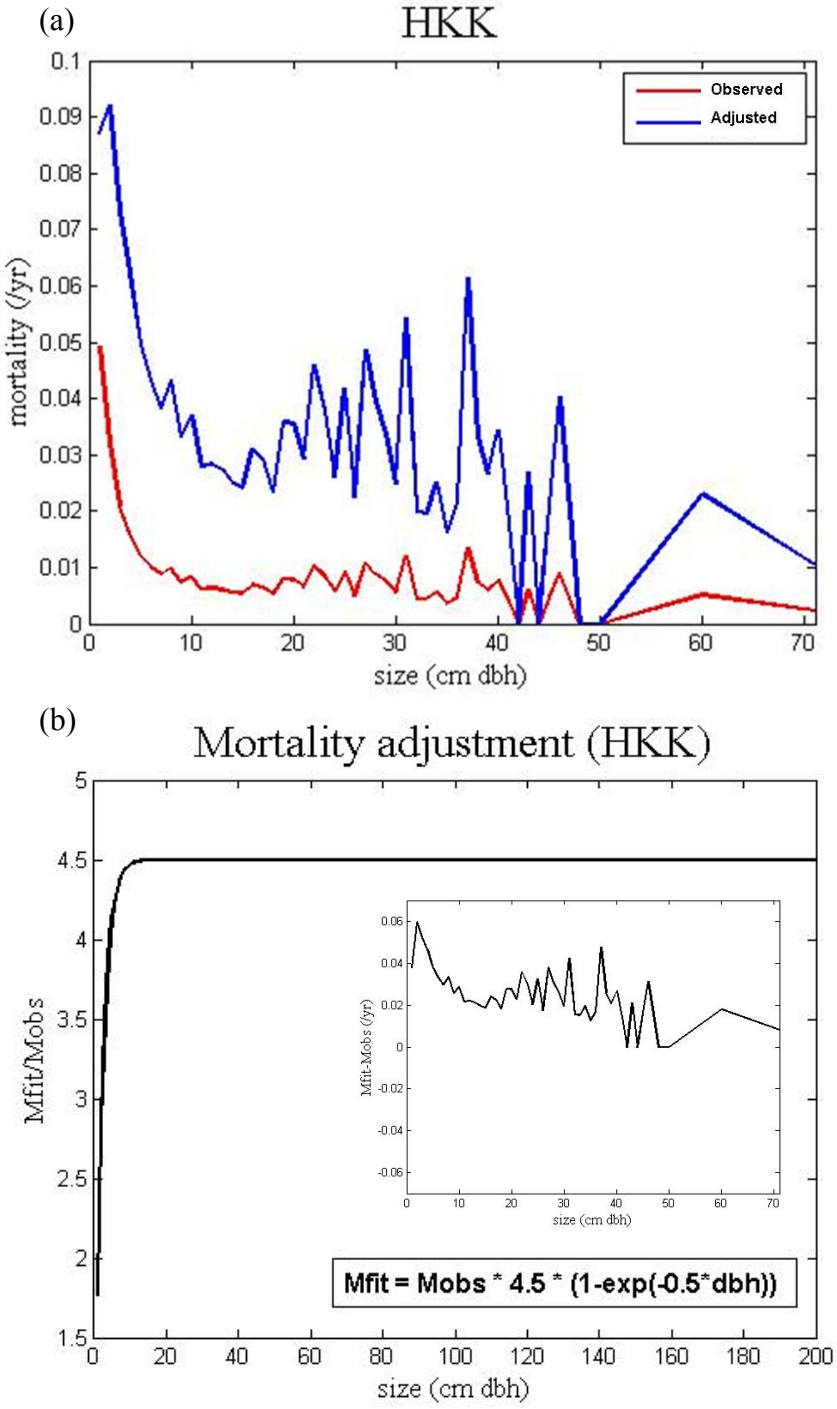

Figure 4.7 Adjusted mortality rates at HKK. (a) Comparison of adjusted (blue line) and observed (red line) mortality rates. (b) The ratio (outer panel) and difference (inner panel) of the fitted (M_{fit}) versus observed (M_{obs}) mortality rates. The equation shows the functional form and parameters used in the adjustment.

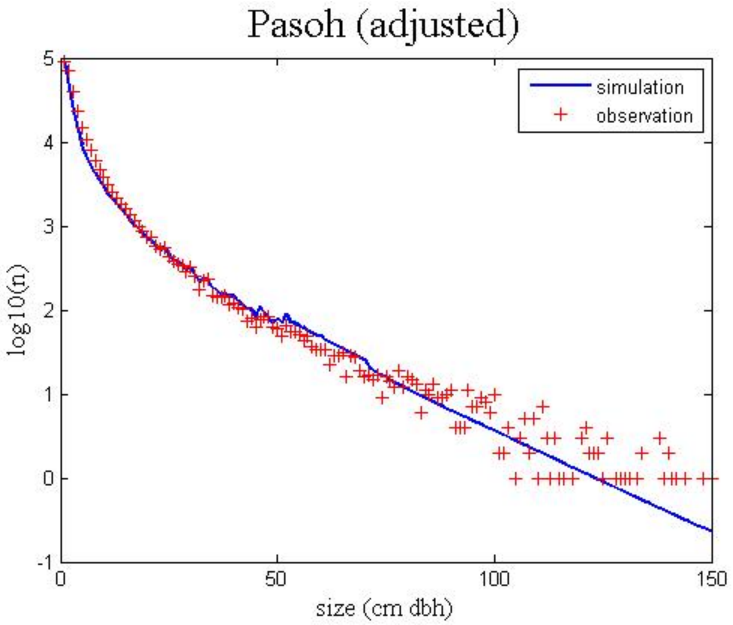

Figure 4.8 Model simulation of stem size distribution at Pasoh, using adjusted tree growth and mortality rates. The blue line is the model output, and the red crosses are the observed size-frequency distribution from the plot census.

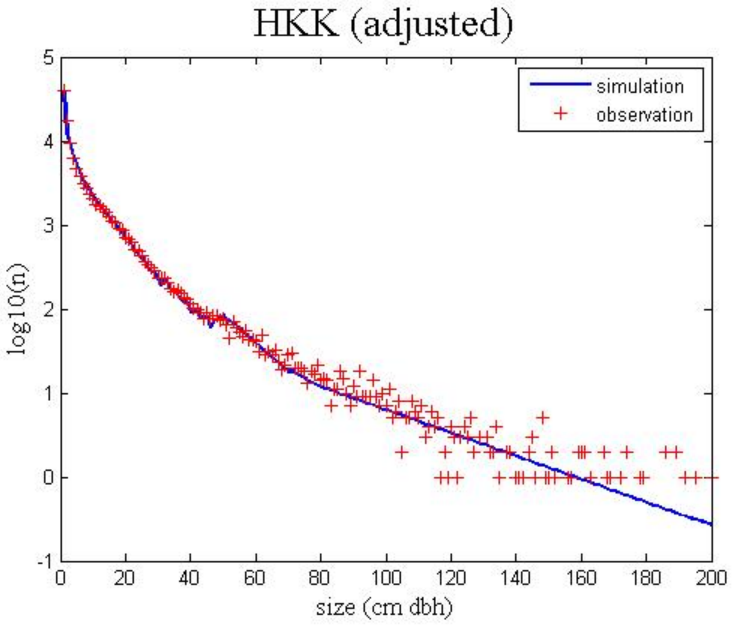

Figure 4.9 Model simulation of stem size distribution at HKK, using adjusted tree growth and mortality rates. The blue line is the model output, and the red crosses are the observed size-frequency distribution from the plot census.

4.3 Comparisons with metabolic scaling theory

In the model developed in the previous section, the growth and mortality rates for each size class were prescribed from the observed mean values calculated for trees of each size class at each site: there are no assumptions of general patterns and/or functional forms of the relationship between those demographic rates and tree stem diameter. Allometric scaling relationships have been used to provide predictions of forest structure and dynamics (e.g. Yoda et al. 1963; Brown 1997; Chave et al. 2005); and more recently, metabolic scaling theory (MST) has been used to relate characteristic properties of forest canopies to stem size (West et al. 2009). Starting from biomechanics and allometric scaling of trees' total mass, incorporating an assumed isometric Euclidean scaling of the canopy and space-filling of the leaves, MST predicts that the size distribution of natural forests should scale as the -2 power of stem radius (Enquist and Niklas 2001; West et al. 1997; West et al. 2009), and that tree growth rate and mortality rate should respectively scale approximately as the 1/3 and -2/3 powers of the stem radius (Enquist et al. 1999).

A test of the inverse square law of stem size-frequency distribution at Lambir, the site which was shown earlier to be the closest to steady-state (Figure 4.1), and thus consistent with the equilibrium assumptions of MST, shows that the observed size structure is consistent with the -2 power law scaling predicted by MST for the mid-sized trees; however, there are deviations for both small trees and trees in the largest size classes (Figure 4.10). Such discrepancies are even greater at Pasoh (Figure 4.11).

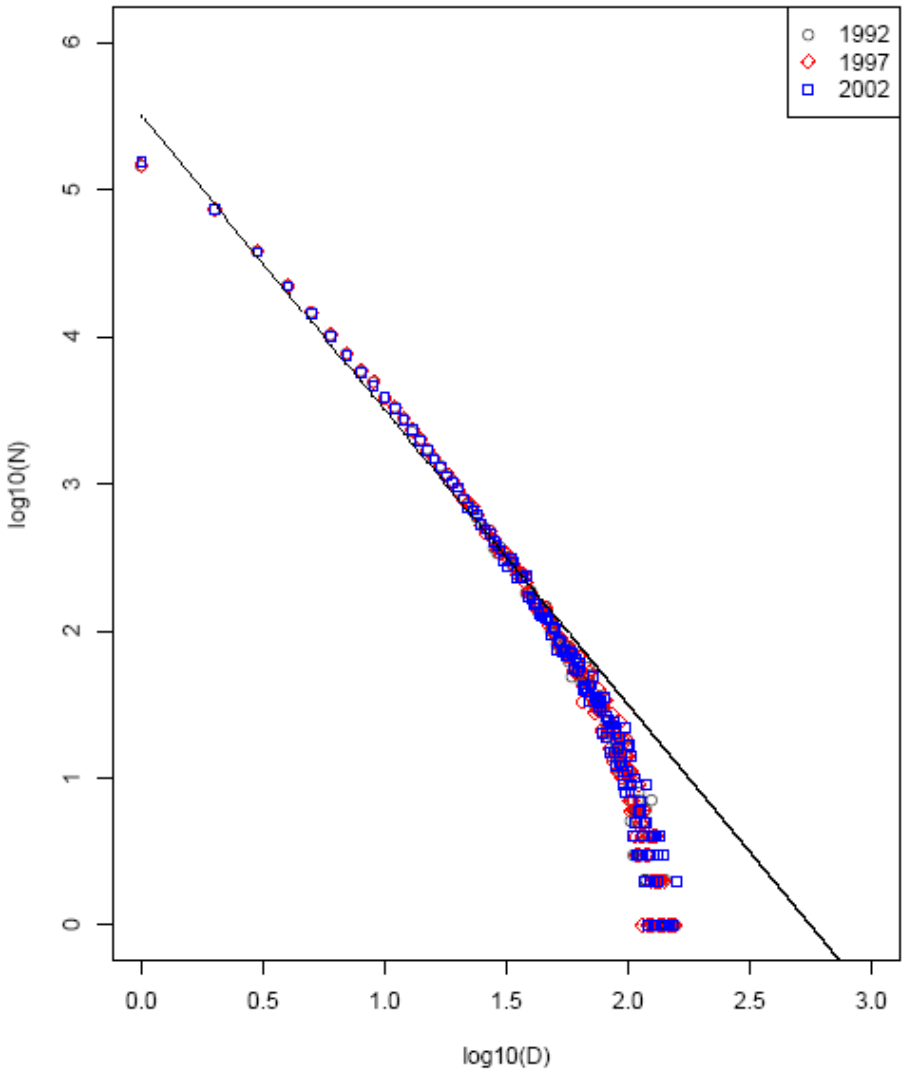

Figure 4.10 Observed stem size-frequency distribution at Lambir. The circles, diamonds, and squares are observations of different censuses (1992, 1997, and 2002, respectively). The straight line is the size distribution predicted by metabolic scaling theory ($N \propto D^{-2}$).

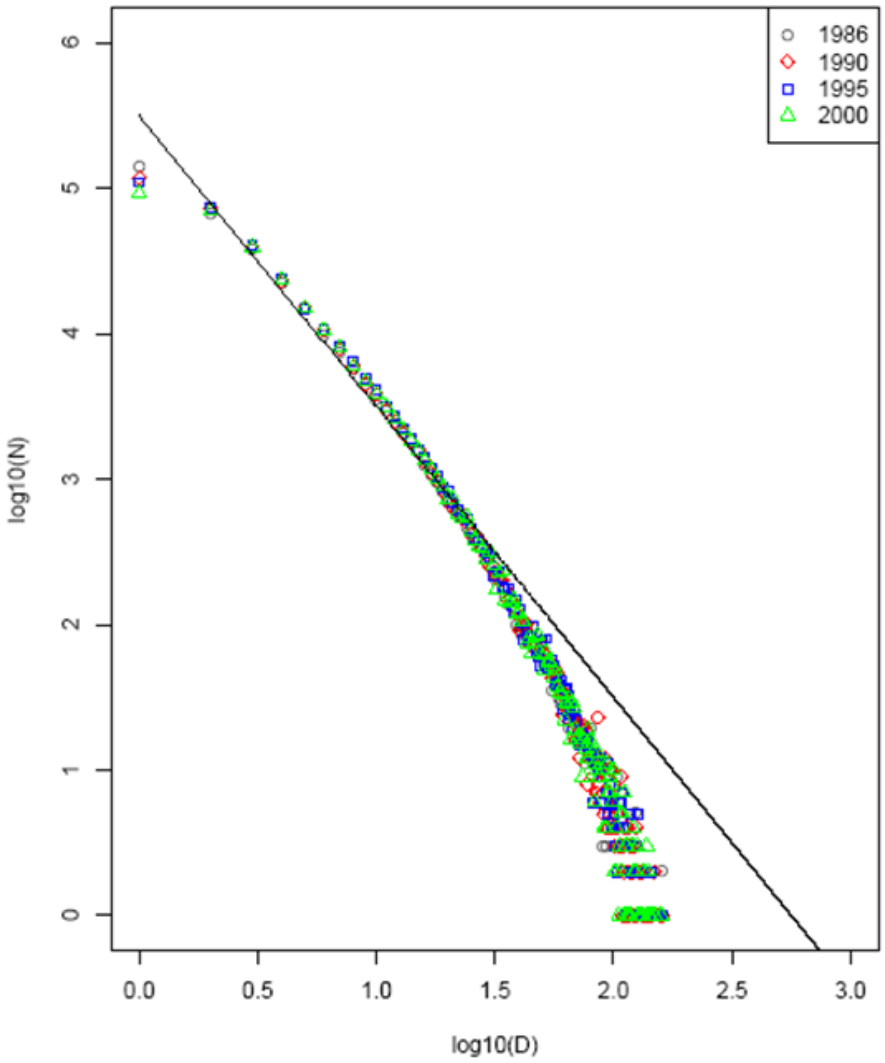

Figure 4.11 Observed stem size-frequency distribution at Pasoh. The circles, diamonds, squares, and triangles are observations of different censuses (1986, 1990, 1995, and 2000, respectively). The straight line is the size distribution predicted by metabolic scaling theory ($N \propto D^{-2}$).

Table 4.2 Exponents of power-law-function fits and metabolic scaling theory (MST) predictions of tree diameter growth rates and mortality rates to tree size.

Site	Growth exponent (95% CI)	Mortality exponent (95% CI)
Lambir	0.59 (0.56 to 0.63)	-0.13 (-0.15 to -0.10)
Pasoh	0.65 (0.62 to 0.68)	0.06 (0.02 to 0.11)
MST prediction	0.33	-0.67

These findings are consistent with the original evaluations of metabolic scaling theory against the observed size structure of other forest plots, in which similar discrepancies occurred in large and small size classes (e.g. Enquist et al. 2009).

Moreover, the exponents of power law functions fitted to the observed growth-size and mortality-size relationships differ considerably from those predicted by metabolic scaling theory at both Lambir and Pasoh, the two sites where the forests were relatively close to steady state (Table 4.2). As Table 4.2 shows, the fitted exponents of the power law functions are significantly different from metabolic scaling theory (1/3 and -2/3 for the growth and mortality exponents, respectively). In both cases, the growth exponents are much higher than the MST prediction; and the mortality exponents are much less negative (or even slightly positive at Pasoh).

However, the power law functional form still seems to be a plausible approximation to the observed growth-size and mortality size relationships and seems to fit the Lambir and Pasoh data reasonably well (Figure 4.12). Thus we can still consider substituting the discrete values of observed tree growth and mortality rates with the power law functions fitted to the data and solve Equation 4.2, which is a

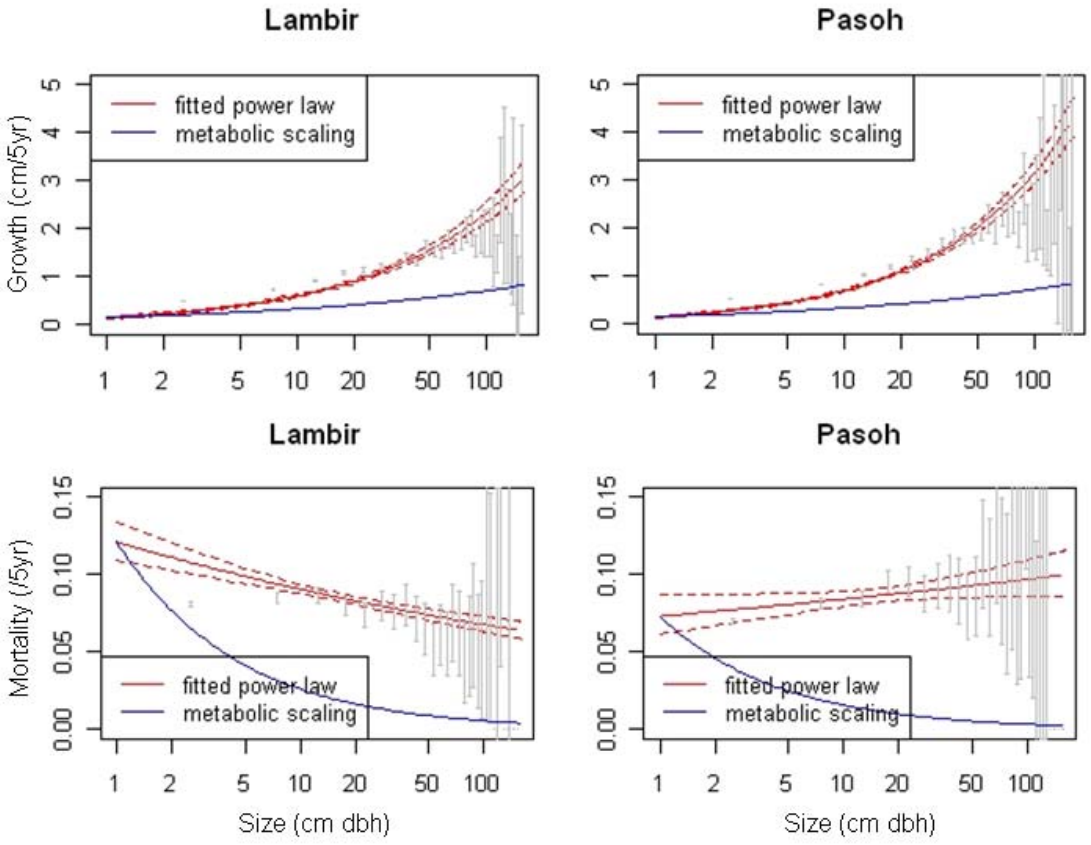

Figure 4.12 Predicted and observed five-year tree growth and mortality rates at Lambir and Pasoh. The grey lines are observed means of growth and mortality rates with 95% confidence intervals. The blue lines are the predicted growth and mortality rates by metabolic scaling theory. The red lines are the fitted power law function curves with 95% confidence intervals (dashed red lines).

continuous time model that provides analytic tractability. The equilibrium solution can be found when the forest is at steady state, i.e.

$$0 = -\frac{\partial}{\partial z}\left[g(z)\ n(z)\right] - \mu(z)\ n(z) \quad , \tag{4.12}$$

where $g(z) = g_0 z^p$ and $\mu(z) = \mu_0 z^q$; p and q are the fitted exponents of growth-size and mortality-size power law functions, and g_0 and μ_0 are the intercepts, respectively. By integrating with respect to z and substituting the boundary condition $n_1 = n(z=1)$, i.e. the observed number of trees in the smallest size class (1 cm dbh), Equation 4.12 can be solved and the solution is:

$$n(z) = n_1 z^{-p} e^{\frac{\mu_0}{g_0}\left(\frac{1-z^{1+q-p}}{1+q-p}\right)} \quad . \tag{4.13}$$

Therefore, with the specified power law relationships of tree growth and mortality rates with size, we can analytically calculate the steady-state stand size structure that arises from given exponents (p, q) and intercepts (g_0, μ_0). Interestingly, the set of exponents proposed by metabolic scaling theory is a special case: with p = 1/3 and q = -2/3, the denominator of the exponential in Equation 4.13 becomes zero (1+q-p=0). It is possible to show that in this case, for particular values of g_0 and μ_0, the otherwise curvilinear n-z relationship becomes a straight-line relationship with slope -2 (see details of the calculations proving this special case in Appendix B).

Thus the metabolic scaling theory prediction of a –2 scaling of the n-z relationship

is a special case of Equation 4.13, and in general, we should expect curvilinear *n*-*z* relationships. Nonetheless, the power law functional form appears to be a reasonable parametric function for describing the observed patterns of growth and mortality (Figure 4.12). When the fitted power law functions for tree growth and mortality rates are used, the partial differential equation model correctly predicts the curvilinear shape of the stand size distributions seen at both Lambir and Pasoh (Figure 4.13).

4.4 Discussion

The results from the case studies of three forest plots provide information on the demographic history and current status of the forests at the three different study sites. Among the three forest plots examined in this study, Lambir is the closest to approaching steady state: the predicted size distribution closely matches the observations (Figure 4.1), indicating that the currently observed tree growth and mortality rates are similar to their historical rates that gave rise to the forest structure. This implies that the forest at Lambir is approximately at equilibrium, i.e. has not experienced any recent change in demography or disturbance that alters the demography of the trees. In contrast, the results of the simulations for Pasoh and HKK both display mismatches between observed and predicted size structure (Figures 4.2 and 4.3). The discrepancies indicate that the observed tree demographic rates are not the long-term mean and the currently observed stem size distributions likely resulted

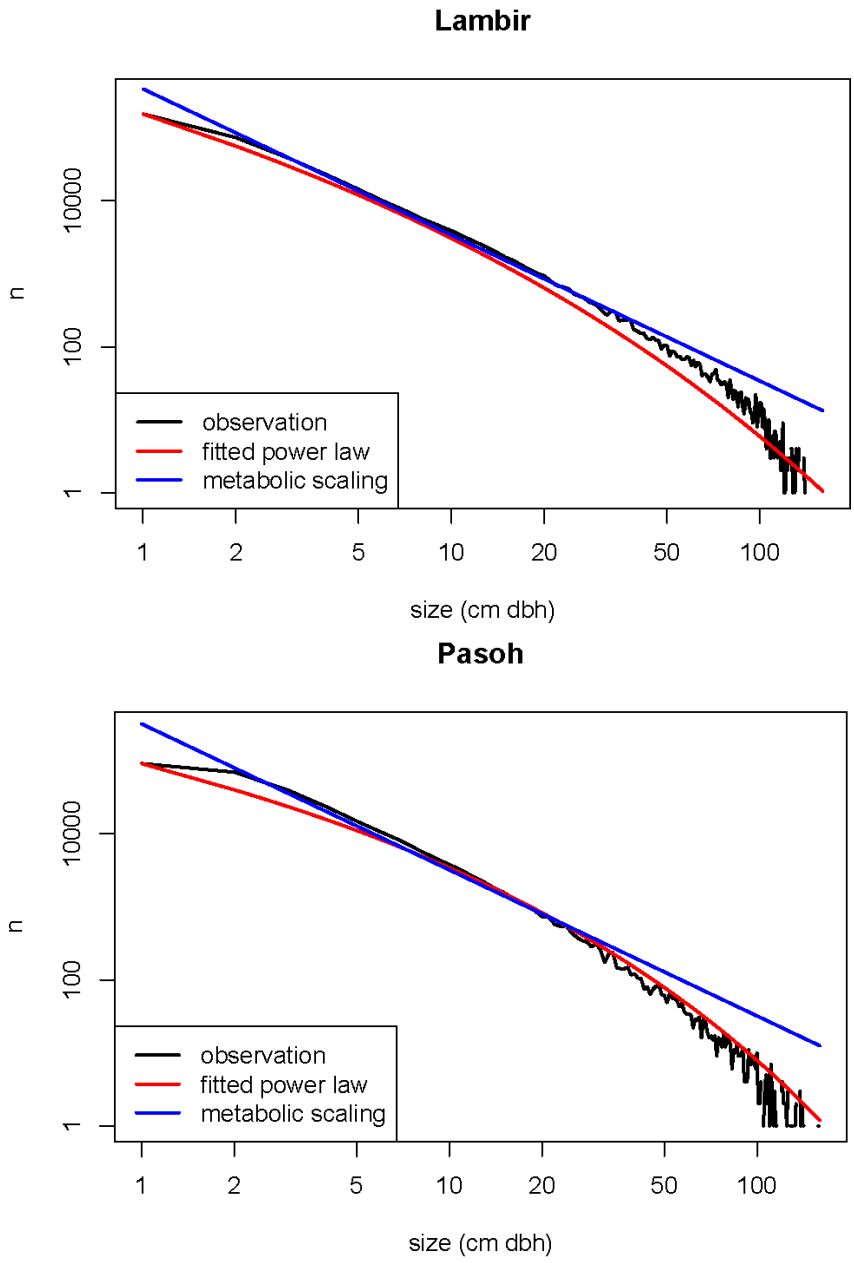

Figure 4.13 Predicted and observed stem size distribution at Lambir and Pasoh. The black lines are observed size distribution. The blue lines are the predictions of metabolic scaling theory ($N \propto D^{-2}$). The red lines are the predictions using the partial differential equation model and power law functional forms for tree growth and mortality rates (Equation 4.13).

from past perturbations or disturbances.

Further analyses of the model using different sets of parameters to find tree growth and mortality that will potentially give rise to the currently observed size structure reveal more clues for the nature and magnitude of the disturbance history of the two sites. The implied historical long-term mean tree growth and mortality rates that would have given rise to the stem size structure of the forest at Pasoh are different from the currently observed growth and mortality rates, with growth 4% lower than the current observed rates (Figure 4.4) and mortality on average 3% higher than the current observed rates (Figure 4.5). Such results imply that no major disturbance has occurred at Pasoh. The forest is relatively close to equilibrium, but has experienced mild perturbations that have reduced tree growth rates and increased mortality. Likely candidates are two fold. First, changes in climate factors (e.g. temperature, precipitation, etc.) may have influenced the forest's demography. We have already seen variations in tree growth rates at Pasoh associated with climate variability (Chapters 2 and 3). Second, small-scale disturbances may have been stronger in the past, but only influenced a small area. The current model does not have a spatial component to test this hypothesis. Nevertheless, it is a plausible explanation: the gaps created in the plot will reduce the overall stem density and the reduced growth and increased mortality of trees in part of the plot will still influence the site-wide mean growth and mortality rates. Pasoh is known to have experienced small-scale wind-throws and animal disturbances, such as wild pigs and termites (Losos and Leigh 2004, Tho 1982).

The analysis at HKK shows a quite different case: the fitted growth rates are almost identical to those observed, except for the smallest size classes (Figure 4.6), but the fitted mortality rates are a lot higher than the observed values, with an average of 0.03 per year and generally 3.5 times higher than the observation (Figure 4.7). This result implies catastrophic disturbance events severe enough to kill large numbers of trees. This is consistent with the findings of a recent study of the disturbance history and historical stand dynamics of the forest at HKK, which indicated widespread disturbances of variable intensity have occurred at least three times in the past century, and background and gap formation were evident in every decade since 1790 (Baker et al. 2005). It is also known that widespread fires occur approximately every 3-10 years in the area; and wind-throws and elephants also cause numerous tree falls and tree damage in the plot (Losos and Leigh 2004).

In Section 4.3, I have compared the metabolic scaling theory predictions of forest size distributions and tree demographic rates with the empirical data and shown that MST does not predict the general pattern of forest structure and dynamics. However, the power law functional form appears to be a reasonable parametric function for describing the observed patterns of growth and mortality (Figure 4.12) and, when inserted in a partial differential equation model, correctly predicts the curvilinear shape of the observed stand size distributions (Figure 4.13).

The potential of the size-structured model using phenomenological functions of tree demographic rates to yield realistic predictions of forest structure leads us to develop a dynamic model that is capable of predicting the forest structure at any stage,

using demographic rates updated at each time step. This new model will be introduced in the next chapter.

Chapter 5

Dynamic scaling theory yields improved predictions of forest structure and dynamics

In the previous chapter, I showed how a size-structured integral projection model that uses simple phenomenological functions to describe size related variation in growth and mortality can be used to relate forest demographic rates to the resulting forest structure. I also tested the ability of power law functional forms (e.g. those proposed by the metabolic scaling theory) to relate characteristic properties of forest canopies to stem size. The functions were able to describe the observed patterns reasonably well, but there were still limitations in the previous formulation. In particular, as in metabolic scaling theory, the demographic rates were assumed to be constant and unaffected by current stand structure. In this chapter I introduce a dynamic scaling theory that yields more accurate predictions of the observed size distributions and growth and mortality rates. The dynamic scaling theory presented here builds upon the basic assumptions of conventional metabolic scaling theory,

retaining the allometric relationship for canopy leaf area as a function of tree size. However, it also incorporates the density-dependent impact of forest structure upon forest light profiles and resulting tree demographic rates. I then show how this model is also capable of predicting the transient, time-dependent dynamics of forest demography and structure as forests reach their steady-state equilibrium, and capturing the characteristic timescales for these processes. In doing so, this dynamic scaling theory bridges the simplicity and generality of metabolic scaling theory and the accuracy and predictive capabilities of empirically-calibrated size-structured models of forest structure and dynamics.

5.1 Introduction

As noted in Chapter 4, metabolic scaling theory (MST) has been proposed as a zeroth-order theory that uses allometric scaling relations between tree size and rates of plant metabolism in conjunction with assumptions regarding the space-filling architecture of plant canopies to predict forest canopy structure and associated rates of tree growth and mortality (West et al. 2009; Enquist et al. 2009). The over-arching prediction of the theory is that “the forest is the tree” (West et al. 2009). This means that the equilibrium size distribution of trees and the distribution of energy and material fluxes across tree size classes scale in an identical manner to the size distribution of branches within trees and the distribution of energy and material fluxes.

Table 5.1 Similarity of predicted scaling relations for branches within a tree and for trees within a forest proposed by metabolic scaling theory (MST; West et al. 2009).

Scaling Quantity	Individual Tree	Entire Forest
Area preserving	$\frac{R_{i+1}}{R_i} = \frac{1}{n^{1/2}}$	$\frac{r_{k+1}}{r_k} = \frac{1}{\lambda^{1/2}}$
Space filling	$\frac{L_{i+1}}{L_i} = \frac{1}{n^{1/3}}$	$\frac{l_{k+1}}{l_k} = \frac{1}{\lambda^{1/3}}$
Biomechanics	$R_i^2 = L_i^3$	$r_k^2 = l_k^3$
Size distribution	$\Delta N_i \propto R_i^{-2} \propto M_i^{-3/4}$	$\Delta n_k \propto r_k^{-2} \propto m_k^{-3/4}$
Energy and material flux	$B_i \propto R_i^2 \propto N_i^L \propto M_i^{3/4}$	$B_k \propto r_k^2 \propto n_k^L \propto m_k^{3/4}$

across branch size classes (Table 5.1; West et al. 2009; West et al. 1999)

In particular, with regard to forest structure and dynamics, MST predicts that the size-frequency distribution of natural forests should scale as the -2 power of stem diameter (Enquist and Niklas 2001; West et al. 1997), and that stem diameter growth rates and mortality rates should respectively scale approximately as the 1/3 and -2/3 powers of the stem diameter (Enquist et al. 1999). However, many studies have found that the exponents or functional forms relating abundance, growth and mortality to tree size often differ from the predictions from metabolic scaling theory (e.g. Muller-Landau et al. 2006a; Muller-Landau et al. 2006b; Russo et al. 2007; Coomes et al. 2003). For example, Table 5.2 shows the observed growth-size and mortality-size exponents fitted to power law functions at three tropical forest sites: Barro Colorado

Island (BCI) in Panama, Lambir in Malaysian Borneo and Pasoh in Peninsular Malaysia. At all three sites the exponents differ markedly from those predicted by MST.

In this chapter I develop a new dynamic scaling theory (DST) that builds upon the principles of MST regarding the allometric scaling of individual plant characteristics, but combines them with the ecological principles of density-dependent, height-structured competition between individual trees for light within forest canopies. I show that DST yields greatly improved predictions of tree demographic rates and size-frequency distributions. I also show that this new model is able to predict realistic time-varying changes in tree growth and mortality rates and forest size structure when stands are perturbed away from equilibrium, and their subsequent dynamical convergence to an equilibrium forest structure and demography.

Table 5.2 Exponents of power-law-function fits of tree diameter growth rates and mortality rates to tree size in three tropical forests. The bottom line shows the predicted exponents in metabolic scaling theory (MST).

Site	Growth exponent (95% CI)	Mortality exponent (95% CI)
Lambir, Malaysia	0.59 (0.56 to 0.63)	-0.13 (-0.15 to -0.10)
Pasoh, Malaysia	0.65 (0.62 to 0.68)	0.06 (0.02 to 0.11)
BCI, Panama	0.70 (0.66 to 0.74)	-0.08 (-0.12 to -0.03)
MST prediction	0.33	-0.67

5.2 Methods

The essential components of DST are summarized in Figure 5.1. On the scale of individual plants, DST adopts the same fundamental assumptions and principles as MST: namely, that a hierarchical, space-filling geometry within individual plant crowns results in a characteristic power law allometric scaling of leaf biomass and resulting leaf area with tree size. At the canopy scale, however, DST replaces MST's assumptions of energetic equivalence, hierarchical space filling geometry, and a steady-state equilibrium forest structure with a dynamical equation describing the demography of a forest canopy in which rates of individual tree growth and death are influenced by density-dependent, height-structured competition for light. As a result, in DST the demographic rates vary depending on the current canopy structure.

The light profile, *I(z,t)*, is calculated in terms of the fraction of incoming light at the top of the canopy reaching each size class (*z*) at time *t*, and is calculated from the canopy's current leaf area index (LAI) profile *L(z,t)* using the Beer-Lambert law (assuming a canopy extinction coefficient *k* of 0.5; Sands 1995). The LAI profile of the forest canopy is, in turn, determined by the current forest structure, using empirical allometric scaling relationships (Reich et al. 1997; Saldarriaga et al. 1988; Moorcroft et al. 2001). Specifically,

$$I(z,t) = e^{-k\int_z^\infty L(z,t)dz} \tag{5.1}$$

$$L(z,t) = B_l(z) \cdot SLA \cdot n(z,t) / A_{plot} \quad , \tag{5.2}$$

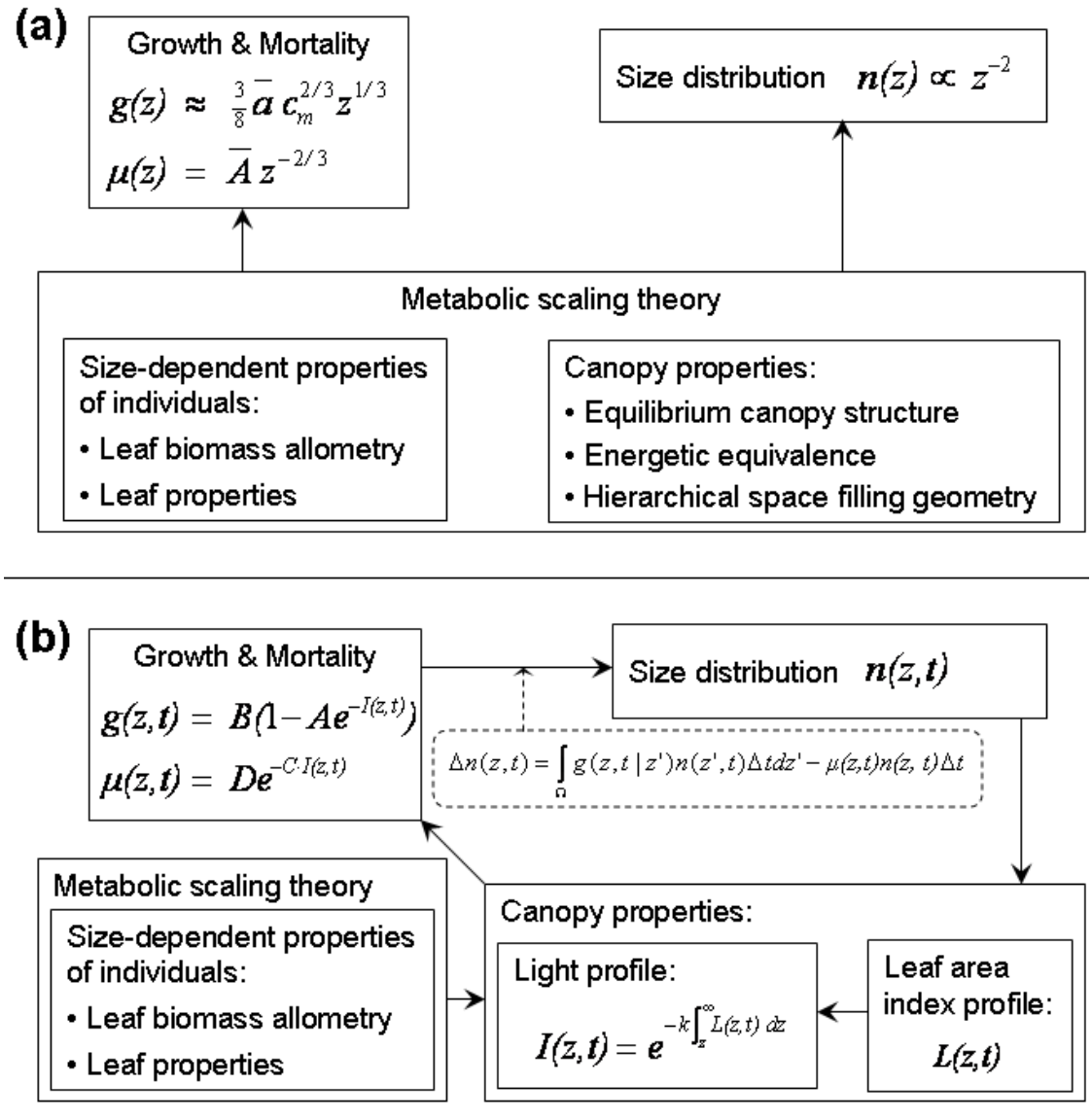

Figure 5.1 Schematic diagrams of (a) Metabolic Scaling Theory (MST) and (b) Dynamic Scaling Theory (DST).

where A_{plot} is the size of the plot, SLA is the specific leaf area and $B_l(z)$ is the function relating plant's leaf biomass B_l to its size z. I used a representative value for the SLA for a tropical tree (16.0 m^2 leaf per kg of leaves; Reich et al. 1997). The allometric scaling relationship for leaf biomass (B_l) is derived from empirical height-diameter (O'Brien et al. unpublished data) and leaf allometric data (Saldarriaga et al. 1988) for tropical trees and using a representative average value for tree wood density of 0.6 g/cm^3. Taken together, these yield the following relationship between a plant's size (cm diameter) and leaf mass (kg biomass):

$$B_l(z) = 0.0316 \cdot z^{1.56} . \tag{5.3}$$

Under the assumption that a tree's growth and mortality rates respectively increase and decrease as exponential functions of the amount of light it receives, the current demographic rates of the canopy are given by:

$$g(z,t) = B(1 - Ae^{-I(z,t)}) \tag{5.4}$$

$$\mu(z,t) = De^{-C \cdot I(z,t)}. \tag{5.5}$$

The coefficients were estimated by fitting these equations to the long-term mean values of the observed growth and mortality rates at each study site using generalized linear models.

Growth and mortality rates are then calculated and used in the integral projection model (see Equations 4.5-4.9 in Section 4.1) to predict the stem size distribution in the following time step. As in Chapter 4, the probabilities of trees growing into larger size

classes follow a Poisson distribution with rate parameter $g(z,t)\,\Delta t$, and the probabilities of death follow a Bernoulli distribution with probability $\mu(z,t)\,\Delta t$ of mortality per individual per time step, where $g(z,t)$ and $\mu(z,t)$ are the current growth and mortality rates calculated using Equations 5.1-5.5. These equations relate $g(z,t)$ and $\mu(z,t)$ to the current canopy structure $n(z,t)$.

The derivation and solution of the integral projection model used in this study (Equation 5.6) are presented and discussed in detail in Chapter 4 (see *4.1 Model formulation*), and thus are not further explained here.

$$\Delta n(z,t) = \int_{\Omega} g(z,t \mid z')n(z',t)\Delta t dz' - \mu(z,t)n(z,t)\Delta t \quad . \qquad (5.6)$$

5.3 Results

I used data from three old-growth forests from the Center for Tropical Forest Science (CTFS) network of large-scale forest dynamics plots: Barro Colorado Island (BCI) in Panama (9°09' N, 79°51' W), Lambir in Malaysian Borneo (4°10' N, 114°01' E) and Pasoh in Peninsular Malaysia (2°58' N, 102°18' E). Descriptions of these forest plots can be found in Chapter 2 (See Section 2.2.1 and Table 2.1). Growth and mortality rates were calculated in the same manner as described in Chapter 4 (see Section 4.2). Table 5.3 lists all the fitted parameters for Equations 5.4 and 5.5 using the observed long-term mean growth and mortality rates of each size class at the three

Table 5.3 Fitted parameters for Equations 5.4 and 5.5 at each study site.

Site	A	B	C	D
Lambir, Malaysia	0.973	4.208	0.411	0.094
Pasoh, Malaysia	1.064	5.386	-0.218	0.080
BCI, Panama	1.114	7.479	0.303	0.110

sites. The size-frequency distributions of all censuses were used for comparison with the model output.

When applied at three old-growth tropical forest sites, the equilibrium forest structure and demography predicted by DST closely matches the observed stand size-frequency distributions (Figure 5.2a-c), and the observed patterns of tree growth and mortality (Figure 5.2d-i). In contrast to MST, which predicts that tree abundance declines as a -2 power of tree size, DST captures the observed curvilinear nature of the log-log relationship between tree size and abundance that is apparent at all three sites (Figure 5.2a-c). DST also yields markedly improved predictions for relationships between tree size and growth and mortality rates at all of the three tropical forest sites (Figure 2d-i).

The replacement of the equilibrium assumption of MST with a dynamic, density-dependent equation of forest growth means that DST can be used to predict the time-dependent changes in the structure and dynamics of the forest canopy over time from any given starting condition. Figure 5.3 shows an example of time-dependent successional dynamics of the BCI forest. Starting from a near-bare ground condition in

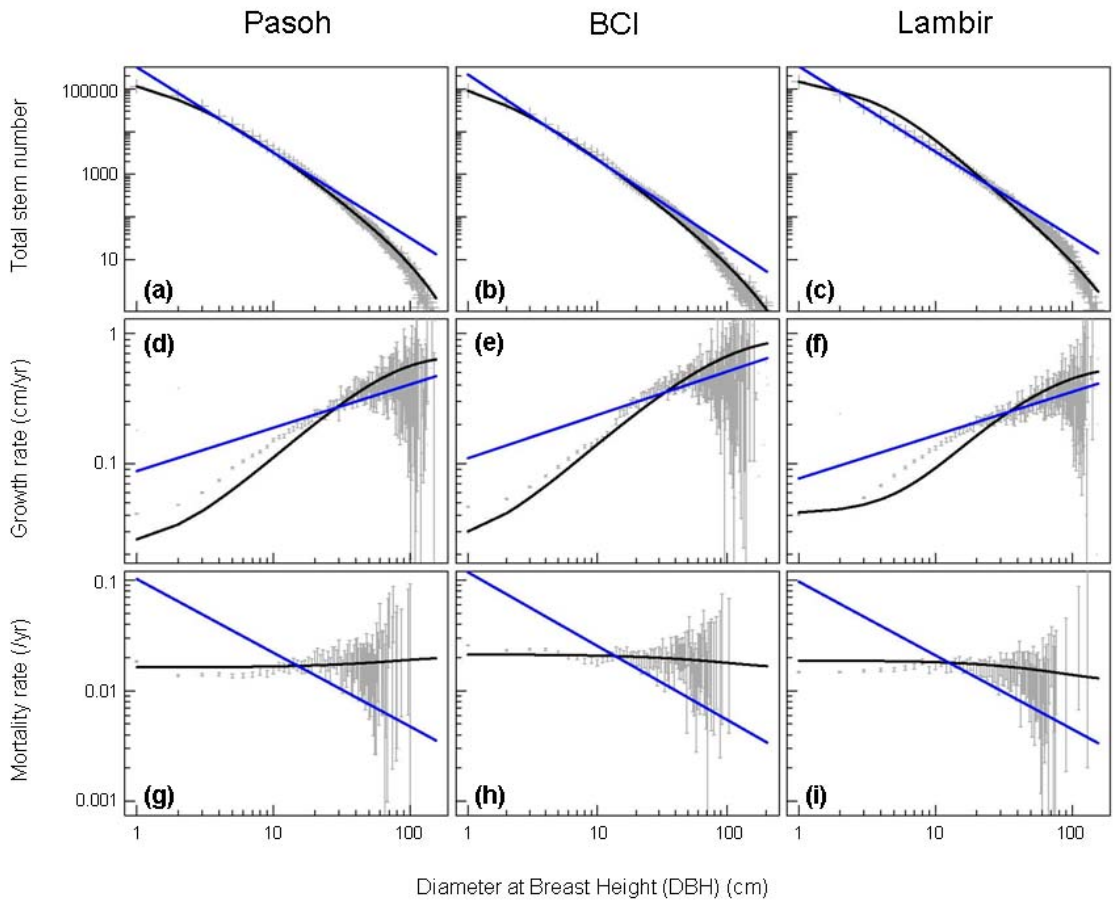

Figure 5.2 Comparisons of DST and MST predictions for three tropical forest sites. (a)-(c) Stem size-frequency distribution. (d)-(f) Diameter growth rate (cm/yr) in relation to tree size. (g)-(i) Mortality rate (/yr) in relation to tree size. Black lines are DST predictions, and blue lines are MST predictions. Observed stem numbers for various censuses are shown as grey crosses in (a)-(c). Grey lines in (d)-(i) are observed means of growth and mortality rates with 95% confidence intervals.

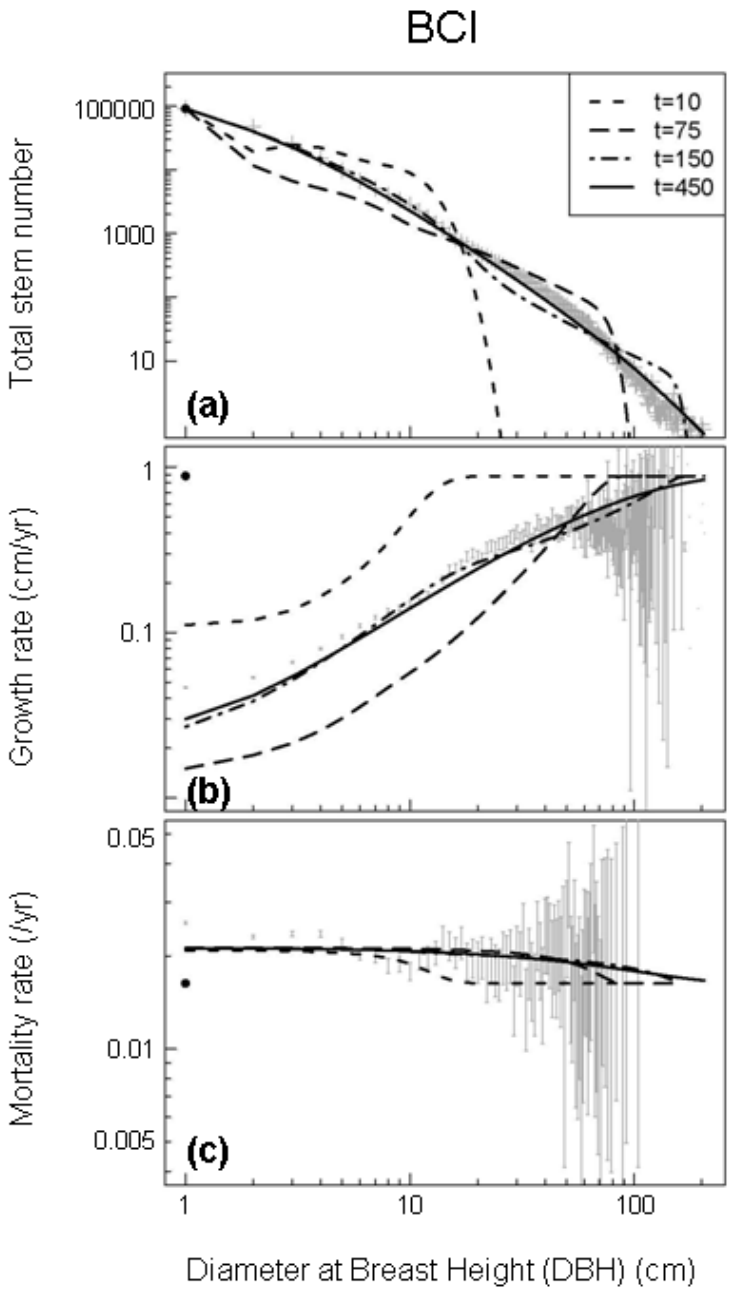

Figure 5.3 DST predictions for BCI at different time steps. (a) Stem size-frequency distribution. (b) Diameter growth rate (cm/yr) in relation to tree size. (c) Mortality rate (yr) in relation to tree size. Observed stem numbers for various censuses are shown as grey crosses in a. Grey lines in (b) and (c) are observed means of growth and mortality rates with 95% confidence intervals.

which only individuals in the smallest (1 cm diameter) size class are present, light availability is initially high, resulting in fast rates of tree growth and relatively lower mortality rates, especially for the largest trees at leading edge of the size distribution. After a decade (short dashed line in Figure 5.3a), the canopy has a large number of trees between 3-15 cm diameter. However, over the following decades, thinning occurs as the rates of tree growth slow and mortality rates increase as light becomes limiting. By 75 years (long dashed line in Figure 5.3a) there are fewer individuals below 20 cm diameter and the number of leading large trees has also decreased significantly. As the canopy continues to develop, the distribution of individuals (Figure 5.3a) and their rates of growth and mortality (Figure 5.3b and 5.3c, respectively) converge to their respective equilibrium patterns, which closely match the observed distributions of these quantities (solid line in Figure 5.3a-c).

5.4 Discussion

As Figure 5.3 illustrates, the non-equilibrium nature of DST reflects the biological reality that the growth rates, mortality rates, and size distribution within the plant canopy interact and dynamically co-evolve to yield the forest's characteristic equilibrium structure and demography. The characteristic equilibrium scaling relationships of abundance, growth and mortality with tree size are thus emergent properties that arise from the interaction between the allometric properties of

individual trees and density-dependent, height-structured competition for light within the forest canopy.

Unlike MST that predicts identical scaling of abundance, growth and mortality with plant size within all forest canopies, the dynamic scaling theory presented here explicitly incorporates site-specific variation in the life-history parameters relating light availability to rates of growth and mortality at each forest site. Embodied in these parameters are site-specific differences in environmental forcing and life-history properties of the species found in different forests. While these site-specific parameters mean that DST is more complex than the universal predictions of zeroth-order MST, it is clear from results shown in Table 5.1 and Figure 5.2 that such site-specific differences in life-history parameters do indeed occur, and that accounting for these differences results in markedly improved predictions of the equilibrium patterns of tree growth and mortality rates as well as the resulting stand structure in different forests.

An important question not addressed by the analysis shown here is understanding the reasons for the life history differences of trees at each study site reflected by the differences in the parameters estimated for the relationships of tree growth and mortality rates against light availability (Equations 5.4 and 5.5; Table 5.3). These differences likely reflect variations both in the intrinsic biological properties of the tree species and in the physical environment such as topography and climate forcing across the sites.

As I have shown here, the incorporation of the dynamical interplay between stand structure, light profiles, and resulting rates of growth and mortality within forest canopies embodied in DST addresses important limitations of MST highlighted in recent studies (e.g. Coomes et al. 2003). Unlike MST, DST can be applied in non-equilibrium situations, including the dynamics of forest re-growth following natural or human disturbances (such as those that have occurred at Huai Kha Khaeng), and transient changes in forest demography and size distributions following climate change.

Chapter 6

Conclusions

As stated in Chapter 1, in this thesis I have sought to better understand how differences in climate impact tropical forest structure and address two inter-related sets of questions:

(1) Are tropical forests changing in their dynamics and structure as a result of on-going climate change? If so, in which direction? And why?

(2) To what extent can we account for the different structure and dynamics of different tropical forests? And to what extent do these differences affect their responses to changes in environmental forcing?

I use both empirical field measurement data analyses and mathematical modeling approaches to address these questions. Here I conclude the thesis with the key results of my analyses and discuss directions of future research.

6.1 Key findings

In Chapters 2 and 3, I addressed the first set of questions I posed in the research objectives (see Section 1.2), i.e. whether and how tropical forests are changing in their dynamics and structure as a result of on-going climate change.

I reviewed changes in tree growth rates at four long-term permanent tropical forest research plots (Pasoh and Lambir in Malaysia, Huai Kha Khaeng in Thailand, and Barro Colorado Island in Panama) in relation to site level differences in temperature, precipitation, and solar radiation. I found a positive correlation between five-year temporal variation in stand-level tree growth rates and variation in incoming solar radiation, and a negative correlation between tree growth rates and night-time temperatures. No significant relationship was found between stand-level tree growth rates and total precipitation at any of the sites in this analysis. Taken alone, neither solar radiation variability nor the negative effects of night-time temperature explain the changes in growth rates at all sites. However, when considered together these two climate variables explain most of the observed changes in tree growth rates over time.

I then presented results from a newly initiated and currently on-going study using dendrometer bands to measure inter- and intra-annual variations in tree growth rates at four tropical forest plots along a latitudinal gradient in Southeast Asia (Pasoh in Malaysia, Huai Kha Khaeng and Khao Chong in Thailand, and Xishuangbanna in China). The results revealed new information about relationships between tree growth and climate variability that were not evident in the analyses using the 5-year census

data. In particular, the positive relationship between precipitation and tree growth rate is seen more clearly with shorter time scale measurements that allow some separation of dry and wet seasons. Moreover, the patterns of growth responses to increasing mean minimum temperature are shown to shift along the latitudinal gradient. These trends are consistent across tree species with different life history traits. Trees respond positively to increases in light availability regardless of their initial size. This pertains except for when precipitation rates are low and the trees are, presumably, water stressed. In addition, I used the dendrometer measurement data to examine patterns of within-site variability in tree demography. My analyses showed that trees of lower wood density generally grow faster in diameter than those of denser wood at all of the three sites examined; and slope steepness exerted positive influences on tree growth at one site (Khao Chong), especially for small-sized trees.

Chapters 4 and 5 addressed the second set of questions in the research objectives, i.e. understanding the differences in structure and dynamics of different tropical forests and relating them to differences in environmental forcing.

I used a size-structured integral projection model that incorporates phenomenological functions to relate current forest demographic rates and the forest structure that would result from these demographic rates if they are maintained. The model provided insights into the demographic history and current status of the forest, as was shown in case studies of three different forest plots in Southeast Asia (Lambir and Pasoh in Malaysia, and Huai Kha Khaeng in Thailand). The predicted size distribution closely matches the observations at Lambir, indicating that the currently

observed tree growth and mortality rates are similar to the historical rates that gave rise to the forest structure. The forest at Lambir is close to its equilibrium size structure. The results of the analysis of Pasoh implied that that no major disturbance has occurred and the forest is relatively close to equilibrium, but has been impacted by either mild disturbances or changes in climate forcing that have reduced tree growth rates and increased mortality rates. In contrast, the model simulation with observed growth and mortality rates at Huai Kha Khaeng over-predicted the size distribution, and further analysis provided evidence for higher mortality rates as a result of major disturbances in the past. I also discussed and compared some of the predictions from metabolic scaling theory (MST), using the same study sites, and found that MST cannot predict the general pattern of forest structure and dynamics. However, the power law functional form proposed in MST appeared to be a reasonable parametric function for describing the observed patterns of growth and mortality.

I then presented a new model, dynamic scaling theory (DST), which builds upon the basic assumptions of conventional metabolic scaling theory, retaining the allometric relationship for canopy leaf area as a function of tree size, but incorporating the density-dependent impact of forest structure upon forest light profiles and resulting tree demographic rates. DST yields more accurate predictions of the observed size distributions and growth and mortality rates than conventional MST. When applied at three old-growth tropical forest sites (Pasoh and Lambir in Malaysia, and Barro Colorado Island in Panama), the equilibrium forest structure and demography predicted by DST closely matched the observed stand size-frequency distributions,

and the observed patterns of tree growth and mortality. DST is also capable of predicting both the transient, time-dependent dynamics of forest demography and structure as forests reach their steady-state equilibrium, and the characteristic timescales for these processes.

6.2 Future directions

Although the results from the dendrometer band study presented in Chapter 3 consisted of only two to three years, or four to six measurement intervals, of tree growth data, they provide a useful complement to the five-year plot census data and valuable insight into changes in tree growth in relation to climate variability in the four Asian tropical forests studied in this project. The geographical positions of the four study sites along the latitudinal and seasonality gradient and the intrinsic similarity among the forests made it possible for comparisons among the responses of those forests to different patterns of changes in environmental forcing. In particular, the shifts in the patterns of growth-temperature relationships from the southern to northern plots suggested possible latitudinal influences on trees' growth responses to increasing mean minimum temperature. This finding offers a plausible explanation for the conflicting trends in tree growth rates observed in different tropical forests (e.g. Clark et al. 2003; Feeley et al. 2007; Phillips et al. 2004). As the dendrometer band study continues and more measurements are made over time, it will be possible to verify these results from the first three years' data with more measurement intervals

encompassing more of the different seasonality and variability in climatic factors. More information of mortality will also be available as time goes by, and it will be possible to examine the relationship between mortality and climate variability on sub-annual time scales. These measurements, combined with the 5-year plot-wide census data, will allow me to gain further insights into the dynamics of these different forests in relation to climate change.

The dynamic scaling theory (DST) presented in Chapter 5 bridges the simplicity and generality of metabolic scaling theory (MST), and the accuracy and predictive capabilities of empirically-calibrated size-structured models of forest structure and dynamics. Whereas the conventional MST only applies to forests at equilibrium (i.e. at steady state; West et al. 2009; Enquist et al. 2009), the incorporation of the dynamic interplay between stand structure, light profiles, and resulting rates of growth and mortality within forest canopies embodied in DST enables it to be applied in non-equilibrium situations. Many studies have found that the exponents or functional forms relating abundance, growth and morality to tree size are often different from the predictions of MST (e.g. Muller-Landau et al. 2006a; Muller-Landau et al. 2006b; Russo et al. 2007; Coomes et al. 2003). But DST explicitly incorporates site-specific variation in the life-history parameters and yields more accurate predictions of the observed stem size distributions and tree growth and mortality rates at each site.

Future work is needed to understand these differences in growth and mortality parameters in relation to differences in both forest composition and climate forcing in order to address the second part of the research question posed in Section 1.2

(understanding the two-way interactions between tropical forest structure and dynamics and their responses to changes in environmental forcing). The new dynamic scaling theory developed here is also capable of predicting the transient, time-dependent dynamics of forest demography and structure as forests reach their steady-state equilibrium, and the characteristic timescales for these processes. Therefore, DST provides a useful framework for studying the dynamics of forest re-growth following natural or human disturbances of any kind and intensity, or transient changes in forest demography and stem size distributions occurring in response to changes in climate forcing.

Appendix A

Supplementary materials for Chapter 3

Table A.1 Results of linear regression models of climate variables (P: precipitation; T: temperature; R: radiation). *: $p \leq 0.05$; (*): $0.05 < p \leq 0.10$.

Sites	X	Y	Slope	d.f.	R^2	p-value
All	P	T	0.033	18	0.54	<0.001*
HKK	P	T	0.020	3	0.33	0.31
KC	P	T	-0.0026	2	0.048	0.78
Pasoh	P	T	-0.0009	3	0.019	0.83
Pasoh	P	R	-0.10	3	0.17	0.50
Pasoh	T	R	3.2	3	0.70	0.08(*)
XSBN	P	T	0.045	4	0.74	0.03*
XSBN	P	R	0.26	4	0.79	0.02*
XSBN	T	R	4.4	4	0.62	0.06(*)

Table A.2 Results of linear regression models of relative growth rates against climate variables (P: precipitation; T: temperature; R: radiation). *: $p \leq 0.05$; (*): $0.05 < p \leq 0.10$.

Sites	Y	Slope	d.f.	R^2	p-value
All	P	0.000074	18	0.49	<0.001*
All	T	0.0013	18	0.32	0.009*
HKK, KC, Pasoh	P	0.000095	12	0.45	0.009*
HKK, KC, Pasoh	T	0.0026	12	0.25	0.07(*)
Pasoh, XSBN	P	0.000064	9	0.62	0.004*
Pasoh, XSBN	T	0.0011	9	0.45	0.02*
Pasoh, XSBN	R	0.000047	9	0.04	0.58
HKK	P	0.000099	3	0.46	0.21
HKK	T	0.0029	3	0.40	0.25
KC	P	0.000053	2	0.19	0.57
KC	T	0.0016	2	0.02	0.84
Pasoh	P	0.000083	3	0.38	0.27
Pasoh	T	-0.014	3	0.83	0.03*
Pasoh	R	-0.00033	3	0.85	0.03*
XSBN	P	0.000069	4	0.84	0.01*
XSBN	T	0.0013	4	0.91	0.003*
XSBN	R	0.00014	4	0.40	0.18

Table A.3 Results of multiple linear regression models of relative growth rates against climate variables (P: precipitation; T: temperature; R: radiation). *: $p \leq 0.05$; (*): $0.05 < p \leq 0.10$.

Sites: H: HKK; K: KC; Pa: Pasoh; X: XSBN

Sites	Y_1	Slope	p-value	Y_2	Slope	p-value	d.f.	R^2	p-value
All	P	0.000063	0.02*	T	0.00034	0.52	17	0.51	0.002*
H, K, Pa	P	0.000084	0.01*	T	0.00020	0.07(*)	11	0.60	0.007*
Pa, X	P	0.000062	0.10(*)	T	0.00007	0.92	8	0.62	0.02*
Pa, X	R	-0.00012	0.16	T	0.0016	0.01*	8	0.58	0.03*
Pa, X	R	-0.00012	0.06(*)	P	0.00009	0.001*	8	0.76	0.004*
H	P	0.000091	0.21	T	0.0026	0.23	2	0.78	0.22
K	P	0.00007	0.64	T	0.0040	0.75	1	0.31	0.83
Pa	P	0.000055	0.06(*)	T	-0.013	0.02*	2	0.98	0.02*
Pa	R	-0.00020	0.53	T	-0.0063	0.63	2	0.87	0.13
Pa	R	-0.00029	0.10(*)	P	0.00003	0.52	2	0.88	0.12
X	P	0.000024	0.45	T	0.00091	0.16	3	0.93	0.02*
X	R	-0.000012	0.83	T	0.0013	0.03*	3	0.91	0.03*
X	R	-0.00010	0.24	P	0.00010	0.03*	3	0.91	0.03*

Table A.4 Results of linear regression models of relative growth rates against wood density. *: $p \leq 0.05$; (*): $0.05 < p \leq 0.10$.

Site	Interval	Slope	d.f.	R^2	p-value
Pasoh	1-2	-0.0067	2442	0.007	<0.001*
Pasoh	2-3	-0.012	1744	0.005	0.005*
Pasoh	3-4	-0.017	1539	0.007	0.002*
Pasoh	4-5	-0.0054	1992	0.002	0.057(*)
Pasoh	5-6	0.0032	1929	0.002	0.05*
KC	1-2	-0.037	1850	0.08	<0.001*
KC	2-3	-0.029	1865	0.05	<0.001*
KC	3-4	-0.037	1840	0.04	<0.001*
KC	4-5	-0.023	2084	0.03	<0.001*
HKK	1-2	-0.014	1435	0.01	<0.001*
HKK	2-3	-0.0054	2135	0.005	<0.001*
HKK	3-4	-0.0018	2117	0.0002	0.57
HKK	4-5	0.00049	2231	4.0×10^{-5}	0.77
HKK	5-6	-0.0036	2271	0.0004	0.34

Table A.5 Results of multiple linear regression models of absolute growth rates against wood density (W), tree size (S), and their interaction (WxS). *: p≤0.05; (*): 0.05<p≤0.10.

Sites: H: HKK; K: KC; Pa: Pasoh.

Interval	Slope-W	p-value	Slope-S	p-value	Slope-WxS	p-value	d.f.	R^2
Pa 1-2	-1.71	0.003*	0.035	<0.001*	0.0013	0.92	2440	0.14
Pa 2-3	-3.73	0.008*	0.027	0.14	0.014	0.65	1742	0.05
Pa 3-4	-5.35	<0.001*	0.025	0.34	-0.037	0.39	1537	0.02
Pa 4-5	-2.13	0.03*	0.0025	0.84	0.0055	0.79	1990	0.008
Pa 5-6	0.55	0.41	-0.00017	0.98	0.0035	0.81	1927	0.002
K 1-2	-8.55	<0.001*	0.079	<0.001*	-0.077	0.01*	1848	0.15
K 2-3	-6.75	<0.001*	0.091	<0.001*	-0.083	0.01*	1863	0.13
K 3-4	-9.41	<0.001*	0.093	<0.001*	-0.059	0.15	1838	0.12
K 4-5	-6.95	<0.001*	0.027	0.15	0.009	0.77	2082	0.07
H 1-2	-3.44	0.03*	0.051	0.004*	-0.029	0.35	1433	0.07
H 2-3	-1.75	0.03*	-0.0049	0.52	0.0023	0.86	2133	0.007
H 3-4	-2.36	0.12	0.015	0.35	0.027	0.32	2115	0.04
H 4-5	1.45	0.07(*)	0.021	0.009*	-0.041	0.003*	2229	0.005
H 5-6	-4.43	0.004*	-0.0003	0.98	0.043	0.09(*)	2269	0.03

Table A.6 Results of multiple linear regression models of relative growth rates against wood density (W), tree size (S), and their interaction (WxS). *: $p \leq 0.05$; (*): $0.05 < p \leq 0.10$.

Sites: H: HKK; K: KC; Pa: Pasoh.

Interval	Slope-W	p-value	Slope-S	p-value	Slope-WxS	p-value	d.f.	R^2
Pa 1-2	-0.011	<0.001*	-0.00015	<0.001*	0.00012	0.03*	2440	0.04
Pa 2-3	-0.019	0.005*	-0.00025	0.005*	0.00018	0.22	1742	0.03
Pa 3-4	-0.020	0.03*	-0.00010	0.39	0.00006	0.75	1537	0.01
Pa 4-5	-0.0085	0.07(*)	-0.00010	0.11	0.00007	0.48	1990	0.01
Pa 5-6	0.0055	0.05*	0.00003	0.48	-0.00006	0.29	1927	0.004
K 1-2	-0.050	<0.001*	-0.00033	<0.001*	0.00039	0.002*	1848	0.11
K 2-3	-0.036	<0.001*	-0.00018	0.02*	0.00018	0.15	1863	0.06
K 3-4	-0.047	<0.001*	-0.00033	0.002*	0.00031	0.08(*)	1838	0.07
K 4-5	-0.036	<0.001*	-0.00026	<0.001*	0.00034	0.006*	2082	0.04
H 1-2	-0.023	<0.001*	-0.00022	0.002*	0.00016	0.20	1433	0.05
H 2-3	-0.0093	<0.001*	-0.00007	0.01*	0.000065	0.15	2133	0.02
H 3-4	-0.0053	0.33	-0.00017	0.003*	2.4×10^{-7}	0.998	2115	0.08
H 4-5	0.00041	0.15	0.000047	0.11	-0.00008	0.14	2229	0.001
H 5-6	-0.0004	0.95	-0.00007	0.24	-0.00015	0.15	2269	0.05

Table A.7 Results of linear regression models of absolute growth rates (AGR) and relative growth rates (RGR) against slope steepness at Huai Kha Khaeng. *: $p \leq 0.05$; (*): $0.05 < p \leq 0.10$.

Growth	Interval	Slope	d.f.	R^2	p-value
AGR	1-2	0.041	1435	0.003	0.04*
AGR	2-3	-0.011	2135	0.0007	0.24
AGR	3-4	0.001	2117	0.0001	0.58
AGR	4-5	-0.0057	2231	0.0002	0.54
AGR	5-6	-0.028	2271	0.001	0.13
RGR	1-2	0.00025	1435	0.007	0.001*
RGR	2-3	-0.00006	2135	0.002	0.07(*)
RGR	3-4	0.000048	2117	0.0003	0.46
RGR	4-5	-0.000038	2231	0.0006	0.24
RGR	5-6	0.000005	2271	1.8×10^{-6}	0.95

Table A.8 Results of multiple linear regression models of absolute growth rates (AGR) and relative growth rates (RGR) against slope steepness (S), tree size (s), and their interaction (Sxs) at Huai Kha Khaeng. *: $p \leq 0.05$; (*): $0.05 < p \leq 0.10$.

Interval	Slope-S	p-value	Slope-s	p-value	Slope-Sxs	p-value	d.f.	R^2
AGR 1-2	0.059	0.07(*)	0.038	<0.001*	-0.00014	0.85	1433	0.06
AGR 2-3	-0.053	<0.001*	-0.013	<0.001*	0.00097	0.001*	2133	0.007
AGR 3-4	-0.014	0.64	0.023	<0.001*	0.00082	0.16	2115	0.04
AGR 4-5	-0.0078	0.62	-0.0024	0.49	0.000034	0.91	2229	0.001
AGR 5-6	0.079	0.01*	0.048	<0.001*	-0.0023	<0.001*	2269	0.03
RGR 1-2	0.00038	0.003*	-0.00007	0.03*	-0.00005	0.09(*)	1433	0.05
RGR 2-3	-0.0001	0.009*	-0.00005	<0.001*	0.000002	0.10(*)	2133	0.01
RGR 3-4	-0.0003	0.74	-0.00017	<0.001*	0.000001	0.74	2115	0.08
RGR 4-5	-0.0008	0.16	-5.5×10^{-6}	0.66	0.6×10^{-7}	0.37	2229	0.001
RGR 5-6	-0.0003	0.80	-0.00015	<0.001*	-2.6×10^{-7}	0.91	2269	0.05

Table A.9 Results of linear regression models of relative growth rates against climate variables for the species sample (P: precipitation; T: temperature; R: radiation). *: $p \leq 0.05$; (*): $0.05 < p \leq 0.10$.

Group	Y	Slope	d.f.	R^2	p-value
Fast-growing emergents	P	0.000042	23	0.11	0.10(*)
Fast-growing emergents	T	0.00044	23	0.03	0.41
Slow-growing emergents	P	0.000078	23	0.22	0.02*
Slow-growing emergents	T	0.0021	23	0.38	0.001*
Legumes	P	0.000075	26	0.19	0.02*
Legumes	T	0.00092	26	0.04	0.34
Burseraceae	P	0.00011	23	0.66	<0.001*
Burseraceae	T	0.0016	23	0.36	0.002*
Pioneers	P	0.000081	18	0.41	0.002*
Pioneers	T	0.0015	18	0.29	0.01*

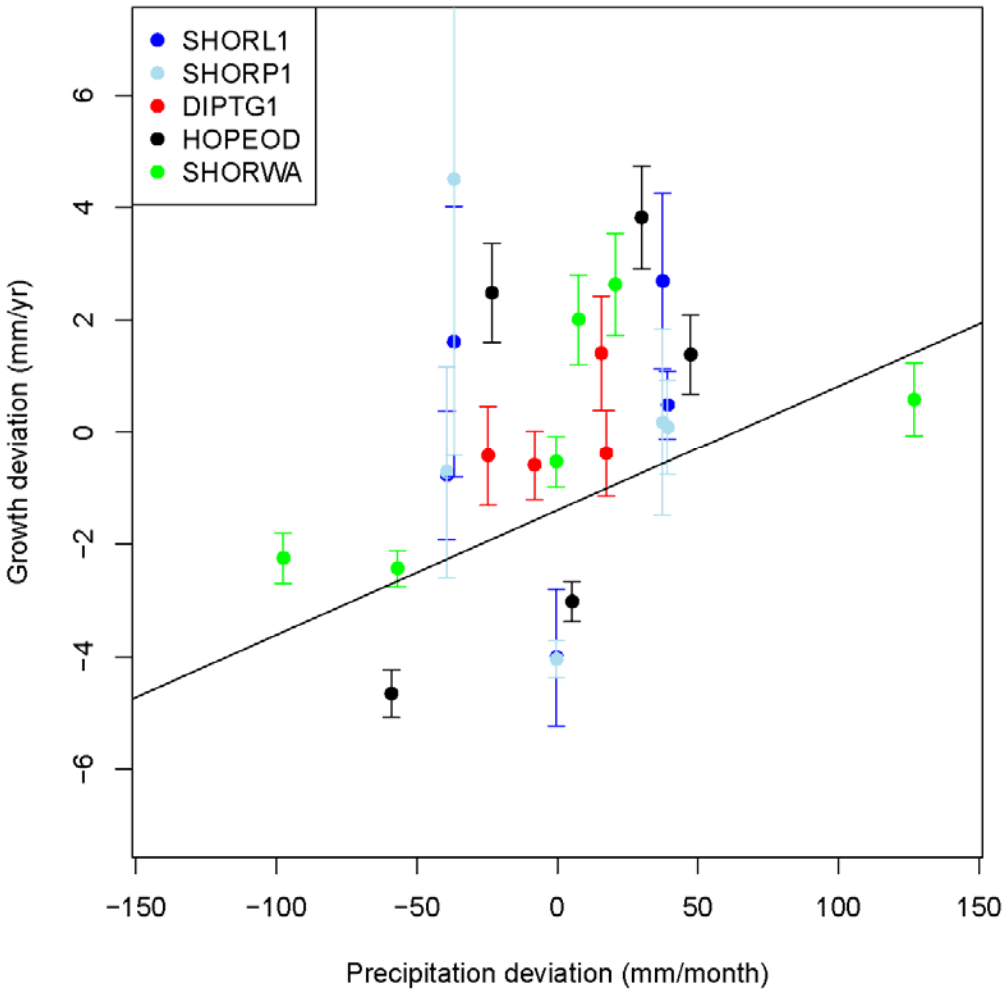

Figure A.1 Mean diameter absolute growth (mm/yr) deviation of fast-growing emergents against monthly total precipitation (mm) deviation. The vertical lines with horizontal bars show the 95% confidence interval of the mean growth rates. The solid black line shows the linear regression across all sites. The species codes of different colors refer to: *Shorea leprosula* at Pasoh (SHORL1, blue), *Shorea parvifolia* at Pasoh (SHORP1, light blue), *Dipterocarpus grandiflorus* at KC (DIPTG1, red), *Hopea odorata* at HKK (HOPEOD, black), and *Parashorea chinensis* at XSBN (SHORWA, green).

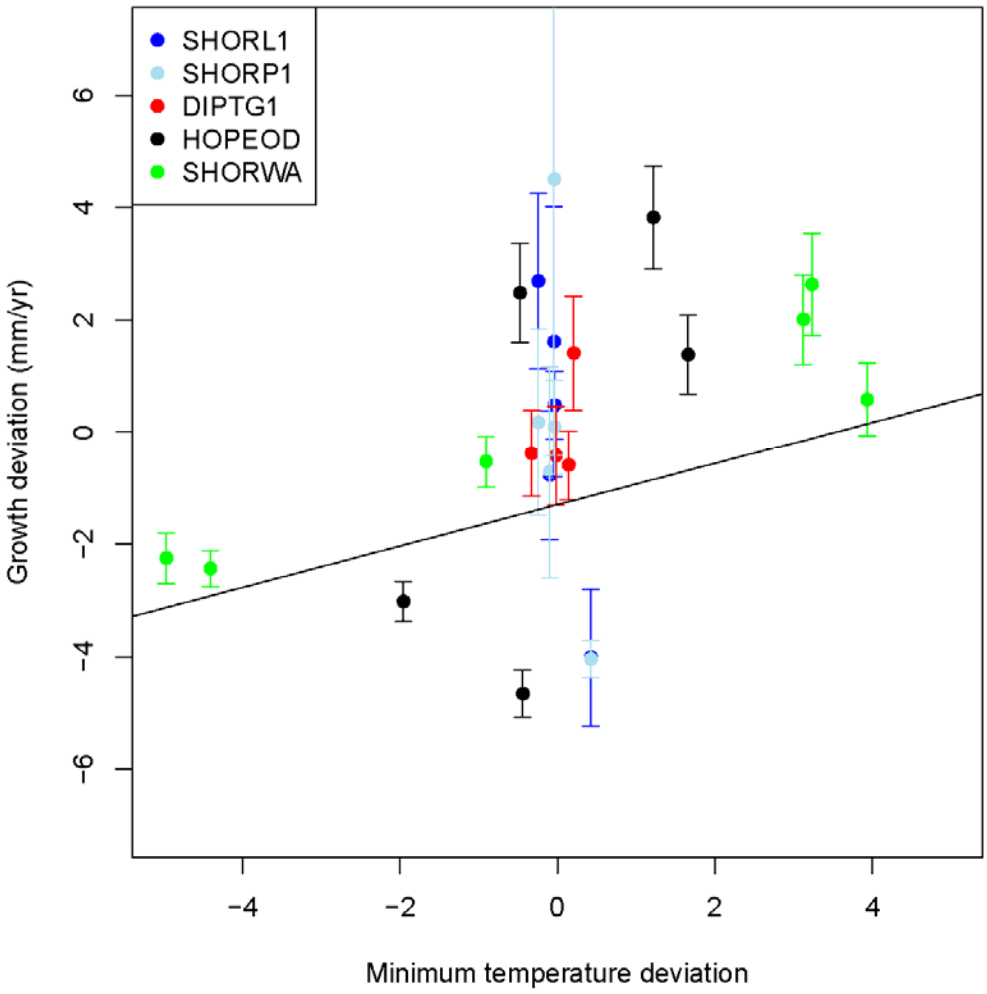

Figure A.2 Mean diameter absolute growth (mm/yr) deviation of fast-growing emergents against monthly mean daily minimum temperature deviation. The vertical lines with horizontal bars show the 95% confidence interval of the mean growth rates. The solid black line shows the linear regression across all sites. The species codes of different colors refer to: *Shorea leprosula* at Pasoh (SHORL1, blue), *Shorea parvifolia* at Pasoh (SHORP1, light blue), *Dipterocarpus grandiflorus* at KC (DIPTG1, red), *Hopea odorata* at HKK (HOPEOD, black), and *Parashorea chinensis* at XSBN (SHORWA, green).

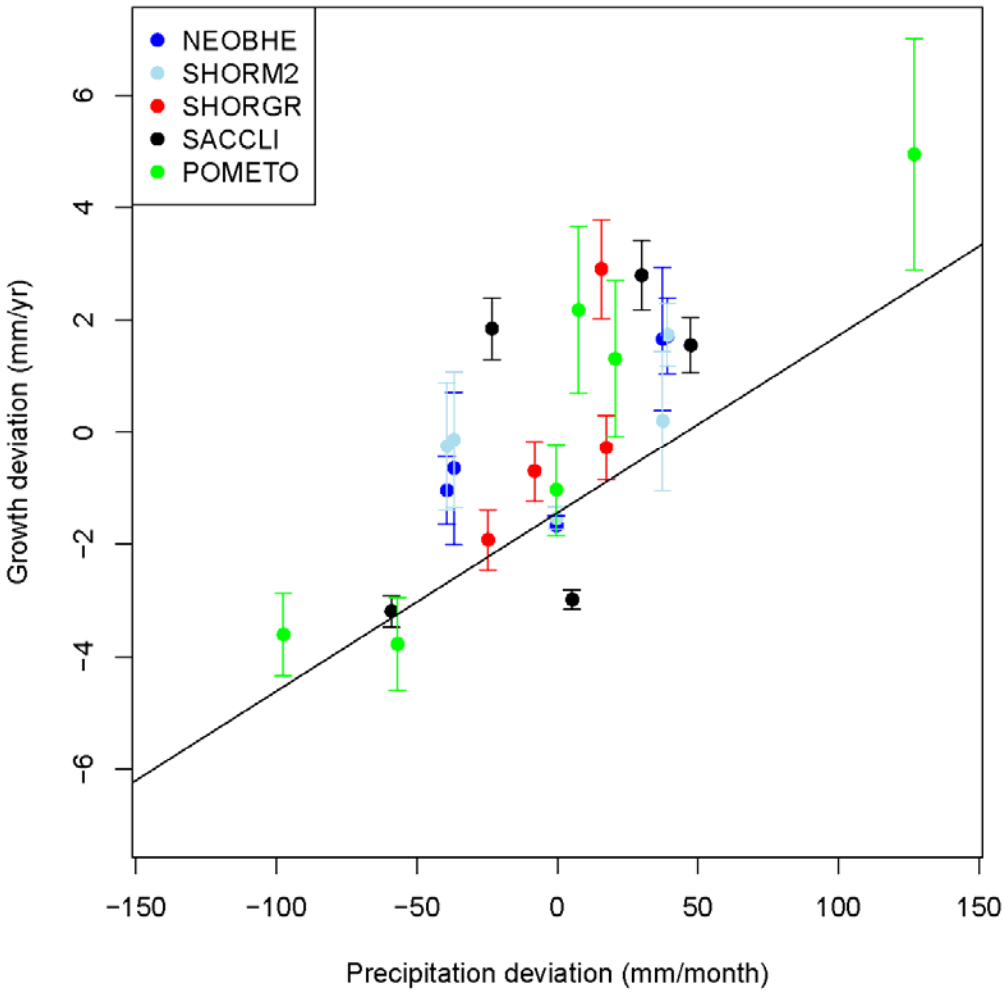

Figure A.3 Mean diameter absolute growth (mm/yr) deviation of slow-growing emergents against monthly total precipitation (mm) deviation. The vertical lines with horizontal bars show the 95% confidence interval of the mean growth rates. The solid black line shows the linear regression across all sites. The species codes of different colors refer to: *Neobalanocarpus heimii* at Pasoh (NEOBHE, blue), *Shorea maxwelliana* at Pasoh (SHORM2, light blue), *Shorea gratissima* at KC (SHORGR, red), *Saccopetalum lineatum* at HKK (SACCLI, black), and *Pometia tomentosa* at XSBN (POMETO, green).

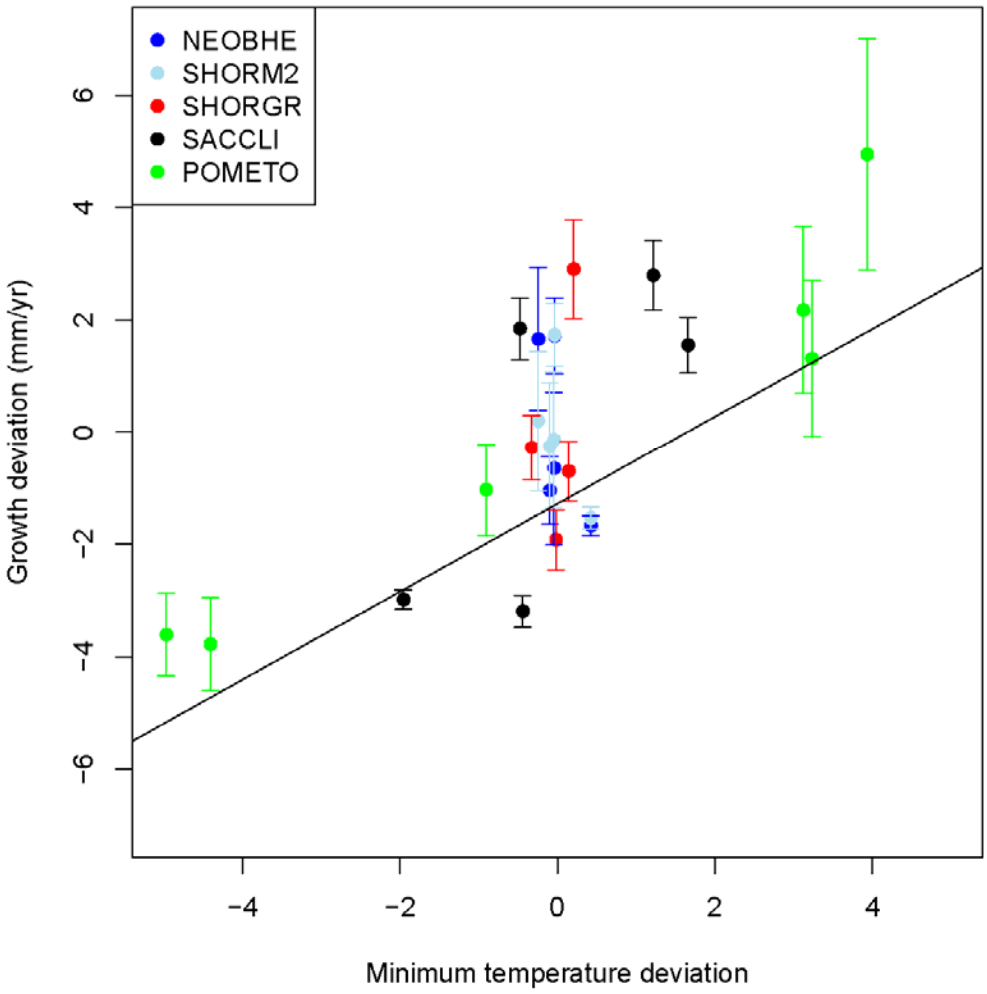

Figure A.4 Mean diameter absolute growth (mm/yr) deviation of slow-growing emergents against monthly mean daily minimum temperature deviation. The vertical lines with horizontal bars show the 95% confidence interval of the mean growth rates. The solid black line shows the linear regression across all sites. The species codes of different colors refer to: *Neobalanocarpus heimii* at Pasoh (NEOBHE, blue), *Shorea maxwelliana* at Pasoh (SHORM2, light blue), *Shorea gratissima* at KC (SHORGR, red), *Saccopetalum lineatum* at HKK (SACCLI, black), and *Pometia tomentosa* at XSBN (POMETO, green).

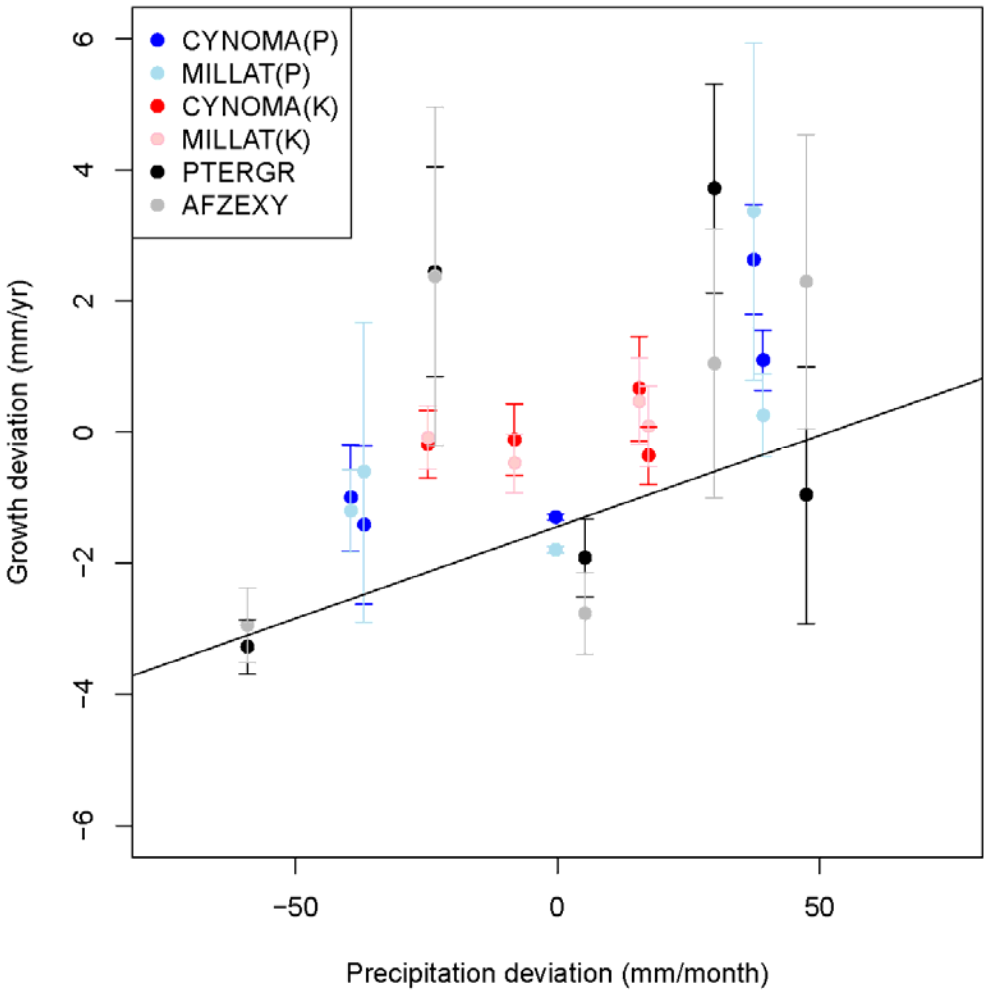

Figure A.5 Mean diameter absolute growth (mm/yr) deviation of Legumes against monthly total precipitation (mm) deviation. The vertical lines with horizontal bars show the 95% confidence interval of the mean growth rates. The solid black line shows the linear regression across all sites. The species codes of different colors refer to: *Cynometra malaccensis* at Pasoh [CYNOMA(P), blue], *Millettia atropurpurea* at Pasoh [MILLAT(P), light blue], *Cynometra malaccensis* at KC [CYNOMA(K), red], *Millettia atropurpurea* at KC [MILLAT(K), pink], *Pterospermum grandiflorum* at HKK (PTERGR, black), and *Afzelia xylocarpa* at HKK (AFZEXY, grey).

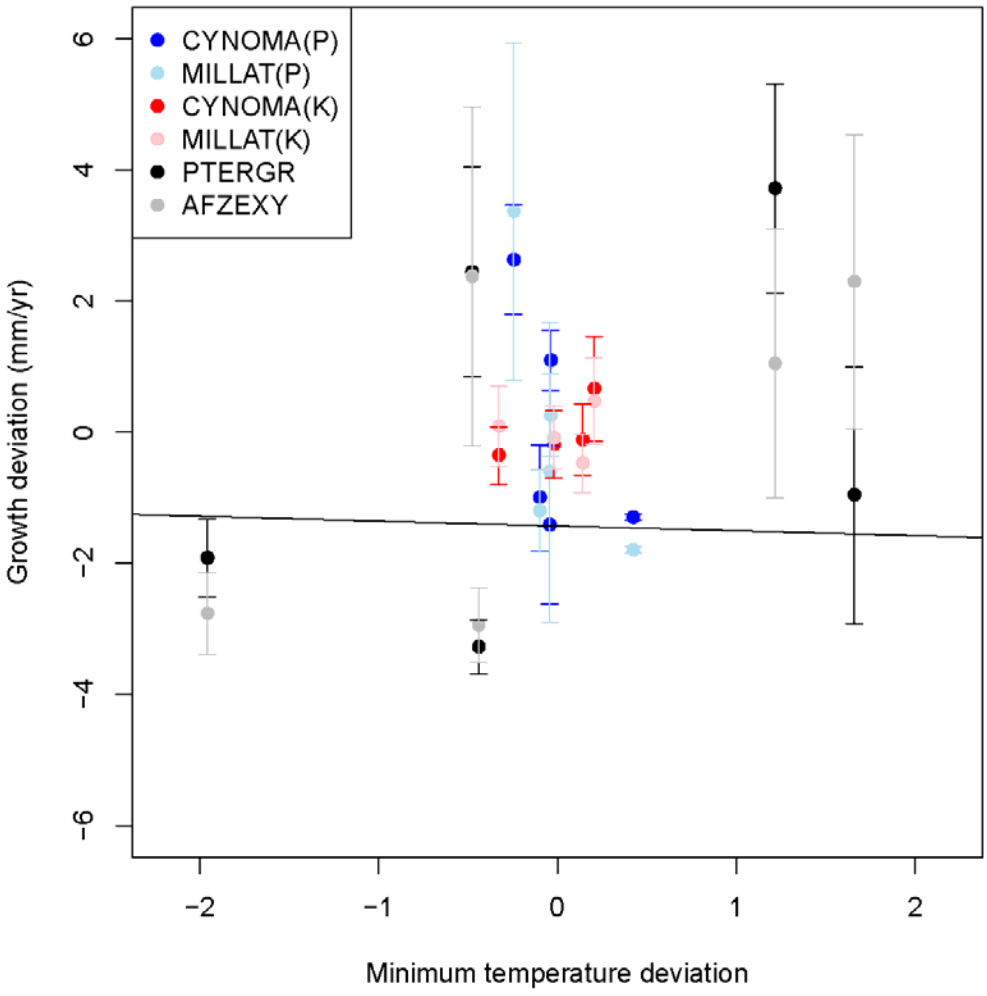

Figure A.6 Mean diameter absolute growth (mm/yr) deviation of Legumes against monthly mean daily minimum temperature deviation. The vertical lines with horizontal bars show the 95% confidence interval of the mean growth rates. The solid black line shows the linear regression across all sites. The species codes of different colors refer to: *Cynometra malaccensis* at Pasoh [CYNOMA(P), blue], *Millettia atropurpurea* at Pasoh [MILLAT(P), light blue], *Cynometra malaccensis* at KC [CYNOMA(K), red], *Millettia atropurpurea* at KC [MILLAT(K), pink], *Pterospermum grandiflorum* at HKK (PTERGR, black), and *Afzelia xylocarpa* at HKK (AFZEXY, grey).

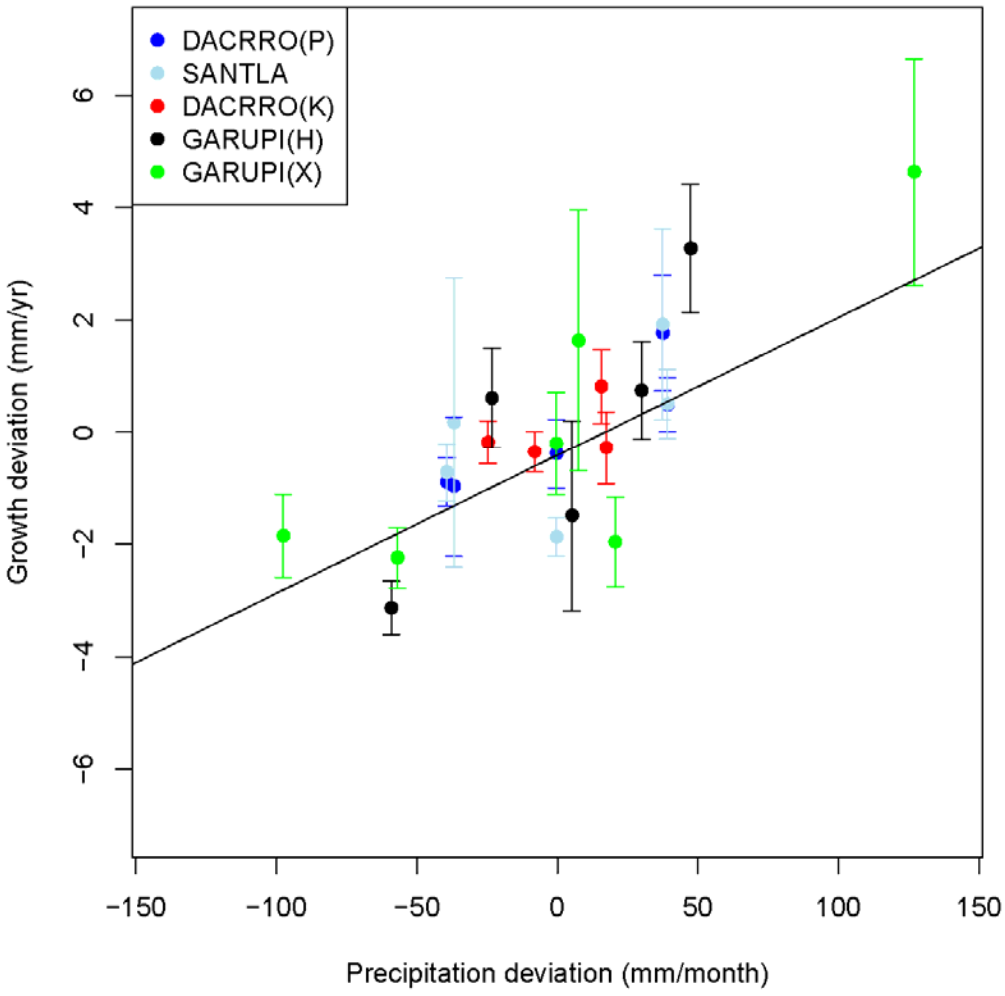

Figure A.7 Mean diameter absolute growth (mm/yr) deviation of Burseraceae against monthly total precipitation (mm) deviation. The vertical lines with horizontal bars show the 95% confidence interval of the mean growth rates. The solid black line shows the linear regression across all sites. The species codes of different colors refer to: *Dacryodes rostrata* at Pasoh [DACRRO(P), blue], *Santiria laevigata* at Pasoh (SANTLA, light blue), *Dacryodes rostrata* at KC [DACRRO(K), red], *Garuga pinnata* at HKK [GARUPI(H), black], and *Garuga pinnata* at XSBN [GARUPI(X), green].

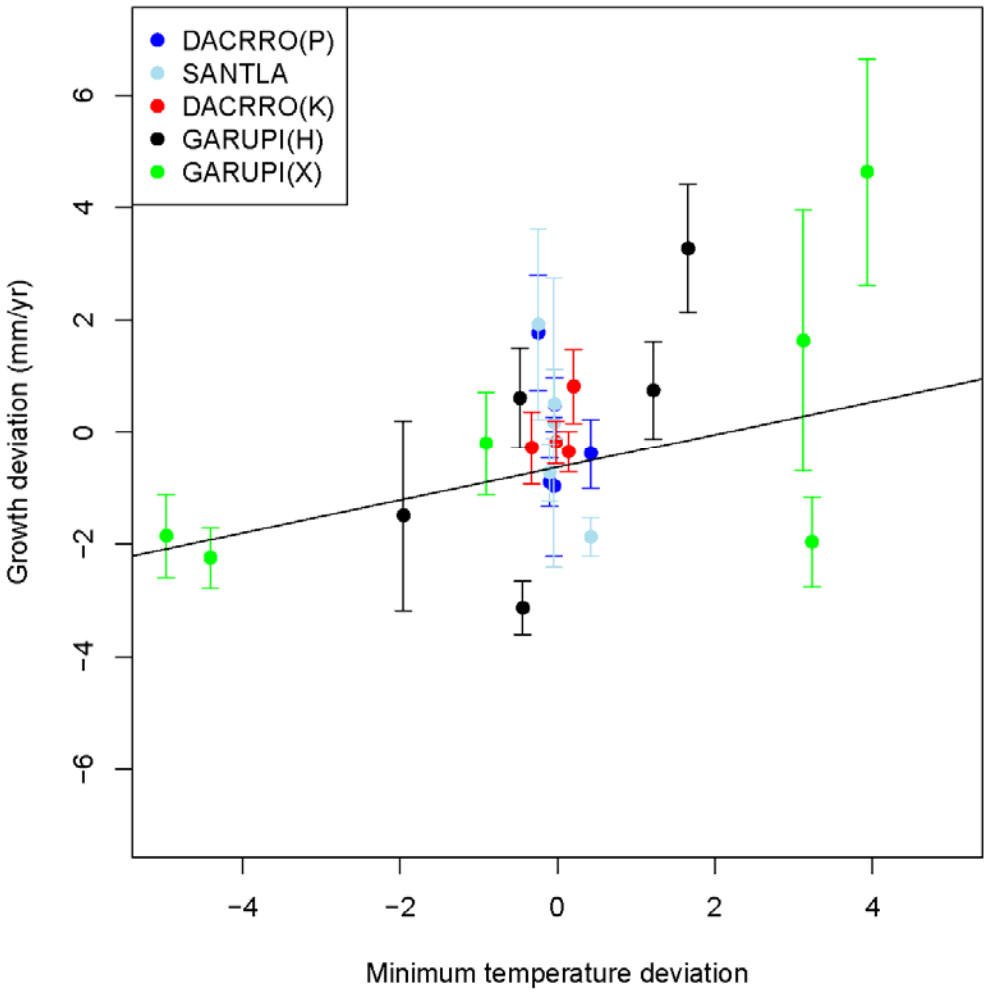

Figure A.8 Mean diameter absolute growth (mm/yr) deviation of Burseraceae against monthly mean daily minimum temperature deviation. The vertical lines with horizontal bars show the 95% confidence interval of the mean growth rates. The solid black line shows the linear regression across all sites. The species codes of different colors refer to: *Dacryodes rostrata* at Pasoh [DACRRO(P), blue], *Santiria laevigata* at Pasoh (SANTLA, light blue), *Dacryodes rostrata* at KC [DACRRO(K), red], *Garuga pinnata* at HKK [GARUPI(H), black], and *Garuga pinnata* at XSBN [GARUPI(X), green].

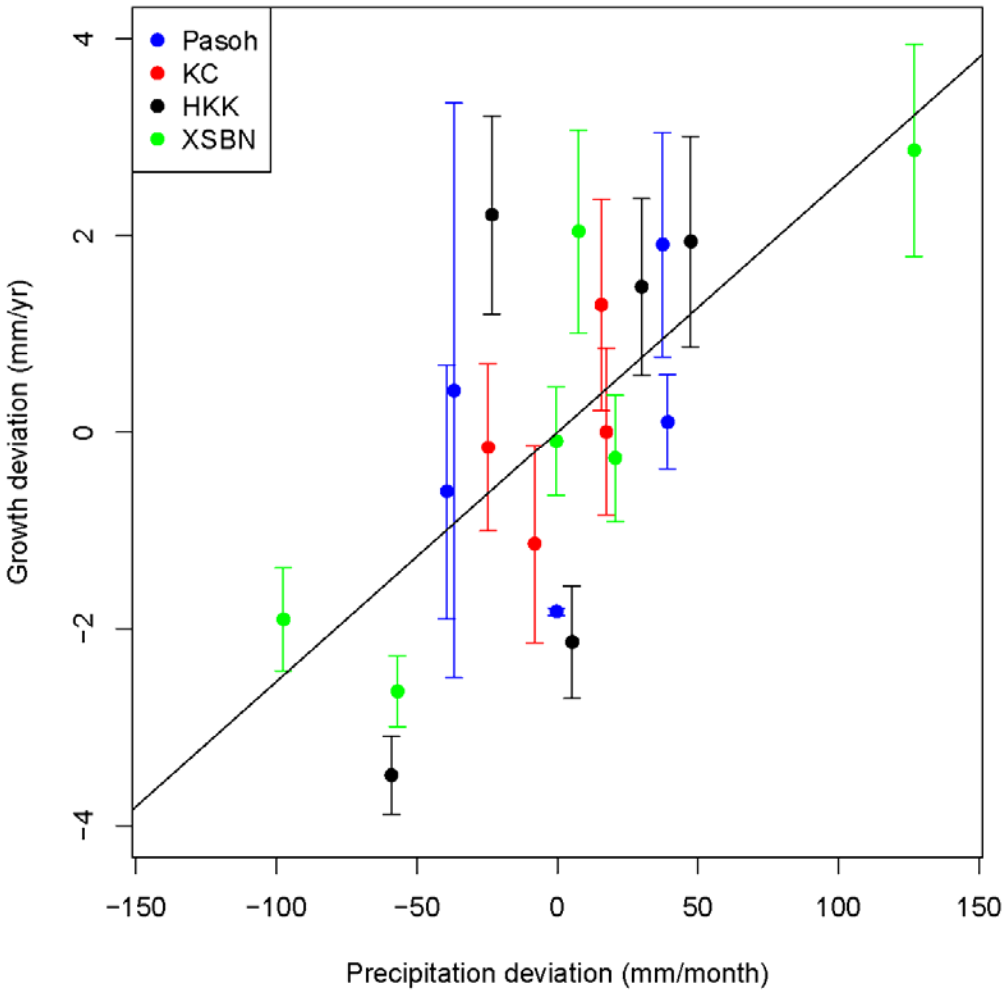

Figure A.9 Mean diameter absolute growth (mm/yr) deviation of pioneers against monthly total precipitation (mm) deviation at Pasoh (blue), KC (red), HKK (black), and XSBN (green). The vertical lines with horizontal bars show the 95% confidence interval of the mean growth rates. The solid black line shows the linear regression across all sites.

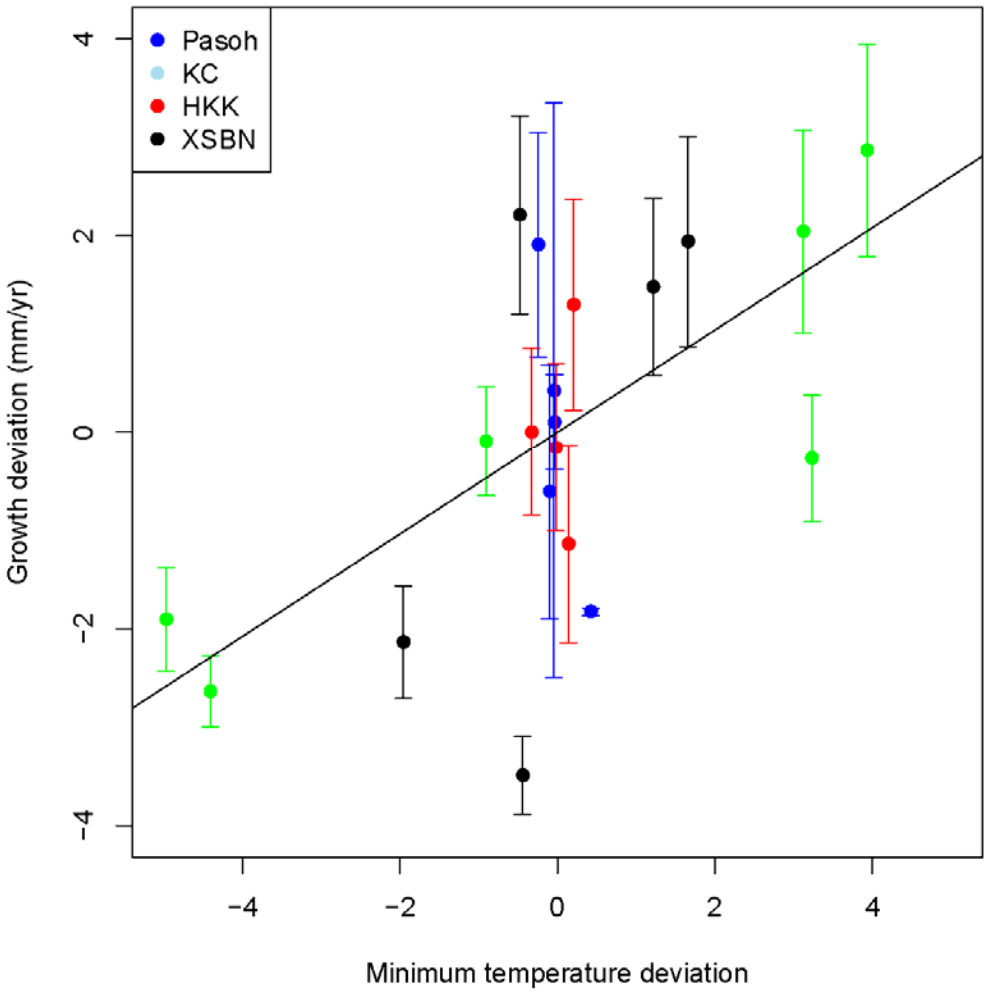

Figure A.10 Mean diameter absolute growth (mm/yr) deviation of pioneers against monthly mean daily minimum temperature deviation at Pasoh (blue), KC (red), HKK (black), and XSBN (green). The vertical lines with horizontal bars show the 95% confidence interval of the mean growth rates. The solid black line shows the linear regression across all sites.

Appendix B

Supplementary materials for Chapter 4

The equilibrium solution for the partial differential model (Equation 4.2) is

$$n(z) = n_1 z^{-p} e^{\frac{\mu_0}{g_0}\left(\frac{1-z^{1+q-p}}{1+q-p}\right)} \quad , \qquad \text{(Equation 4.13)}$$

when the steady-state equation (Equation 4.12) is solved by incorporating the power law functions for growth and mortality rates, i.e. $g(z) = g_0 z^p$ and $\mu(z) = \mu_0 z^q$, and substituting the boundary condition $n_1 = n(z=1)$ (see Section 4.3).

However, the set of exponents proposed by metabolic scaling theory is a special case: with p = 1/3 and q = -2/3, the denominator of the exponential in Equation 4.13 becomes zero (1+q-p=0). In this case, we can still approximate the solution by invoking the Taylor expansion for power law functions, i.e.

$$a^x = \sum_{k=0}^{\infty} \frac{(x \ln a)^k}{k!}. \qquad \text{(B.1)}$$

Then the power law function z^{1+q-p} becomes:

$$z^{1+q-p} = 1 + (1+q-p)\ln z + (1+q-p)^2 \ln z^2 + \cdots \quad . \tag{B.2}$$

When $1+q-p \rightarrow 0$, the higher-order terms are negligible and

$$z^{1+q-p} \approx 1 + (1+q-p)\ln z \quad . \tag{B.3}$$

Equation 4.13 now becomes:

$$\begin{aligned} n(z) &= n_1 z^{-p} e^{\frac{\mu_0}{g_0}\left(\frac{1-z^{1+q-p}}{1+q-p}\right)} \\ &= n_1 z^{-p} e^{-\frac{\mu_0}{g_0}\ln z} \\ &= n_1 z^{-p} \cdot z^{-\frac{\mu_0}{g_0}} \end{aligned} \tag{B.4}$$

Thus if $p = 1/3$ and $\mu_0/g_0 = 5/3$ (as was predicted for a Costa Rican forest in Enquist et al. 2009, $\mu_0 = 0.20$ and $g_0 = 0.12$), then

$$n(z) = n_1 z^{-p-\frac{\mu_0}{g_0}} = n_1 z^{-2} \quad . \tag{B.5}$$

Therefore, MST is shown to be a special case to the general solution of Equation 4.2 and the slope of the *n-z* relationship approaches -2 for particular values of g_0 and μ_0.

Bibliography

Asner, G. P., D. Nepstad, G. Cardinot, and D. Ray. 2004. Drought stress and carbon uptake in an Amazon forest measured with spaceborne imaging spectroscopy. Proceedings of the National Academy of Science USA 101: 6039-6044.

Baker, P. J., S. Bunyavejchewin, C. D. Oliver, and P. S. Ashton. 2005. Disturbance history and historical stand dynamics of a seasonal tropical forest in western Thailand. Ecological Monographs 75(3): 317-343.

Baker, T. R., O. L. Phillips, Y. Malhi, S. Almeida, L. Arroyo, A. Di Fiore, T. Erwin, et al. 2004a. Variation in wood density determines spatial patterns in Amazonian forest biomass. Global Change Biology 10: 545-562.

Baker, T. R., O. L. Phillips, Y. Malhi, S. Almeida, L. Arroyo, A. Di Fiore, T. Erwin, et al. 2004b. Increasing biomass in Amazonian forest plots. Philosophical Transactions of the Royal Society of London B 359: 353-365.

Bawa, K. S. and A. Markham. 1995. Climate change and tropical forests. Trends in Ecology and Evolution 10: 348-349.

Brown, S. 1997. Estimating Biomass and Biomass Change in Tropical Forests: a Primer. Rome: Food and Agriculture Organization of the United Nations.

Chave, J., R. Condit, S. Lao, J. P. Caspersen, R. B. Foster, and S. P. Hubbell. 2003. Spatial and temporal variation of biomass in a tropical forest: results from a large census plot in Panama. Journal of Ecology 91: 240-252.

Chave, J., C. Andalo, S. Brown, M. A. Cairns, J. Q. Chambers, D. Eamus, H. Fölster, et al. 2005. Tree allometry and improved estimation of carbon stocks and balance in tropical forests. Oecologia 145: 87-99.

Chave, J., H. C. Muller-Landau, T. R. Baker, T. A. Easdale, H. t. Steege, and C. O. Webb. 2006. Regional and phylogenetic variation of wood density across 2456 neotropical tree species. Ecological Applications 16: 2356-2367.

Chave, J., R. Condit, H. C. Muller-Landau, S. C. Thomas, P. S. Ashton, S. Bunyavejchewin, L. L. Co, et al. 2008. Assessing evidence for a pervasive alteration in tropical tree communities. PLoS Biology 6: 455-462.

Chen, M., P. Xie, J. E. Janowiak, and P. A. Arkin. 2002. Global land precipitation: a 50-yr monthly analysis based on gauge observations. Journal of Hydrometeorology 3: 249-266.

Childs, D. Z., M. Rees, K. E. Rose, P. J. Grubb, and S. P. Ellner. 2003. Evolution of complex flowering strategies: an age- and size-structured integral projection model. Proceedings of the Royal Society B 270: 1829-1838.

Clark, D. A. and D. B. Clark 1992. Life history diversity of canopy and emergent tres in a neotropical rain forest. Ecological Monographs 62: 315-344.

Clark, D. B., D. A. Clark, and P. M. Rich. 1993. Comparative analysis of microhabitat utilization by saplings of nine tree species in Neotropical rain forest. Biotropica 25: 397-407.

Clark, D. A., S. C. Piper, C. D. Keeling, and D. B. Clark. 2003. Tropical rain forest tree growth and atmospheric carbon dynamics linked to interannual temperature variation during 1984-2000. Proceedings of the National Academy of Science USA 100: 5852-5857.

Clark, D. A. 2004a. Sources or sinks? The responses of tropical forests to current and future climate and atmospheric composition. Philosophical Transactions of the Royal Society of London B 359: 477-491.

Clark, D. A. 2004b. Tropical forests and global warming: slowing it down or speeding it up? Frontiers in Ecology and the Environment 2: 73-80.

Clark, D. A. 2007. Detecting tropical forests' responses to global climatic and atmospheric change: current challenges and a way forward. Biotropica 39: 4-19.

Clark, D. B., D. A. Clark, and S. F. Oberbauer. 2010. Annual wood production in a tropical rain forest in NE Costa Rica linked to climatic variation but not to increasing CO2. Global Change Biology 16: 747-759.

Condit, R., S. P. Hubbell, and R. B. Foster. 1996. Assessing the response of plant functional types to climatic change in tropical forests. Journal of Vegetation Science 7: 405-416.

Condit, R. 1998. Tropical forest census plots. Berlin: Springer-Verlag and Georgetown, TX: R. G. Landes Company.

Condit, R., P. Ashton, S. Bunyavejchewin, H. S. Dattaraja, S. Davies, S. Esufali, E. Corneille, et al. 2006. The importance of demographic niches to tree diversity. Science 313: 98-101.

Coomes, D. A., R. P. Duncan, R. B. Allen, and J. Truscott. 2003. Disturbances prevent stem size-density distributions in natural forests from following scaling relationships. Ecology Letters 6: 980-989.

Da Costa, A. C. L., D. Galbraith, S. Almeida, B. T. T. Portela, M. da Costa, J. de Athaydes Silva, A. P. Braga, et al. 2010. Effect of 7 yr of experimental drought on vegetation dynamics and biomass storage of an eastern Amazonian rainforest. New Phytologist 187: 579-591.

Da Silva, R. P., J. dos Santos, E. S. Tribuzy, J. Q. Chambers, S. Nakamura, and N. Higuchi. 2002. Diameter increment and growth patterns for individual tree growing in Central Amazon, Brazil. Forest Ecology and Management 166: 295-301.

Davies, S. J., P. A. Palmiotto, P. S. Ashton, H. S. Lee, and J. V. LaFrankie. 1998. Comparative ecology of 11 sympatric species of *Macaranga* in Borneo: tree distribution in relation to horizontal and vertical resource heterogeneity. Journal of Ecology 86: 662-673.

Dawkins, H. C. and D. R. B. Field. 1978. A long-term surveillance system for British woodland vegetation. Oxford: Department of Forestry, Oxford University.

Dixon, R. K., S. Brown, R. A. Houghton, A. M. Solomon, M. c. Trexler, and J. Wisniewski. 1994. Carbon pools and flux of global forest ecosystems. Science 263: 185-190.

Easterling, M. R., S. P. Ellner, and P. M. Dixon. 2000. Size-specific sensitivity: applying a new structured population model. Ecology 81(3): 694-708.

Enquist, B. J., G. B. West, E. L. Charnov, and J. H. Brown. 1999. Allometric scaling of production and life-history variation in vascular plants. Nature 401: 907-911.

Enquist, B. J. and K. J. Niklas. 2001. Invariant scaling relations across tree-dominated communities. Nature 410: 655-660.

Enquist, B. J., G. B. West, and J. H. Brown. 2009. Extensions and evaluations of a general quantitative theory of forest structure and dynamics. Proceedings of the National Academy of Science USA 106: 7046-7051.

Feeley, K. J., S. J. Wright, M. N. N. Supardi, A. R. Kassim, and S. J. Davies. 2007. Decelerating growth in tropical forest trees. Ecology 10: 461-469.

Gloor, M., O. L. Phillips, J. J. Lloyd, S. L. Lewis, Y. Malhi, T. R. Baker, G. López-Gonzalez, et al. 2009. Does the disturbance hypothesis explain the biomass increase in basin-wide Amazon forest plot data? Global Change Biology 15: 2418-2430.

Graham, E. A., S. S. Mulkey, K. Kitajima, N. G. Phillips, and S. J. Wright. 2003. Cloud cover limits net CO_2 uptake and growth of a rainforest tree during tropical rainy seasons. Proceedings of the National Academy of Science USA 100: 572-576.

IPCC. 2007. Climate change 2007: The physical science basis. Contribution of working group I to the fourth assessment report of the intergovernmental panel on climate change. Cambridge and New York: Cambridge University Press.

Keeland, B. D. and R. R. Sharitz. 1993. Accuracy of tree growth measurements using dendrometer bands. Canadian Journal of Forest Research 23: 2454–2457.

King, D. A., S. J. Davies, M. N. N. Supardi, and S. Tan. 2005. Tree growth is related to light interception and wood density in two mixed dipterocarp forests in Malaysia. Functional Ecology 19: 445-453.

Kohyama, T. 1992. Size-structured multi-species model of rain forest trees. Functional Ecology 6: 206-212.

Kohyama, T. 1993. Size-structured tree populations in gap-dynamic forest – the forest architecture hypothesis for the stable coexistence of species. Journal of Ecology 81: 131-143.

Kohyama, T. and N. Shigesada. 1995. A size-distribution-based model of forest dynamics along a latitudinal environmental gradient. Vegetatio 121: 117-126.

Lewis, S. L., O. L. Phillips, T. R. Baker, J. J. Lloyd, Y. Malhi, S. Almeida, N. Higuchi, et al. 2004. Concerted changes in tropical forest structure and dynamics: evidence from 50 South American long-term plots. Philosophical Transactions of the Royal Society of London B 359: 421-436.

Losos, E. C. and E. G. Leigh. 2004. Tropical forest diversity and dynamism: findings from a network of large-scale tropical forest plots. Chicago: The University of Chicago Press.

Malhi, Y., O. L. Phillips, J. Lloyd, T. R. Baker, J. Wright, S. Almeida, L. Arroyo, et al. 2002. An international network to monitor the structure, composition and

dynamics of Amazonian forests (RAINFOR). Journal of Vegetation Science 13: 439-450.

Malhi, Y. and O. L. Phillips. 2004. Tropical forests and global atmospheric change: a synthesis. Philosophical Transactions of the Royal Society of London B 359: 549-555.

Malhi, Y. and J. Wright. 2004. Spatial patterns and recent trends in the climate of tropical rainforest regions. Philosophical Transactions of the Royal Society of London B 359: 311-329.

Midgley, J. J. 2001. Do mixed-species mixed-size indigenous forests also follow the self-thinning line? Trends in Ecology & Evolution 16: 661-662.

Moorcroft, P. R., G. C. Hurtt, and S. W. Pacala. 2001. A method for scaling vegetation dynamics: The ecosystem demography model (ED). Ecological Monographs 71: 557-585.

Muller-Landau, H. C. 2004. Interspecific and inter-site variation in wood specific gravity of tropical trees. Biotropica 36: 20–32.

Muller-Landau, H. C., R. S. Condit, J. Chave, S. C. Thomas, S. A. Bohlman, S. Bunyavejchewin, S. Davies, et al. 2006a. Testing metabolic ecology theory for allometric scaling of tree size, growth and mortality in tropical forests. Ecology Letters 9: 575-588.

Muller-Landau, H. C., R. S. Condit, K. E. Harms, C. O. Marks, S. C. Thomas, S. Bunyavejchewin, G. Chuyong, et al. 2006b. Comparing tropical forest tree size distributions with the prediction of metabolic ecology and equilibrium models. Ecology Letters 9: 589-602.

Muller-Landau, H. C. and S. X. Dong. 2008. Metal band dendrometer protocol. Version: November 2008. http://www.ctfs.si.edu/data///documents/Metal_Band_Dendrometer_Protocol_20081119_archive.pdf

Murphy, P. G. and A. E. Lugo. 1986. Ecology of tropical dry forest. Annual Review of Ecology and Systematics 17: 67-88.

Nemani, R. R., C. D. Keeling, H. Hashimoto, W. M. Jolly, S. C. Piper, C. J. Tucker, R. B. Myneni, and S. W. Running. 2003. Climate-driven increases in global terrestrial net primary production from 1983 to 1999. Science 300: 1560-1563.

O'Brien, J. J., S. F. Oberbauer, D. B. Clark, and D. A. Clark. 2008. Phenology and stem diamter increment seasonality in a Costa Rican wet tropical forest. Biotropica 40: 151-159.

Pelissier, R. and J.P. Pascal. 2000. Two-year tree growth patterns investigated from monthly girth records using dendrometer bands in a wet evergreen forest in India. Journal of Tropical Ecology 16: 429–446.

Phillips, O. L., T. R. Baker, L. Arroyo, N. Higuchi, T. Killeen, W. F. Laurance, S. L. Lewis, et al. 2004. Pattern and process in Amazon tree turnover, 1976-2001. Philosophical Transactions of the Royal Society of London B 359: 381-407.

Poorter, L., F. Bongers, F. J. Sterck, and W. Hannsjörg. 2005. Beyond the regeneration phase: differentiation of height-light trajectories among tropical tree species. Journal of Ecology 93: 256-267.

Reich, P. B., M. B. Walters, and D. S. Ellsworth. 1997. From tropics to tundra: global convergence in plant functioning. Proceedings of the National Academy of Science USA 94: 13730-13734.

Rice, A. H., E. H. Pyle, S. R. Saleska, L. Hutrya, M. Palace, M. Keller, P. B. de Camargo, K. Portilho, D. F. Marques, and S. C. Wofsy. 2004. Carbon balance and vegetation dynamics in an old-growth Amazonian forest. Ecological applications 14: S55-S71.

Rolim, S. G., R. M. Jesus, H. E. M. Nascimento, H. T. Z. d. Couto, and J. Q. Chambers. 2005. Biomass change in an Atlantic tropical moist forest: the ENSO effect in permanent sample plots over a 22-year period. Oecologia 142: 238–246.

Ropelewski, C. F., J. E. Janowiak, and M. S. Halpert. 1985. The analysis and display of real time surface climate data. Monthly Weather Review 113: 1101-1106.

Russo, S. E., S. K. Wiser, and D. A. Coomes. 2007. Growth-size scaling relationships of woody plant species differ from predictions of the Metabolic Ecology Model. Ecology Letters 10: 889-901.

Saldarriaga, J., D. C. West, M. L. Tharp, and C. Uhl. 1988. Long-term chronosequence of forest succession in the upper Rio Negro of Colombia and Venezuela. Journal of Ecology 76: 938-958.

Sands, P. J. 1995. Modelling canopy production. II. From single-leaf photosynthetic parameters to daily canopy photosynthesis. Australian Journal of Plant Physiology 22: 603-614.

Suzuki, E. 1999. Diversity in specific gravity and water content of wood among Bornean tropical rainforest trees. Ecological Research 14: 211-224.

Tho, Y. P. 1982. Gap formation by the termite *Microcerotermes dubius* in lowland forests of Peninsular Malaysia. Malaysian Forester 45: 184-192.

West, G. B., J. H. Brown, and B. J. Enquist. 1997. A general model for the origin of allometric scaling laws in biology. Science 276: 122-126.

West, G. B., J. H. Brown, and B. J. Enquist. 1999. A general model for the structure and allometry of plant vascular systems. Nature 400: 664-667.

West, G. B., B. J. Enquist, and J. H. Brown. 2009. A general quantitative theory of forest structure and dynamics. Proceedings of the National Academy of Science USA 106: 7040-7045.

Whitfield, J. 2001. All creatures great and small. Nature 413: 342-344.

Wilson, E. O. 1988. The current state of biological diversity. In Biodiversity, ed. E. O. Wilson, 3-18. Washington, D.C.: National Academy Press.

Wright, S. J. and O. Calderon. 2006. Seasonal, El Niño and longer term changes in flower and seed production in a moist tropical forest. Ecology Letters 9: 35-44.

Yan, J., G. Zhou, D. Zhang, X. Tang, and X. Wang. 2006. Different patterns of changes in the dry season diameter at breast height of dominant and evergreen tree species in a mature subtropical forest in South China. Journal of Integrative Plant Biology 48: 906-913.

Yoda, K., T. Kira, H. Ogawa, and K. Hozumi. 1963. Self-thinning in overcrowded pure stands under cultivated and natural conditions. Journal of Biology, Osaka City University 14: 106-129.

Zhang, Y., W. B. Rossow, A. A. Lacis, V. Oinas, and M. I. Mishchenko. 2004. Calculation of radiative fluxes from the surface to top of atmosphere based on ISCCP and other global data sets: refinements of the radiative transfer model and the input data. Journal of Geophysical Research 109: D19105.